主論文

Synthetic Studies on Carbon Nanobelt

カーボンナノベルトの合成研究

Akiko Yagi (Iwata)

八木（岩田）亜樹子

2016

Preface

The studies presented in this thesis have been carried out under the direction of Professor Kenichiro Itami at Department of Chemistry, Graduate School of Science, Nagoya University between April 2010 and March 2016. This thesis is concerned with synthetic studies on carbon nanobelt.

I would like to express my sincerest gratitude to Professor Kenichiro Itami for great support, valuable suggestions and hearty encouragement throughout this work. I would like to express my great appreciation to Itami ERATO Group Leader Yasutomo Segawa for his kind guidance, helpful discussions, technical assistance and enthusiasm during the course of this study. I appreciate to Lecturer Hideto Ito for his helpful suggestions. I also appreciate Associate Professor Junichiro Yamaguchi, Associate Professor Shinya Hagihara, and Assistant Professor Kei Murakami for their insightful comments and helpful discussions.

I would like to express my heartfelt appreciation to Professor Ken-Tsung Wong and Professor Cathleen M. Crudden for giving me an opportunity to visit National Taiwan University and Queen's University as an exchange student, great supports and valuable suggestions. I would also like to thank Dr. Shu-Hua Chou, Dr. Erik Keske, Dr. Patrick Eisenberger, and all members in both Wong's and Crudden's laboratories.

I would like to express my gratitude to Professor Shigehiro Yamaguchi and Professor Susumu Saito for their helpful guidance and encouragement.

I must make special mention of Dr. Gandikota Venkataramana, Dr. Hiroshi Ueno, Mr. Katsuma Matsui, Mr. Keishu Okada, Ms. Akiko Gocho for great collaborations and their valuable discussions and encouragement.

I heartily thank to

Dr. Shuichi Yanagisawa	Dr. Masakazu Nambo	Ms. Hiromi Sekizawa
Dr. Debashis Mandal	Dr. Kirika Ueda	Dr. Haruka Omachi
Dr. Katsuaki Kawasumi	Mr. Takuya Yamamoto	Mr. Toshiki Kojima

Mr. Satoshi Tani
Ms. Sanae Matsuura
Mr. Hiroyuki Ishikawa
Dr. Kei Muto
Mr. Takahiro Uehara
Ms. Yukari Mitamura
Mr. Kakishi Uno
Ms. Natsumi Kubota
Mr. Shin Suzuki
Mr. Tsuyoshi Oshima
Ms. Kaho Maeda
Ms. Mari Shibata
Mr. Keiichiro Murai
Mr. Shuya Yamada
Ms. Eri Ito
Mr. Jumpei Suzuki
Ms. Yip Shu Jan
Dr. Kazuya Yamaguchi
Dr. Eiji Yamaguchi
Dr. Hua Zhang
Dr. Guillaume Povie
Dr. Sylvia Kirchberg
Mr. Christoph Rosorius
Mr. Dominik J. Bergmann
Dr. Kathryn. M. Chepiga
Mr. Jake Schlessinger
Ms. Yui Ueyama
Ms. Nanako Kato
Dr. Kazuhiro Hata
Dr. Atsushi Yamaguchi
Mr. Kyohei Ozaki
Ms. Hiromi Yoshida
Mr. Tomonori Kajino
Mr. Tetsushi Yoshidomi
Mr. Hiroki Kondo
Ms. Yuko Kamada
Mr. Ryosuke Takise
Mr. Jun Orii
Mr. Kiyotaka Mori
Mr. Takahiro Kawakami
Ms. Masako Fushimi
Mr. Yuta Yano
Mr. Kazushi Kumazawa
Ms. Wakana Hayashi
Dr. Kenji Mochida
Dr. Lingkui Meng
Dr. Asraa Ziadi
Dr. Jiao Jiao
Mr. Kaoru Arisue
Dr. Anna Junker
Dr. Friederike Sibbel
Dr. Eva Koch
Ms. Huimin Dai
Mr. Chunxiao Li
Mr. Satoru Kawai
Dr. Takehisa Maekawa
Mr. Kazuma Amaike
Mr. Kazuki Kimura
Mr. Yuuki Ishii
Ms. Keika Hattori
Mr. Takao Fujikawa
Ms. Misaho Araki
Mr. Yutaro Saito
Mr. Masahiko Yoshimura
Mr. Kenta Kato
Mr. Shun Yamashita
Ms. Chisa Kobayashi
Ms. Manami Muraki
Mr. Ryotaro Yamada
Mr. Yoshito Koga
Mr. Wataru Matsuoka
Dr. Petr Šenel
Mr. Shin Miyamura
Mr. Taito Hatakeyama
Mr. Takeshi Kaneda
Dr. Atsushi Kinoshita
Dr. Lilia Lohrey
Dr. Nils Schröder
Mr. Artur Kokornaczyk
Mr. Shijian Jin
Ms. Rika Kato
Ms. Akemi Saito

and all past members of Itami group for their enthusiasm and kind consideration.

I am grateful to the Japan Society for the Promotion of Science (JSPS) for the research fellowship for young scientists (DC1). I also thank to Integrative Graduate Education and

Research Program in Green Natural Sciences (IGER) for the financial support.

Finally, I would like to express my deep appreciation to my family, Mr. Teiichi Yagi, Mrs. Keiko Yagi, Ms. Nanae Yagi and Mr. Shogo Iwata for their constant assistance and encouragement.

Akiko Yagi (Iwata)

Department of Chemistry
Graduate School of Science
Nagoya University
2016

Contents

General Introduction

Motivation of this study

The synthesis of novel π-conjugated compounds has been a significant topic of research for many synthetic chemists, triggering numerous discoveries in chemistry and materials science (Figure 1). For example, pentacene, a planar fused aromatic hydrocarbon, has been used as a semiconductor material in organic field-effect transistors.[1] Owing to high levels of charge mobility derived from its small band gap, pentacene exhibits remarkable performance despite consisting only of sp^2-hybridized carbons and hydrogens. After the first synthesis of pentacene in 1961,[2] its synthetic methods have been continually improved. Various derivatives of pentacene have also been synthesized to make better materials in a range of applications. Fullerenes are also representative of π-conjugated compounds whose synthesis had a large influence on science.[3] Since their discovery in 1985,[4] fullerenes have been promising materials in applications that include radiation sources, field-emission displays and solar cells. In addition to industrial applications, fullerenes have also found use in the medical and pharmaceutical fields. While the efficient bulk production methods of fullerene have been developed, another important milestones include organic synthesis of C_{60} in 2002 that paved a way for rational synthesis of other fullerenes.[5] One of the important roles of synthetic chemists is to construct molecules that lead to such breakthroughs in science.

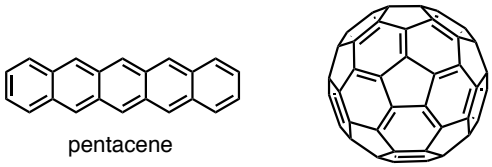

Figure 1. Examples of π-conjugated compounds whose synthesis changed the world.

Belt-shaped aromatic hydrocarbons such as cyclacenes and cyclophenacenes are π-conjugated compounds that have fascinated scientists for a long time (Figure 2).[6] Intrinsically planar aromatic rings are bent to construct such belt-shaped structures, producing unusual structural characteristics and high strain energies. Because of the rigid structure, their π-systems are immobilized perpendicularly to the inner and outer belt surfaces. These unprecedented

structural features have attracted much interest as novel aromatic compounds, leading to subsequent theoretical studies.[7] To date, several interesting properties such as small band gaps and structure–reactivity relationships have been predicted. Besides the interests from the past, various applications in supramolecular chemistry and materials science are expected owing to their three-dimensional molecular shapes with central cavities in recent years. The electronic properties of belt-shaped aromatic hydrocarbons predicted by theoretical studies are also promising for their applications as semiconductor materials, which are essential for the present technological developments. Furthermore, belt-shaped aromatic hydrocarbons have attracted much attention from nanocarbon science as the partial structures of carbon nanotubes, which are promising materials because of their mechanical, electronic, and optical properties.[8,9,10] Therefore, belt-shaped aromatic hydrocarbons have been desired strongly for a long time. In fact, their synthesis has been extensively examined since 1987.[11] Nevertheless, no belt-shaped aromatic hydrocarbon has been obtained yet. The author challenged the synthesis of a belt-shaped aromatic hydrocarbon. General introduction describes the historical background that led to the research in this thesis.

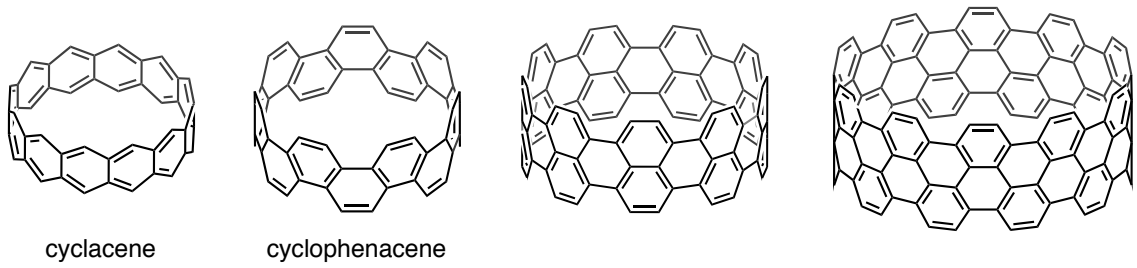

Figure 2. Representative belt-shaped aromatic hydrocarbons.

Synthetic studies on belt-shaped aromatic hydrocarbons

The synthesis of belt-shaped aromatic hydrocarbons has been studied since a long time ago. Cyclacenes were first proposed by Heilbonner in 1954.[12] Thereafter, the theoretical studies on cyclacenes have been conducted, and their high reactivity derived from a small singlet–triplet energy gap has been predicted.[13] The synthetic studies on cyclacenes were started by the Stoddart group in 1987 (Scheme 1a).[11, 14] Sequential Diels–Alder reactions between bisdienophile **1** and bisdiene **2** provided macrocycle **3**, which was subsequently deoxygenated, dehydrated, and reduced, affording octahydro[12]cyclacene **4**. Although the transformation of cyclacene **4** to [12]cyclacene was attempted several times, all these efforts were unsuccessful. In 1996, Cory and co-workers reported a synthetic study aimed at [8]cyclacene (Scheme 1b).[15] They also carried out the Diels–Alder reaction of bisdiene **5** and bisquinone **6** to construct a carbon skeleton of [8]cyclacene. Although macrocycle **7** was obtained, all the attempts for the subsequent transformation to [8]cyclacene were not successful. Even though the carbon skeletons of cyclacenes were constructed successfully, the isolation of them was failed, most likely, due to their low stability. In 1983, Vögtle described a belt-shaped aromatic hydrocarbon known as "Vögtle's belt" and embarked on its synthetic study in 1991 (Scheme 1c).[16] Although a precursor macrocycle **10** has been synthesized by the coupling of thiol **8** with alkyl halide **9**, the transformation of **10** to the belt has not been reported yet. Iyoda reported the synthetic study of [10]cyclophenacene in 2007 (Scheme 1d).[6] First, phenanthrene-containing benz[12]annulene **12** was synthesized by the reduction of compound **11**. Compound **12** can be converted to [10]cyclophenacene by oxidative cyclization, and they detected [10]cyclophenacene among the products of a photocyclization reaction of compound **12** by LD-TOF MS. These two results indicate that the construction of highly strained belt structures remained as a great challenge at that time. For the successful synthesis of belt-shaped aromatic hydrocarbons, new potential targets or more promising synthetic methodologies were required.

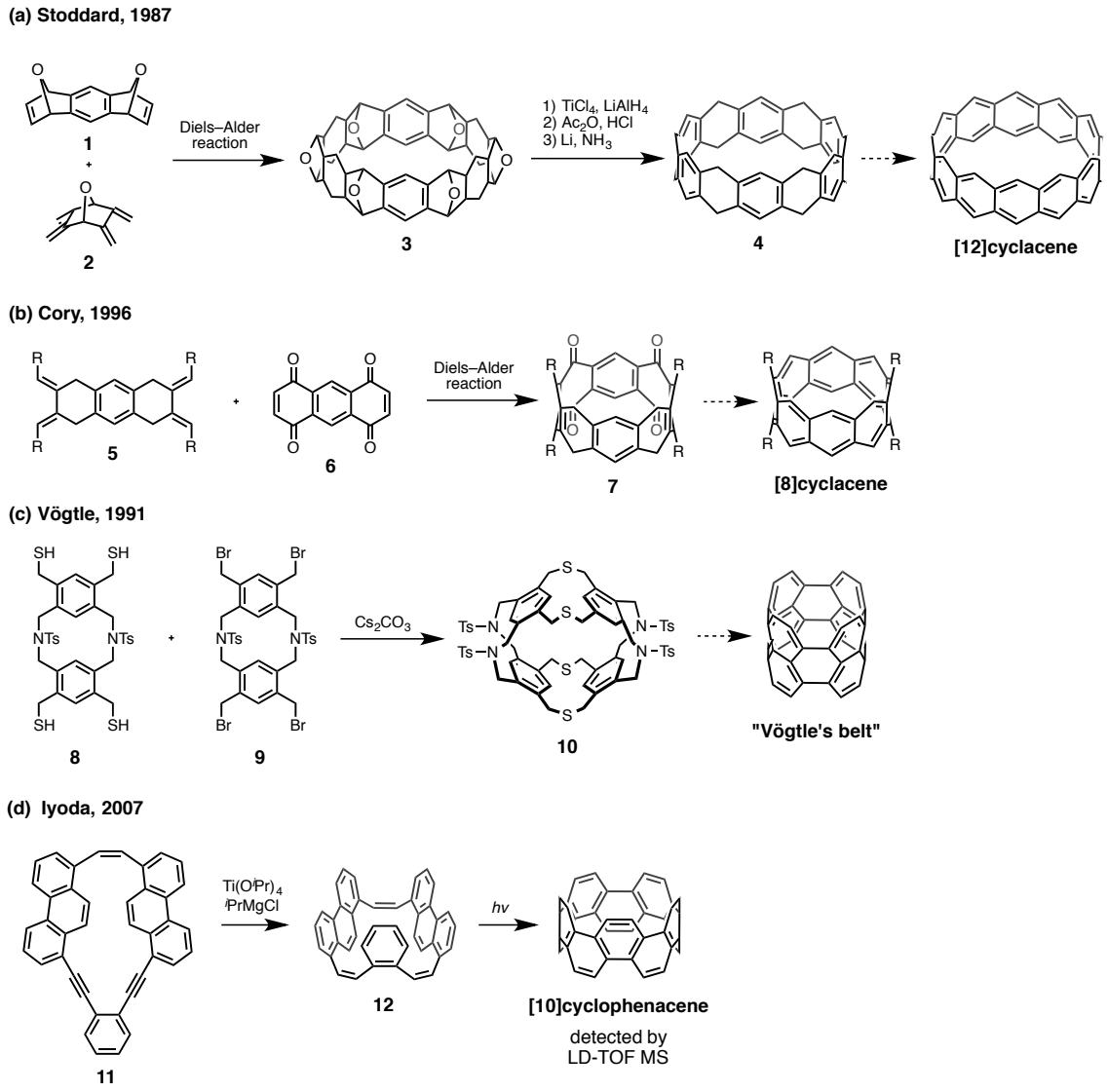

Scheme 1. Synthetic studies on belt-shaped aromatic hydrocarbons.

Synthesis of partial structures of armchair-type carbon nanotubes

On the other hand, since the first discovery of carbon nanotubes by Iijima in 1991,[8] molecules representing partial structures of carbon nanotubes have been the center of attention in synthetic chemistry. In 2003, Nakamura and co-workers reported the synthesis of compound **14** containing a π-conjugated system of [10]cyclophenacene (Scheme 2a).[17] The multimethylation of C_{60} with an organocopper reagent afforded compound **13**, which was converted to compound **14** through protection, multiphenylation, and deprotection. The synthesis of compound **14** enabled the first analysis of the cyclophenacene-like structure. In addition, the group of Gan very recently reported the synthesis of a compound containing

π-system of Vögtle's belt by multiamination of C_{70}.[18] In 2012, Scott and co-workers reported the synthesis of the compound **17**, which has the end-cap structure of carbon nanotubes (Scheme 2b).[19] Compound **15** was transformed to compound **16** by a five-fold Negishi coupling reaction with 2,6-dichlorophenylzinc chloride. Subsequently, a ten-fold C–C bond formation was achieved by flash vacuum pyrolysis (1100 °C, 0.25 Torr, gas phase), affording hemispherical end-cap **17**. Notably, the compounds known as "half Vögtle's belt" were also synthesized.[20] Teropyrenophane **20** was synthesized in 2009 by Bodwell and co-workers (Scheme 2c).[20a] They obtained macrocycle **19** *via* formylation followed by the intramolecular McMurry coupling of the formyl groups in compound **18**. An ensuing oxidation of macrocycle **19** with DDQ afforded a teropyrenophane **20** with a curved π-conjugated structure. These molecules have generated a huge interest in the synthesis of other partial structures of carbon nanotubes including belt-shaped aromatic hydrocarbons.

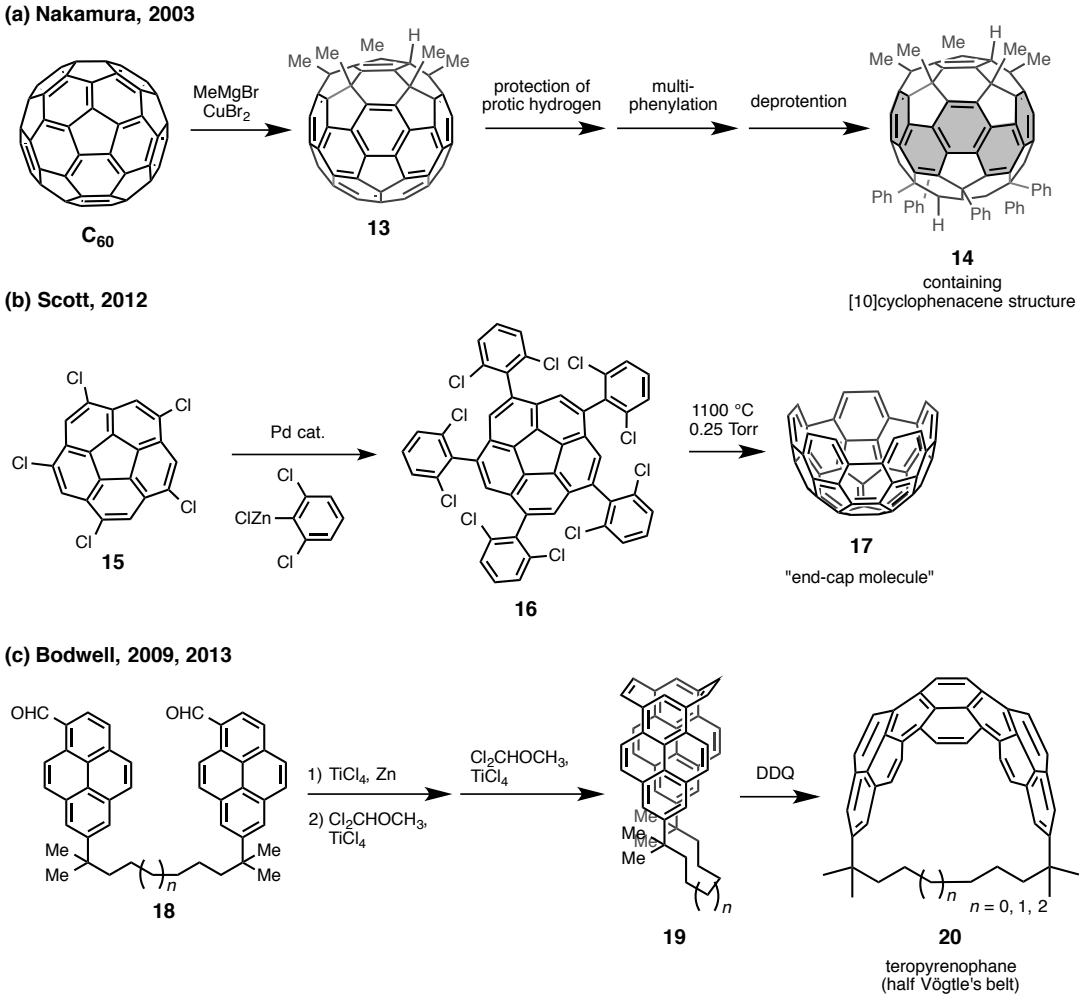

Scheme 2. (a) Nakamura's "extraction" of cyclophenacene structure from C_{60}. (b) Synthesis of an end-cap molecule by Scott. (c) Synthesis of teropyrenophane by Bodwell.

Meanwhile, another type of carbon nanotube segments has been recently synthesized. Cycloparaphenylene (CPP) is a ring-shaped aromatic hydrocarbon in which the benzene rings are connected circularly at their *para* positions (Figure 3). The synthetic studies on CPP began in the 1930s by chemists who were attracted to its beautiful structure.[21] However, the synthesis of CPP was not accomplished for almost 80 years. Inspired by the discovery of carbon nanotubes, CPP also received much attention as the shortest segment of armchair-type carbon nanotubes, and its synthetic study was embarked again. The biggest challenge in the synthesis of [*n*]CPPs was the formation of a macrocycle, which usually contains high levels of intrinsic ring strain as in the belt-shaped aromatic hydrocarbons. The Jasti/Bertozzi, Itami, and Yamago research groups addressed the problem with the synthesis of unstrained macrocyclic CPP precursors (Scheme 3). The group of Jasti and Bertozzi used L-shaped building blocks consisting of phenyl-substituted cyclohexadienes.[22] Because cyclohexadiene moieties can be converted with relative ease to benzene rings *via* reductive aromatization, these L-shaped units can be regarded as the terphenyl precursors. A coupling of these L-shaped units afforded the corresponding macrocycles where the cyclohexadiene moieties occupied the corners, thus generating unstrained CPP precursors. In the final step, these cyclohexadiene moieties were subjected to reductive aromatization, furnishing the corresponding CPPs. The group of Itami, on the other hand, used 1,4-diphenylcyclohexanes as the L-shaped terphenyl precursors.[23] The macrocycles obtained by the coupling of the L-shaped units were subsequently transformed into the corresponding CPP by oxidative aromatization. Yamago and co-workers used *cis*-platinum complexes as the unstrained CPP precursors.[24] First, macrocyclic platinum-bridged biphenyls were synthesized from $PtCl_2$(cod) **21** and 4,4′-bis(trimethylstannyl)biphenyl **22**. Then, the reductive elimination between the biphenyl ligands afforded the CPPs. Each method was further developed by the three research groups and applied to the synthesis of a series of CPPs. Today, [*n*]CPPs (*n* = 5–16, 18) have been synthesized.[25] Their properties have also been investigated exclusively.[26,27] Some CPPs became commercially available.[28] CPP synthesis has become a landmark in the synthesis of other ring-shaped aromatic compounds.

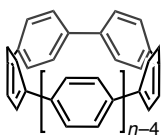

[*n*]cycloparaphenylene ([*n*]CPP, *n* = 5–16, 18)

Figure 3. Cycloparaphenylene.

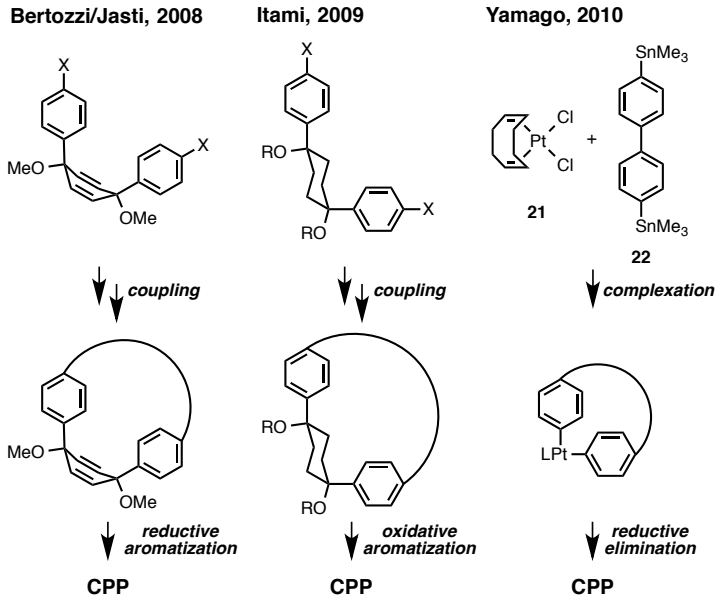

Scheme 3. Strategies for the synthesis of CPP.

Synthesis of carbon nanorings

The synthetic strategies for [*n*]CPP can also be applied to the synthesis of several types of strained ring-shaped compounds. When substituted benzene rings (e.g., tetraphenylbenzene[29]), polycyclic aromatic hydrocarbons (e.g., naphthalene[30], pyrene[31], and chrysene[32]), or heteroarenes (e.g., pyridine,[33] thiophene,[34] anthraquinone,[35] carbazole,[36] and perylene diimide[37]) are used in addition to benzene rings, CPP derivatives known as "carbon nanorings" are obtained. By using suitable synthetic methodologies developed for [*n*]CPPs by Jasti, Itami, and Yamago, diverse carbon nanorings have been synthesized (Figure 4).[38] Some of the carbon nanorings have been classified as molecules with partial structures of armchair-type carbon nanotubes. The successful synthesis of various carbon nanorings demonstrates that the design and synthesis of numerous novel ring-shaped compounds are feasible. Moreover, the structural, photophysical, and electrochemical properties of these carbon nanorings have been intensely investigated. Several features and applications specific to each carbon nanoring have been reported. These researches pioneered a new field in the chemistry of π-conjugated compounds.

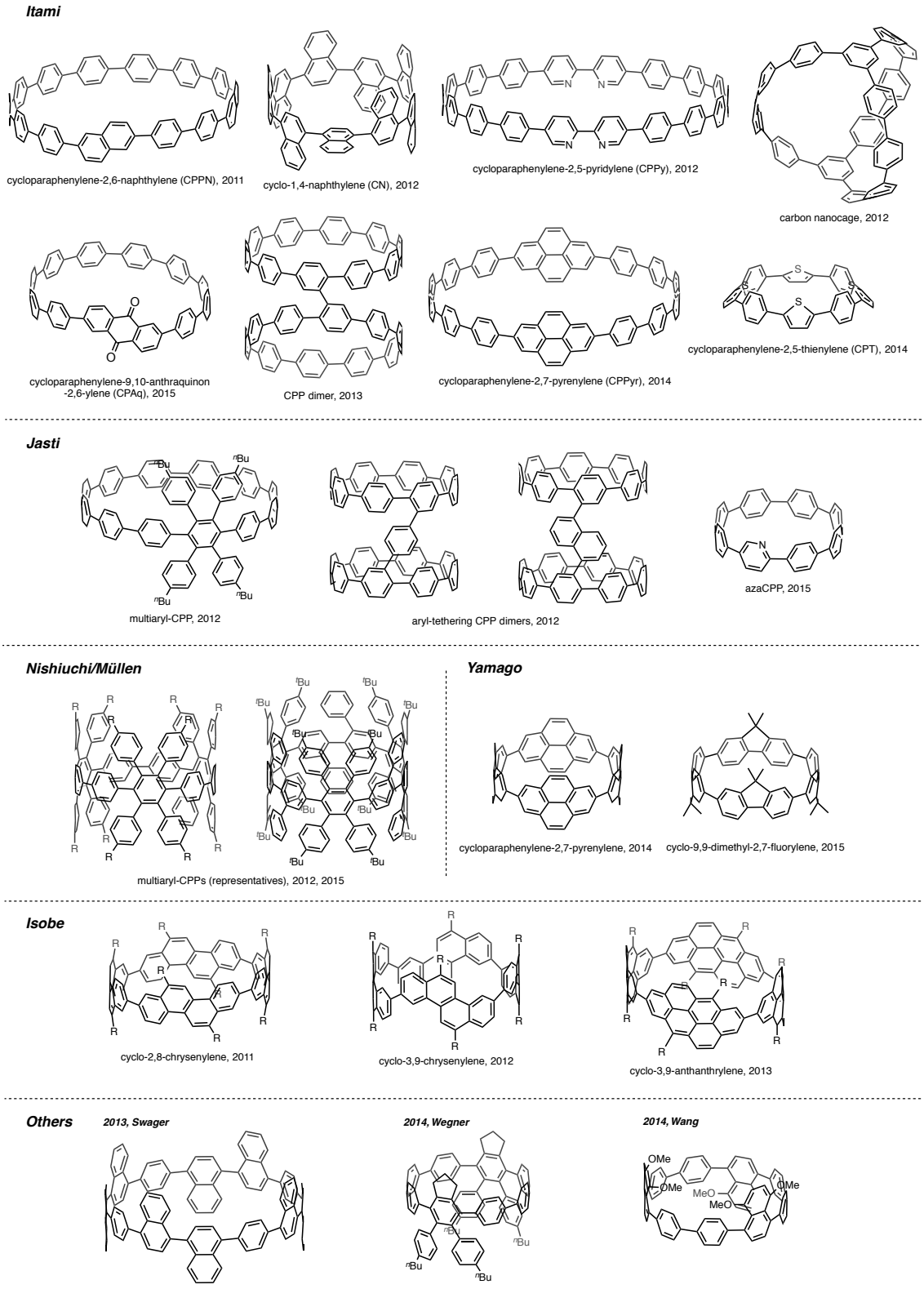

Figure 4. Representative carbon nanorings.

Working hypothesis: synthesis of a carbon nanobelt from carbon nanorings

By the generation of various types of carbon nanorings, clear definitions for "belt"-shaped aromatic hydrocarbons and "ring"-shaped aromatic hydrocarbons became required. In this thesis, they are defined as follows; upon cleavage of one carbon–carbon bond, ring-shaped aromatic hydrocarbons open to give a linear structure (Figure 5, left), while for belt-shaped aromatic hydrocarbons cleavage of at least two carbon–carbon bonds is necessary in order to open their cyclic structures (Figure 5, right). According to these definitions, CPPs and related carbon nanorings are classified into ring-shaped aromatic hydrocarbons, and cyclacenes, cyclophenacene, as well as Vögtle's belt can be called belt-shaped aromatic hydrocarbons.

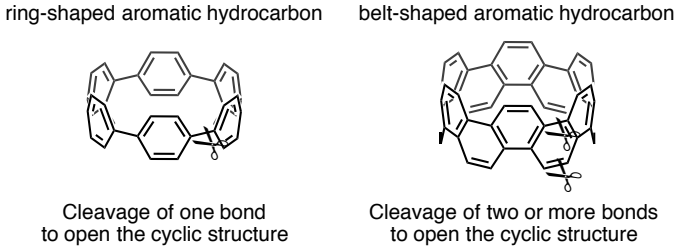

Figure 5. The definition of ring-shaped aromatic hydrocarbons and belt-shaped aromatic hydrocarbons used in this study.

Belt-shaped aromatic hydrocarbons have not been synthesized yet, whereas structurally close compounds have been obtained after long synthetic efforts. To synthesize belt-shaped aromatic hydrocarbons, new synthetic routes should be developed. The author envisioned that belt-shaped aromatic hydrocarbons can be synthesized from carbon nanorings that are specially designed for this purpose. Since the synthesis of carbon nanorings has been fully established as mentioned above, specific carbon nanorings can be designed and synthesized as the potential precursors for belt-shaped aromatic hydrocarbons. The stepwise extension of the π-conjugated system on the carbon nanorings would lead a belt-shaped aromatic hydrocarbon. For example, in a carbon nanoring having arene rings such as pyrene, the arene rings may act as the "foothold" moiety, enabling the extension of π-conjugated system on the carbon nanoring (Scheme 5a). A carbon nanoring consisting solely of π-extended arene rings such as naphthalene rings is also a potential precursor for a belt-shaped aromatic hydrocarbon (Scheme 5b). The coupling of neighboring arene rings would form the desired belt-shaped aromatic hydrocarbon. These transformations would require a slight increase in strain energies because of the intrinsic strain

in the carbon nanorings. Considering the recent progress in π-extension reactions as well, these synthetic strategies are promising novel routes for belt-shaped aromatic hydrocarbons. In this study, the author named the target compound *carbon nanobelt* considering the nickname of CPP derivatives as *carbon nanoring* (Scheme 5).

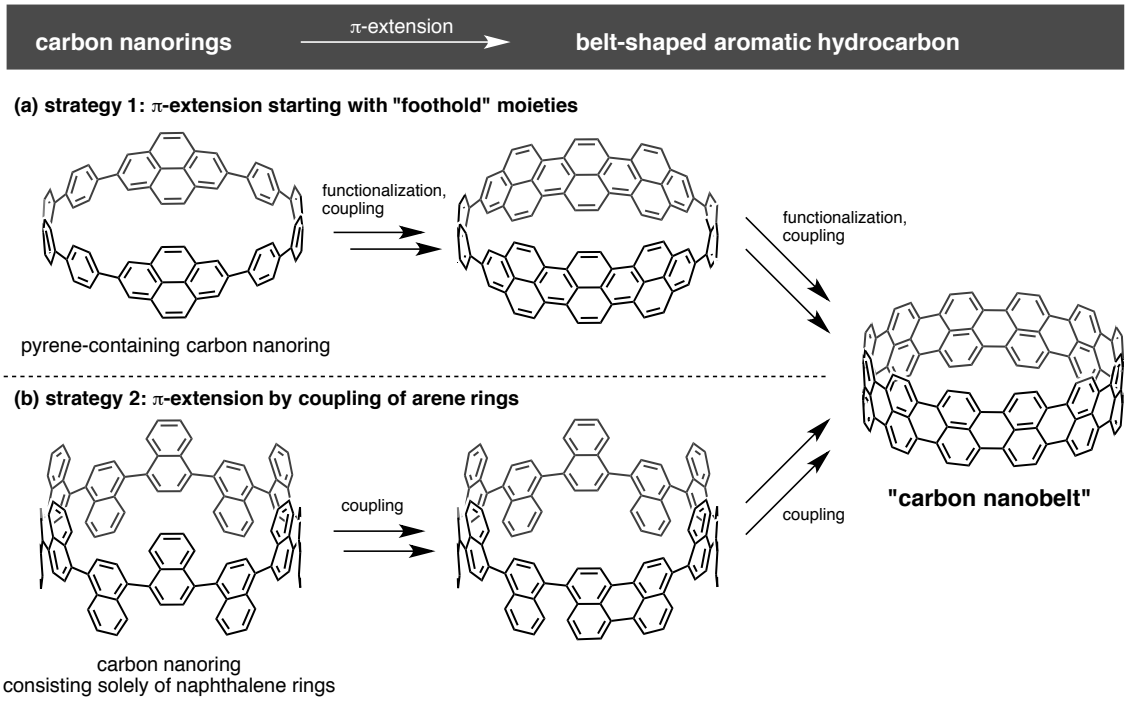

Scheme 5. Strategies for the synthesis of carbon nanobelt from carbon nanorings.

Overview of this thesis

In the PhD study, the author has focused on the synthesis of a carbon nanobelt using novel carbon nanorings. Based on the working hypothesis mentioned above, the carbon nanorings were designed and synthesized. The structural and electronic properties of the novel carbon nanorings, potential precursors for carbon nanobelts, were investigated to better understand their inherent characteristics. Finally, the transformation of the carbon nanorings to the carbon nanobelt was attempted.

Chapter 1 describes the first synthesis of a carbon nanoring bearing a “foothold” moiety for the construction of a belt structure (Figure 6). The author designed a pyrene-containing carbon nanoring, which can in principle be transformed to the carbon nanobelt by stepwise π-extension starting with the pyrene rings. By applying the methods developed for the synthesis of CPPs, cyclo[12]paraphenylene-[2]2,7-pyrenylene ([12,2]CPPyr) was synthesized. Moreover, the photophysical properties of [12,2]CPPyr were investigated to determine the characteristics of the carbon nanoring bearing two pyrene moieties.

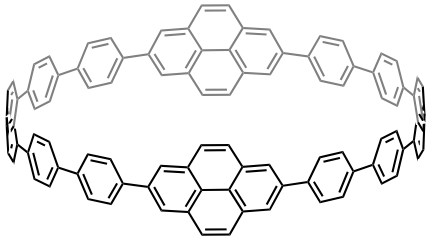

cyclo[12]paraphenylene-[2]2,7-pyrenylene
([12,2]CPPyr)

· the first carbon nanoring having a "foothold" for stepwise π-extension
· photophysical properties characteritic to pyrene-cotaining carbon nanoring

Figure 6. [12,2]CPPyr, a carbon nanobelt.

Chapter 2 describes the synthesis of another promising precursor for carbon nanobelt. [9]Cyclo-1,4-naphthylene ([9]CN), where nine naphthalene rings are connected together at their 1- and 4-positions, has been successfully synthesized (Figure 7). [9]CN is the first carbon nanoring consisting solely of π-extended arene rings. A careful analysis revealed the unique properties of [9]CN generated by connecting nine naphthalene rings circularly.

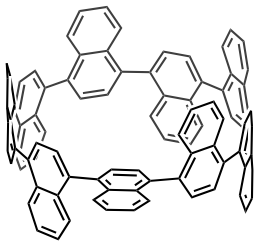

[9]cyclo-1,4-naphthylene
([9]CN)

· *the first carbon nanoring consisting solely of naphthalene rings*
· *unique properties generated by connecting nine naphthalene rings circulaly*

Figure 7. [9]CN, a precursor of carbon nanobelt.

The establishment of synthetic route to [9]CN led to the synthesis of other ring sizes of [*n*]CN (*n* = 8, 10, 12, 16) as described in Chapter 3 (Figure 8). This work is a significant step towards the synthesis of the carbon nanobelt, in terms of creating different sizes of precursors. The structural and photophysical properties of these CNs were investigated to determine their size dependence. Furthermore, the theoretical studies on [*n*]CN (*n* = 6–16) were performed to obtain extensive information about CNs as potential precursors for carbon nanobelts.

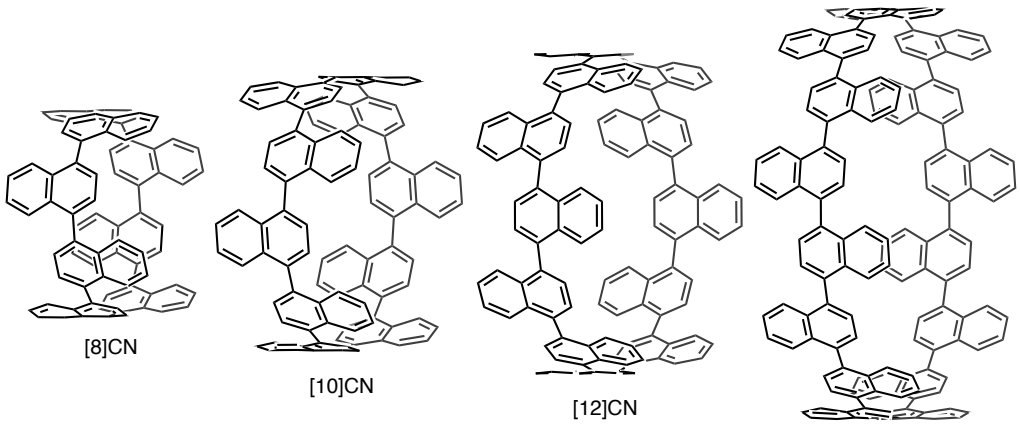

· *several sizes of precursors for carbon nanobelt*
· *size-dependency on structural, photophysical, and electrochemical properties*

Figure 8. Structures of [8]-, [10]-, [12]-, and [16]CN.

In Chapter 4, the synthesis of carbon nanobelt was challenged by employing CNs as precursors (Figure 9). The sequential cyclodehydrogenation reaction is expected to transform CNs to carbon nanobelts straightforwardly. The reaction conditions were investigated, and products expected as nanorings with highly fused π-systems were produced. Based on obtained results, the perspective was described towards the first synthesis of carbon nanobelt.

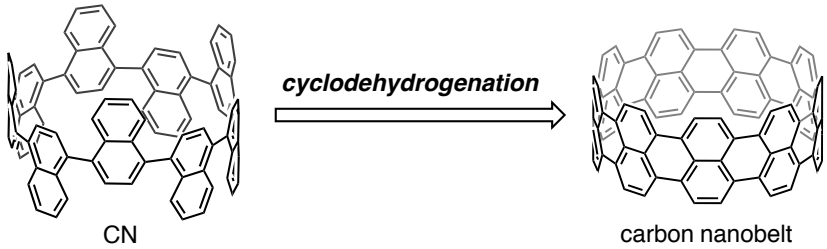

Figure 9. Cyclodehydrogenation of CNs towards carbon nanobelts.

References

1. Kelley, T. W.; Baude, P. F.; Gerlach, C.; Ender, D. E.; Muyres, D. W.; Haase, M. A.; Vogel, D. E.; Theiss, S. D. *Chem. Mater*. **2004**, *16*, 4413.
2. Bruckner, V.; Tomasz, J. *Acta. Chim. Hung*. **1961**, *28*, 405.
3. Hirsch, A.; Brettreich, M. Wiley-VCH, Weinheim, **2005**.
4. Kroto, H. W.; Heath, J. R.; O'Brien, S. C.; Curl, R. F.; Smalley, R. E. *Nature* **1985**, *318*, 162.
5. Scott, L. T.; Boorum, M. M.; McMahon, B. J.; Hagen, S.; Mack, J.; Blank, J.; Wegner, H.; de Meijere, A. *Science* **2002**, *295*, 1500.
6. Petrukhina, M. A.; Scott, L. T. Fragments of Fullerenes and Carbon Nanotube: Designed Synthesis, Unusual Reactions, and Coordination Chemistry Eds.; Wiley: Hoboken, 2012
7. (a) Sato, T.; Tanaka, M.; Yamabe, T. *Synth. Met.* **1999**, *103*, 2525. (b) Li, J.; Zhang, Y.; Zhang, M. *Chem. Phys. Lett.* **2002**, *364*, 338. (c) Matsuo, Y.; Tahara, K.; Nakamura, E. *Org. Lett.* **2003**, *5*, 3181. (d) Yumura, T.; Bandow, S.; Yoshizawa, K.; Iijima, S. *J. Phys. Chem. B* **2004**, *108*, 11426. (e) Galano, A. *Chem. Phys.* **2006**, *327*, 159. (f) Yumura, T.; Nozaki, D.; Hirahara, K.; Bandow, S.; Iijima, S.; Yoshizawa, K. *Annu. Rep. Prog. Chem., Sect. C: Phys. Chem.* **2006**, *102*, 71. (g) Baldoni, M.; Sgamellotti, A.; Mercuri, F. *Org. Lett.* **2007**, *9*, 4267. (h) Liu, L. V.; Tian, W. Q.; Chen, Y. K.; Zhanga, Y. A.; Wang, Y. A. *Nanoscale* **2010**, *2*, 254. (i) Fort, E. H.; Scott, L. T. *J. Mater. Chem.* **2011**, *21*, 1373. (j) Martín-Martínez, F. J.; Melchor, S.; Dobado, J. A. *Phys. Chem. Chem. Phys.* **2011**, *13*, 12844.
8. Iijima, S. *Nature* **1991**, *354*, 56.
9. Dresselhaus, M.; Dresselhaus, G.; Avouris, P. Carbon Nanotubes: Synthesis, Properties, Applications, Springer, 2001.
10. (a) Avouris, P.; Chen, Z.; Perebeinos, V. *Nat. Nanotech.* **2007**, *2*, 605. (b) Avouris, P.; Freitag, M.; Perebeinos, V. *Nat. Photon.* **2008**, *2*, 341. (c) Sgobba, V.; Guldi, D. M. *Chem. Soc. Rev.* **2009**, *38*, 165.
11. Kohnke, F. H.; Slawin A. M. Z.; Stoddart, J. F.; Williams, D. J. *Angew. Chem.* **1987**, *99*, 941.
12. Heilbronner, E. *Helv. Chim. Acta* **1954**, *268*, 845.
13. (a) Choi, H. S.; Kim, K. S. *Angew. Chem., Int. Ed.* **1999**, *38*, 2256. (b) Chen, Z.; Jiang, D.; Lu, X.; Bettinger, H. F.; Dai, S.; Schleyer, P. V. R.; Houk, K. N. *Org. Lett.* **2007**, *9*, 5449.

14. (a) Ashton, P. R.; Isaacs, N. S.; Kohnke, F. H.; Slawin, A. M. Z.; Spencer, C. M.; Stoddart, J. F.; Williams, D. J. *Angew. Chem., Int. Ed. Engl.* **1988***, 27*, 966. (b) Kohnke, F. H.; Stoddart, J. F. *Pure Appl. Chem.* **1989***, 61*, 1581. (c) Kohnke, F. H.; Mathias, J. P.; Stoddart, J. F. *Angew. Chem., Int. Ed. Engl.* **1989**, *28*, 1103. (d) Girreser, U.; Giuffrida, D.; Kohnke, F. H.; Mathias, J. P.; Philp, D.; Stoddart, J. F. *Pure Appl. Chem.* **1993***, 65*, 119.
15. (a) Cory, R. M.; McPhail, C. L.; Dikmans, A. J.; Vittal, J. J. *Tetrahedron Lett.* **1996***, 37*, 1983. (b) Cory, R. M.; McPhail, C. L. *Tetrahedron Lett.* **1996***, 37*, 1987.
16. (a) Vögtle, F. *Top. Curr. Chem.* **1983**, *115*, 157. (b) Vögtle, F.; Schröder, A.; Karbach, D. *Angew. Chem., Int. Ed. Engl.* **1991***, 30*, 575.
17. Nakamura, E.; Tahara, K.; Matsuo, Y.; Sawamura, M. *J. Am. Chem. Soc.* **2003***, 125*, 2834.
18. Li, Y.; Xu, D.; Gan, L. *Angew. Chem., Int. Ed.* **2016**, *early view.*
19. Scott, L. T.; Jackson, E. A.; Zhang, Q.; Steinberg, B. D.; Bancu, M.; Li, B. *J. Am. Chem. Soc.* **2012***, 134*, 107.
20. (a) Merner, B. L.; Dawe, L. N.; Bodwell, G. J. *Angew. Chem., Int. Ed.* **2009***, 48*, 5487. (b) Merner, B. L.; Unikela, K. S.; Dawe, L. N.; Thompson, D. W.; Bodwell, G. J. *Chem. Commun.* **2013***, 49*, 5930.
21. (a) Perkh, V. C.; Guha, P. C. *J. Indian Chem. Soc.* **1934**, *11*, 95. (b) Friederich, R.; Nieger, M.; Vögtle, F. *Chem. Ber.* **1993**, *126*, 1723.
22. Jasti, R.; Bhattacharjee, J.; Neaton, J. B.; Bertozzi, C. R. *J. Am. Chem. Soc.* **2008**, *130*, 17646.
23. Takaba, H.; Omachi, H.; Yamamoto, Y.; Bouffard, J.; Itami, K. *Angew. Chem., Int. Ed.* **2009**, *48*, 6112.
24. Yamago, S.; Watanabe, Y.; Iwamoto, T. *Angew. Chem., Int. Ed.* **2010**, *49*, 757.
25. Reviews for synthesis of CPPs: (a) Omachi, H.; Segawa, Y.; Itami, K. *Acc. Chem. Res.* **2012**, *45*. 1378. (b) Sisto, T. J.; Jasti, R. *Synlett* **2012**, *23*, 483. (c) Yamago, S.; Kayahara, E.; Iwamoto, T. *Chem. Rec.* **2014**, *14*, 84. (d) Lewis, S. E. *Chem. Soc. Rev.* **2015**, *44*, 2221. (e) Darzi, E. R.; Jasti, R. *Chem. Soc. Rev.* **2015**, *44*, 6401. (f) Evans, P.; Jasti, R. in *Polyarenes I, Vol. 349* (Eds.: J. S. Siegel, Y.-T. Wu), Springer Berlin Heidelberg, **2014**, pp. 249.
26. Properties of CPPs: (a) Segawa, Y.; Omachi, H.; Itami, K. *Org. Lett.* **2010**, *12*, 2262. (b) Segawa, Y.; Fukazawa, A.; Matsuura, S.; Omachi, H.; Yamaguchi, S.; Irle, S.; Itami, K. *Org. Biomol. Chem.* **2012**, *10*, 5979. (c) Nishihara, T.; Segawa, Y.; Itami, K.; Kanemitsu,

Y. *J. Phys. Chem. Lett.* **2012**, *3*, 3125. (d) Fujitsuka, M.; Cho, D. W.; Iwamoto, T.; Yamago, S.; Majima, T. *Phys. Chem. Chem. Phys.* **2012**, *14*, 14585. (e) Camacho, C.; Niehaus, T. A.; Itami, K.; Irle, S. *Chem. Sci.* **2013**, *4*, 187. (f) Kayahara, E.; Kouyama, T.; Kato, T.; Takaya, H.; Yasuda, N.; Yamago, S. *Angew. Chem., Int. Ed.* **2013**, *52*, 13722. (g) Nishihara, T.; Segawa, Y.; Itami, K.; Kanemitsu, Y. *Chem. Sci.* **2014**, *5*, 2293. (h) Fujitsuka, M.; Lu, C.; Iwamoto, T.; Kayahara, E.; Yamago, S.; Majima, T. *J. Phys. Chem. A* **2014**, *118*, 4527. (i) Adamska, L.; Nayyar, I.; Chen, H.; Swan, A. K.; Oldani, N.; Fernandez-Alberti, S.; Golder, M. R.; Jasti, R.; Doorn, S. K.; Tretiak, S. *Nano Lett.* **2014**, *14*, 6539. (j) Fujitsuka, M.; Tojo, S.; Iwamoto, T.; Kayahara, E.; Yamago, S.; Majima, T. *J. Phys. Chem. Lett.* **2014**, *5*, 2302.

27. CPP complexes with guest molecules: (a) Iwamoto, T.; Watanabe, Y.; Sadahiro, T.; Haino, T.; Yamago, S. *Angew. Chem., Int. Ed.* **2011**, *50*, 8342. (b) Iwamoto, T.; Watanabe, Y.; Takaya, H.; Haino, T.; Yasuda, N.; Yamago, S. *Chem. Eur. J.* **2013***, 19*, 14061. (c) Nakanishi, Y.; Omachi, H.; Matsuura, S.; Miyata, Y.; Kitaura, R.; Segawa, Y.; Itami, K.; Shinohara, H. *Angew. Chem., Int. Ed.* **2014***, 53*, 3102. (d) Isobe, H.; Hitosugi, S.; Yamasaki, T.; Iizuka, R. *Chem. Sci.* **2013***, 4*, 1293. (e) Hitosugi, S.; Iizuka, R.; Yamasaki, T.; Zhang, R.; Murata, Y.; Isobe, H. *Org. Lett.* **2013***, 15*, 3199. (f) Sato, S.; Yamasaki, T.; Isobe, H. *Proc. Natl. Acad. Sci. U.S.A.* **2014***, 111*, 8374. (g) Alvarez, M. P.; Burrezo, P. M.; Kertesz, M.; Iwamoto, T.; Yamago, S.; Xia, J.; Jasti, R. Navarrete, J. T. L.; Taravillo, M.; Baonza, V. G.; Casado, J. *Angew. Chem., Int. Ed.* **2014***, 53*, 7033. (h) Iwamoto, T.; Slanina, Z.; Mizorogi, N.; Guo, J.; Akasaka, T.; Nagase, S.; Takaya, H.; Yasuda, N.; Kato, T.; Yamago, S. *Chem. Eur. J.* **2014***, 20*, 14403. (i) Alvarez, M. P.; Burrezob, P. M.; Iwamoto, T.; Taravilloa, M.; Baonzaa, V. G.; Navarreteb, J. T. L.; Yamago, S.; Casado, J. *Faraday Discuss.* **2014**, *173*, 157. (j) Matsuno, T.; Sato, S.; Iizukab, R.; Isobe, H. *Chem. Sci.* **2015***, 6*, 909. (k) Ueno, H.; Nishihara, T.; Segawa, Y.; Itami, K. *Angew. Chem., Int. Ed.* **2015**, *54*, 3707.

28. Tokyo Chemical Industry Co., Ltd. (TCI), catalog no. C2449 ([12]CPP); Kanto Chemical Co., Inc., catalog No. 08131-35 ([9]CPP), 08132-35 ([12]CPP), and 08137-65 ([15]CPP).

29. (a) Sisto, T. J.; Tian, X.; Jasti, R. *J. Org. Chem.* **2012***, 77*, 5857. (b) Nishiuchi, T.; Feng, X.; Enkelmann, V.; Wagner, M.; Müllen, K. *Chem. Eur. J.* **2012***, 18*, 16621. (c) Golling, F. E.; Quernheim, M.; Wagner, M.; Nishiuchi, T.; Müllen, K. *Angew. Chem., Int. Ed.* **2014**, *53*, 1525. (d) Quernheim, M.; Golling, F. E.; Zhang, W.; Wagner, M.; Räder, H.-J.;

Nishiuchi, T.; Müllen, K. *Angew. Chem., Int. Ed.* **2015**, *54*, 10341.

30. Yagi, A.; Segawa, Y.; Itami, K. *J. Am. Chem. Soc.* **2012***, 134*, 2962.
31. Iwamoto, T.; Watanabe, Y.; Sakamoto, Y.; Suzuki, T.; Yamago, S. *Angew. Chem., Int. Ed.* **2014***, 53*, 6430.
32. (a) Hitosugi, S.; Nakanishi, W.; Yamasaki, T.; Isobe, H. *Nat. Commun.* **2011***, 2*, 492. (b) Hitosugi, S.; Yamasaki, T.; Isobe, H. *J. Am. Chem. Soc.* **2012***, 134*, 12442.
33. (a) Matsui, K.; Segawa, Y.; Itami, K. *Org. Lett.* **2012***, 14*, 1888. (b) Darzi, E. R.; Hirst, E. S.; Weber, C. D.; Zakharov, L. N.; Lonergan, M. C.; Jasti, R. *ACS Cent. Sci.* **2015**, *1*, 335.
34. (a) Ito, H.; Mitamura, Y.; Segawa, Y.; Itami, K. *Angew. Chem., Int. Ed.* **2015**, *54*, 159. (b) Thakellapalli, H.; Farajidizaji, B.; Butcher, T. W.; Akhmedov, N. G.; Popp, B. V.; Petersen, J. L.; Wang, K. K. *Org. Lett.* **2015**, *17*, 3470.
35. Kuwabara, T.; Orii, J.; Segawa, Y.; Itami, K. *Angew. Chem., Int. Ed.* **2015**, *54*, 9646.
36. Myśliwiec, D.; Kondratowicz, M.; Lis, T.; Chmielewski, P. J.; Stępień, M. *J. Am. Chem. Soc.* **2015**, *137*, 1643.
37. Ball, M.; Fowler, B.; Li, P.; Joyce, L. A.; Li, F.; Liu, T.; Paley, D.; Zhong, Y.; Li, H.; Xiao, S.; Ng, F.; Steigerwald, M. L.; Nuckolls, C. *J. Am. Chem. Soc.* **2015**, *137*, 9982.
38. The carbon nanorings in Figure 4: (a) Omachi, H.; Segawa, Y. ; Itami, K. *Org. Lett.* **2011**, *13*, 2480. (b) Matsui, K.; Segawa, Y.; Namikawa, T.; Kamada, K.; Itami, K. *Chem. Sci.* **2013**, *4*, 84. (c) Matsui, K.; Segawa, Y.; Itami, K. *J. Am. Chem. Soc.* **2014**, *136*, 16452. (d) Ishii, Y.; Nakanishi, Y.; Omachi, H.; Matsuura, S.; Matsui, K.; Shinohara, H.; Segawa, Y.; Itami, K. *Chem. Sci.* **2012**, *3*, 2340. (e) Yagi, A.; Venkataramana, G.: Segawa, Y.; Itami, K. *Chem. Commun.* **2013**, *50*, 957. (f) Kayahara, E; Qu, R.; Kojima, M.; Iwamoto, T.; Suzuki, T.; Yamago, S. *Chem. Eur. J.* **2015**, *21*, 18939. (g) Matsuo, T.; Kamata, S.; Hitosugi, S.; Isobe, H. *Chem. Sci.* **2013**, *4*, 3179. (h) Batson J. M.; Swager, T. M. *Synlett*, **2013**, *24*, 2545. (i) Tran-Van, A.-F.; Huxol, E.; Basler, J. M.; Neuburger, M.; Adjizian, J.-J.; Ewels, C. P.; Wegner, H. A. *Org. Lett.* **2014***, 16*, 1594. (j) Huang, C.; Huang, Y.; Akhmedov, N. G.; Popp, B. V.; Peterson J. L.; Wang, K. K. *Org. Lett.,* **2014**, *16*, 2672.

Chapter 1

Synthesis and Properties of Cycloparaphenylene-2,7-pyrenylene

Abstract: The synthesis of cyclo[12]paraphenylene[2]-2,7-pyrenylene ([12,2]CPPyr), a possible precursor for carbon nanobelt, is described. Through stepwise construction of a macrocycle using palladium- and nickel catalysts followed by aromatization of cyclohexane units, [12,2]CPPyr was synthesized in five steps from commercially available compounds. The UV-vis absorption and fluorescence spectra as well as TD-DFT calculations clarified the unique photophysical and electronic properties of [12,2]CPPyr.

1. Introduction

One possible route toward carbon nanobelt is stepwise construction of the π-extended structure on carbon nanorings. In so doing, a "foothold" moiety is demanded on the carbon nanorings, and we selected pyrene as a possible "foothold" moiety. Pyrene core is known to undergo various electrophilic aromatic substitution reactions at its 1-, 3-, 6-, and 8-positions.[1] Therefore, in a carbon nanoring consisting of pyrene rings and benzene rings, site-selective functionalization on pyrene rings is possible (Figure 1). Introduction of some functional groups to pyrene rings and following annulation with neighboring benzene rings can construct π-extended units on the carbon nanoring.[2] It is expected that sequential π-extension starting with the "foothold" pyrene on the carbon nanoring would finally lead to the carbon nanobelt.

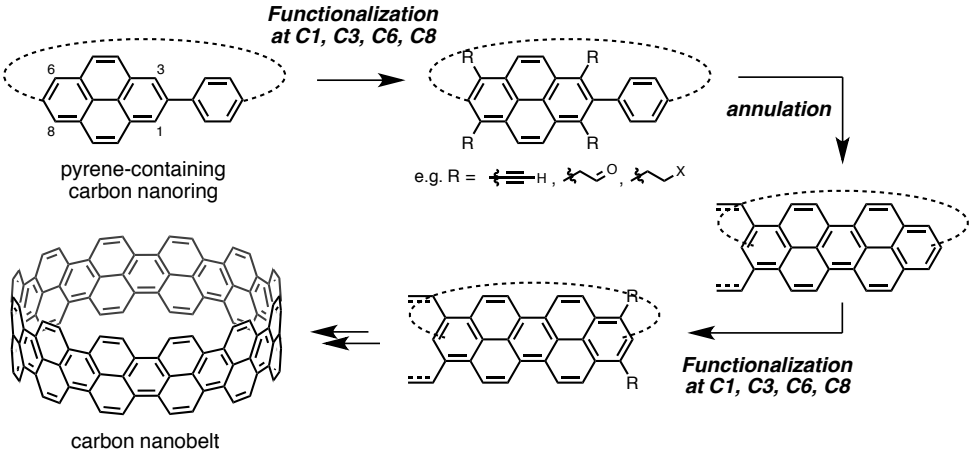

Figure 1. Synthesis of carbon nanobelt from a pyrene-containing carbon nanoring.

As a pyrene-containing carbon nanoring, cycloparaphenylene-2,7-pyrenylene (CPPyr) was designed in this work (Figure 2).[3] For the synthesis of CPPyr, our general and modular synthetic strategy using a benzene-convertible L-shaped cyclohexane unit can be applied.[4] In our previous syntheses of CPP derivatives, coupling of the L-shaped units with 1,4-diborylbenzene, 4,4'-diborylbiphenyl,[5] 2,6-diborylnaphthalene,[6] and 5,5'-dibromo-2,2'-bipyridyl[7] furnished macrocyclic intermediates for CPPs and their derivatives such as cycloparaphenylene-2,6-naphthylene (CPPN) and cycloparaphenylene-2,5-pyridylene (CPPy). CPPyr can be synthesized by a stepwise coupling of the L-shaped units and 2,7-diborylpyrene followed by aromatization of cyclohexane moieties.

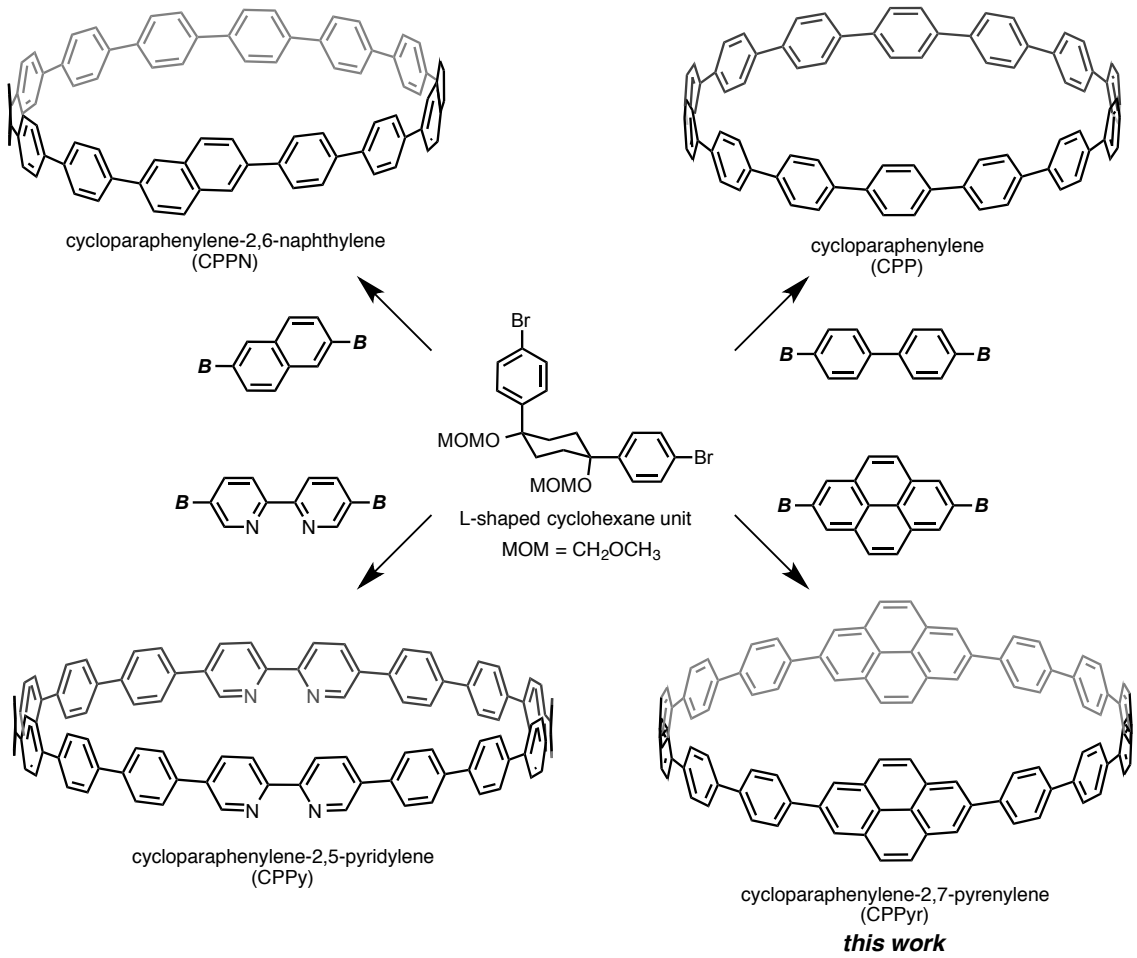

Figure 2. Strategy for the synthesis of CPPyr.

In this chapter, the synthesis of cyclo[12]paraphenyrene[2]-2,7-pyrenylene ([12,2]CPPyr), which consists of twelve benzene rings and two pyrene rings, is described. The photophysical properties of [12,2]CPPyr are also discussed.

2. Results and discussion

2-1. Synthesis of [12,2]CPPyr

The synthesis of a [12,2]CPPyr (**5**) is shown in Scheme 1. The L-shaped unit **1** and 2,7-diborylpyrene **2** were prepared from commercially available reagents according to reported methods.[8,9] The Suzuki–Miyaura cross-coupling of **2** with an excess amount of **1** produced a pyrene-containing U-shaped unit **3** in 69% yield. The homocoupling of **3** promoted by $Ni(cod)_2$/2,2'-bipyridyl gave the corresponding box-shaped macrocycle **4** in 17% yield. In order to inhibit oligomerization of **3**, the reaction was performed under quite dilute conditions (1 mM). Finally, **4** was subjected to aromatization with $NaHSO_4$ in 1,2,4-trichlorobenzene at 150 °C and [12,2]CPPyr **5** was obtained in 18% yield as a pale yellow solid. The high-temperature reaction in 1,2,4-trichlorobenzene was needed to accomplish the aromatization step. [12,2]CPPyr **5** was soluble to chlorinated solvents such as dichloromethane and chloroform, whereas it had poor solubility in other solvents such as ethyl acetate, methanol, and hexane. In the ^{1}H NMR spectrum of **5**, two singlet signals that would be expected for a 2,7-disubstituted pyrene were observed: δ = 8.06 and 8.37 ppm in $CDCl_3$. A broadened singlet signal belonging on the paraphenylene moieties was observed in similar chemical shift (7.68 ppm) to that of [16]CPP (7.69 ppm).[5a]

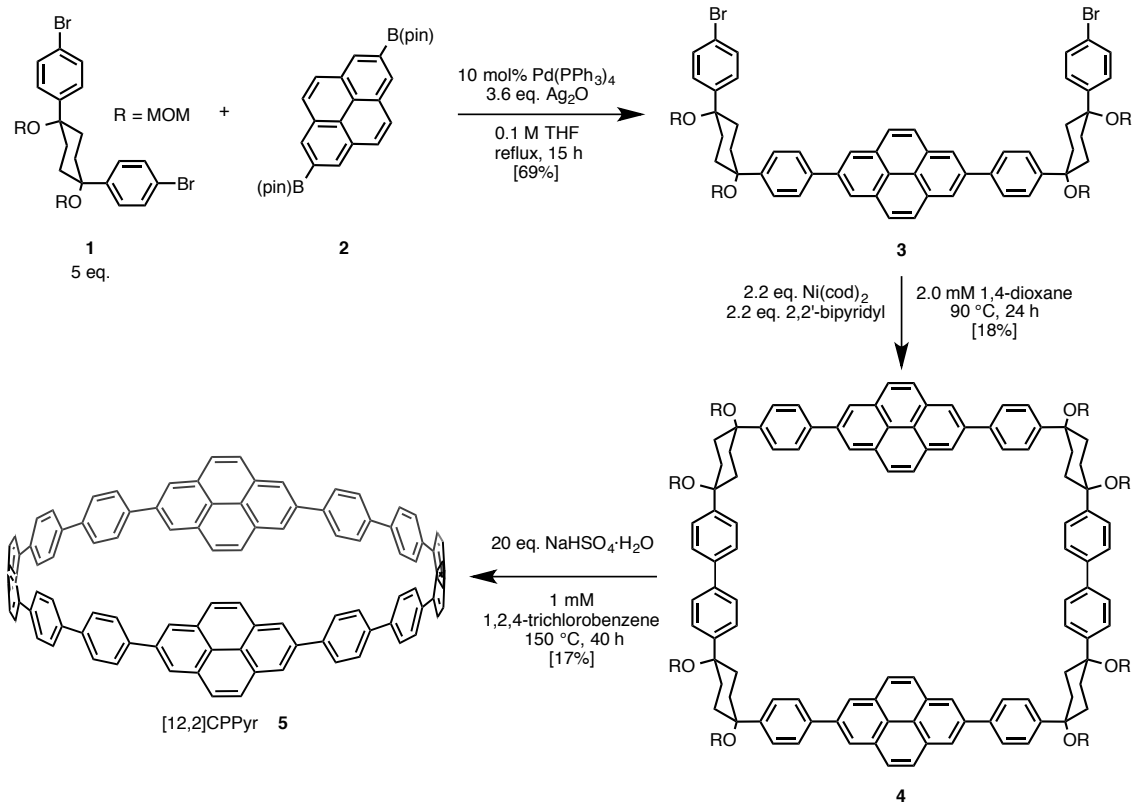

Scheme 1. Synthesis of [12,2]CPPyr **5**.

2-2. Strain energy of [12,2]CPPyr

To estimate the strain energy of [12,2]CPPyr **5**, the DFT calculation was performed at B3LYP/6-31G(d) level (Figure 3). By the hypothetical homodesmotic reactions, where [12]terphenyl and [2]2,7-diphenylpyrene are produced from [12,2]CPPyr and [14]binaphthyl, the strain energy strain energy of **5** was estimated (Scheme 2).[10] The values for heat of formation (Δ*H*) were applied to the reaction formula to obtain the strain energy. It was found that the strain energy of **5** (37.9 kcal·mol^{-1}) is close to that of [16]CPP, which is the same ring size as **5**.

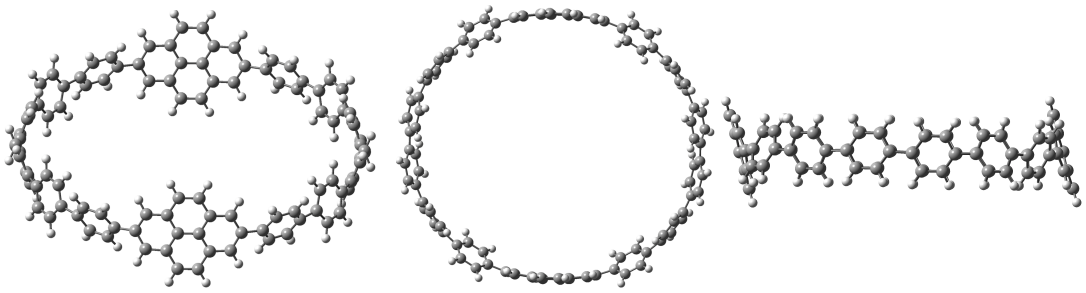

Figure 3. Optimized structure of [12,2]CPPyr **5** (optimized at the B3LYP/6-31G(d) level).

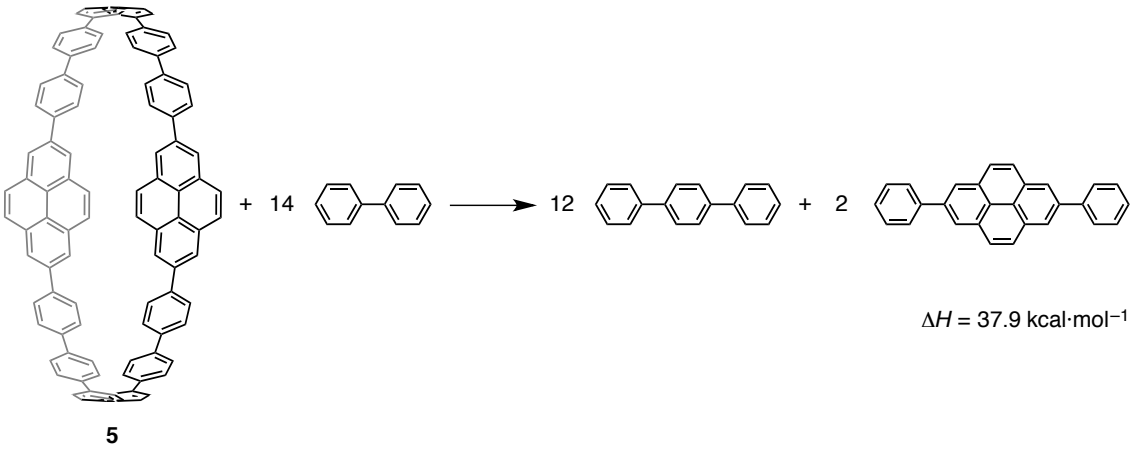

Scheme 2. Homodesmotic reactions for estimating the strain energies (Δ*H*) of **5**.

2-3 Photophysical properties of [12,2]CPPyr

The UV-vis absorption and fluorescence of a [12,2]CPPyr **5** were investigated to elucidate the effect of pyrene on electronic properties of [12,2]CPPyr structure. Spectra of **5** taken as a dichloromethane solution are shown in Figure 4. Absorption peaks were observed at 328 nm and 343 nm with a shoulder on the long-wavelength side. The most intense absorption maximum (λ_{abs}) was observed at 343 nm and the molecular absorption coefficient (ε) was 6.1×10^5 $cm^{-1}M^{-1}$. Similar to [12]–[18]CPPs, **5** showed intense blue photoluminescence.[11,12] Emission maxima (λ_{em}) was observed at 430 nm under excitation at 343 nm. Excimer emission was not observed even at the concentration of 10^{-3} M. The absolute fluorescence quantum yield (Φ_F) of **5** determined by a calibrated integrating sphere system was 0.21±0.03. This value is lower than those of CPPs ([9]–[16]CPP, Φ_F = 0.73–0.90).[12] On the other hand, the fluorescence life time of **5** was long (τ_s = 25.6 ns) in comparison with those of CPPs ([9]CPP and [12]CPP, τ_s = 10.6, 2.2 ns, respectively). Taking the long fluorescence lifetime of pyrenes[13] into consideration, inserted pyrenes would contribute to the long fluorescence life time of **5**. The radiative and nonradiative decay rate constants ($k_r = 8.4 \times 10^6$ s^{-1}, $k_{nr} = 3.1 \times 10^7$ s^{-1}) were determined from the observed quantum yield and fluorescence lifetime as well as the following equations: $\Phi_F = k_r \times \tau_s$ and $k_r + k_{nr} = \tau_s^{-1}$. The k_r values are one- or two orders of magnitude lower than those of CPPs ($k_r = 6.9 \times 10^7$ s^{-1} and $k_r = 4.0 \times 10^8$ s^{-1} for [9]CPP and [12]CPP, respectively), whereas the k_{nr} values are comparable to each other (~10^7 s^{-1}). The spectra of pyrene and [16]CPP are also shown in Figure 4. The UV-vis spectrum of **5** seems to be a combination of two independent spectra of pyrene and [16]CPP. The fluorescence spectrum of **5** is red-shifted from those of pyrene and [16]CPP.

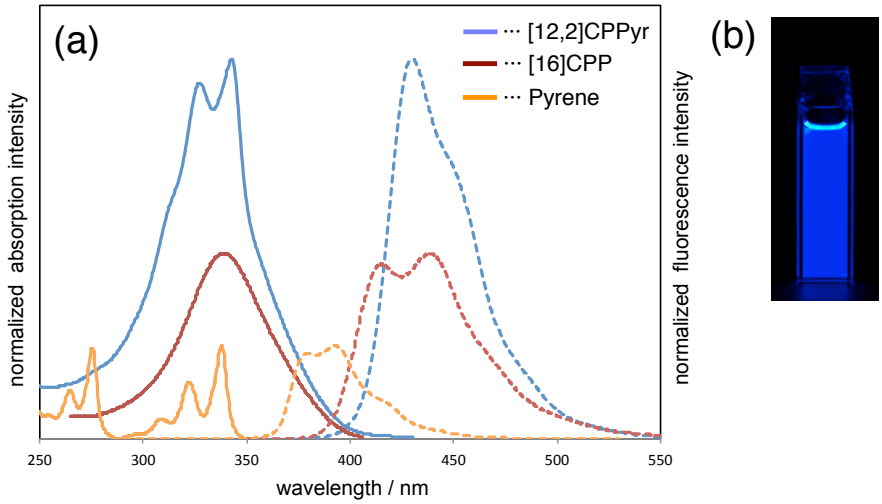

Figure 4. (a) UV-vis absorption (solid lines) and fluorescence spectra (broken lines) of dichloromethane solution of **5** (blue line), chloroform solution of [16]CPP (red line) and chloroform solution of pyrene (orange line). (b) Fluorescence of **5**.

To understand the electronic nature of a [12,2]CPPyr **5**, TD-DFT (time-dependent density functional theory) study was performed at the B3LYP/6-31G(d) level. Shown in Figure 5 are the energy diagrams and pictorial representations of six frontier molecular orbitals (MOs) of **5**. The orbitals of HOMO–1 and HOMO–2 as well as those of LUMO+1 and LUMO+2 are degenerate. In comparison with [16]CPP, the shapes and energy levels of HOMO and LUMO of **5** are very similar to those of [16]CPP: –5.32 eV (HOMO), –1.61 eV (LUMO). However, HOMO–1, HOMO–2, LUMO+1 and LUMO+2 of **5** are localized on two pyrene moieties. Additionally, the shapes of these MOs of **5** are consistent with the HOMO and LUMO of pyrene and 2,7-diphenylpyrene.[14] The fact that frontier MOs of pyrene still remain even in **5** is the main reason why the shape of absorption spectrum of **5** shows additivity in the spectra of pyrene and [16]CPP. In contrast, frontier MOs of pyrene are no longer HOMO and LUMO of **5** so that the emission wavelength are mostly dependent on the cyclic paraphenylene substructure.

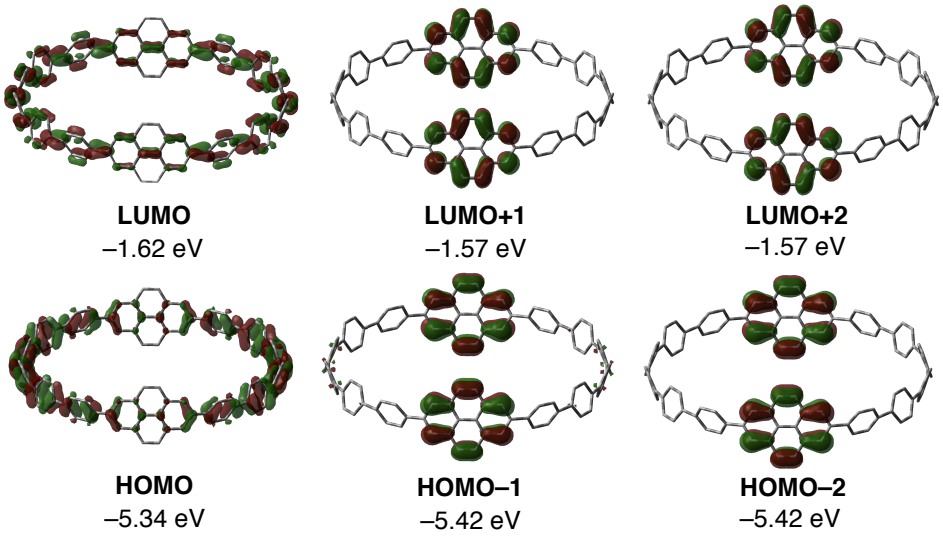

Figure 5. Frontier MOs of [12,2]CPPyr **(5)** calculated at the B3LYP/6-31G(d) level.

3. Conclusion

In this chapter, the synthesis of [12,2]CPPyr (**5**), a potential precursor for carbon nanobelt, is described. paradium-catalyzed and nickel-mediated stepwise coupling reactions of cyclohexane-based L-shaped unit with 2,7-diborylpyrene and following acid-mediated aromatization successfully afforded **5**. A [12,2]CPPyr **5** has higher molecular absorption coefficient, lower fluorescence quantum yield, and longer fluorescence lifetime (τ_s = 25.6 ns) than those of CPPs. The fact that the absorption of **5** shows a simple combination of those of CPP and pyrene reflects the poor conjugation of paraphenylene and 2,7-pyrenylene.

Aimed at obtaining a carbon nanoring having more pyrene rings than **5**, the synthesis of cyclo[12]paraphenylene-[4]2,7-pyrenylene ([12,4]CPPyr, **6**) was also attempted as shown in Scheme 3. Although the mass peak of **6** was detected from the final product, the isolation of **6** was unsuccessful due probably to poor solubility derived from its large size. The size of **6** is in accordance with that of [20]CPP, which has not been synthesized yet.

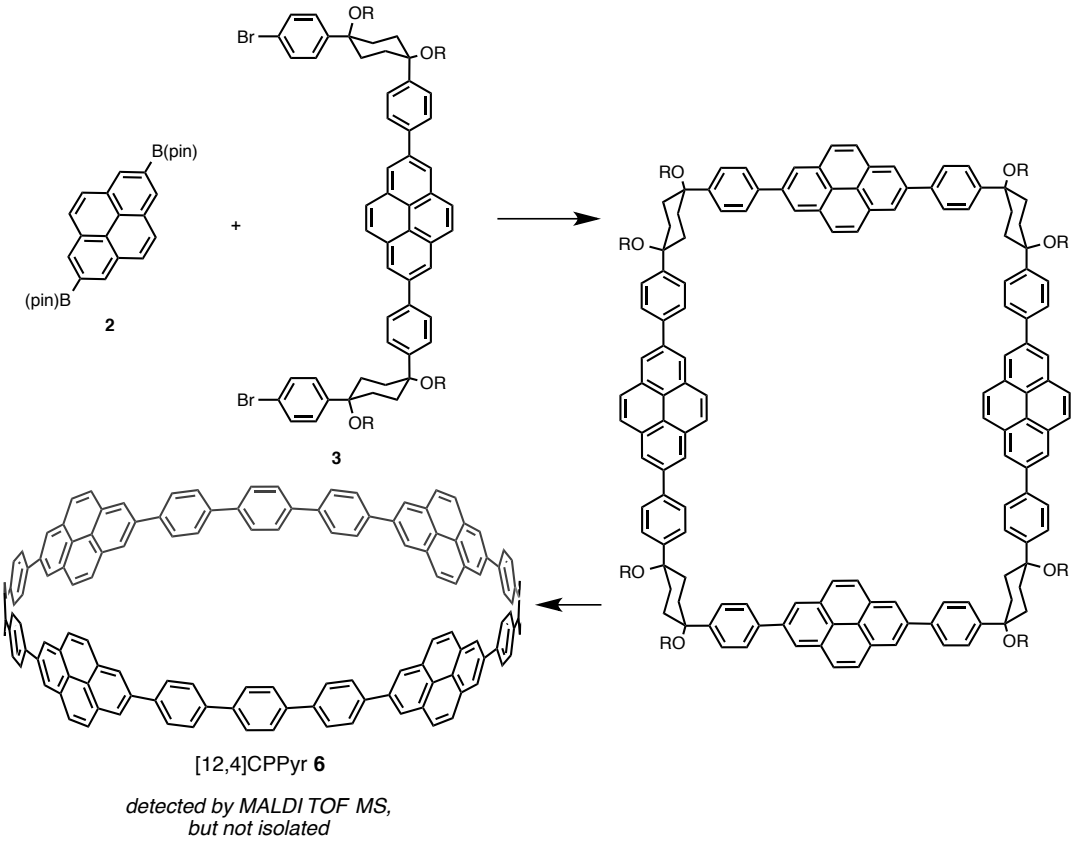

Scheme 3. Attempt for the synthesis of [12,4]CPPyr **6**.

Toward the synthesis of carbon nanobelt, this study should go the next step of aromatic electrophilic substitution of pyrene rings. Here, the problem is poor solubility of **5** owing to its large size. As well as the investigation of the reaction conditions for functionalization of **5**, the synthesis of small sizes of CPPyr, *i.e.* soluble CPPyr, is also worth tackling in future.

4. Experimental section

4-1. General

Unless otherwise noted, all materials including dry solvents (dimethylsulfoxide (DMSO)) were obtained from commercial suppliers and used without further purification. Tetrahydrofuran (THF) and *m*-xylene were purified by passing through a solvent purification system (Glass Contour). All reactions were performed using standard vacuum-line and Schlenk techniques. Work-up and purification procedures were carried out with reagent-grade solvents under air. *cis*-1,4-Bis(4-bromophenyl)-1,4-bis(methoxymethoxy)cyclohexane (**1**) and 2,7-bis(4,4,5,5-tetramethyl-1,3,2-dioxaborolan-2-yl)pyrene (**2**) were synthesized according to reported procedures.

Analytical thin-layer chromatography (TLC) was performed using E. Merck silica gel 60 F254 precoated plates (0.25 mm). The developed chromatogram was analyzed by UV lamp (254 nm). Flash column chromatography was performed with E. Merck silica gel 60 (230–400 mesh). Preparative recycling gel permeation chromatography (GPC) was performed with JAI LC-9204 instrument equipped with JAIGEL-2H/JAIGEL-2H columns using chloroform as an eluent. High-resolution mass spectra (HRMS) were obtained from a JEOL JMS700 (fast atom bombardment mass spectrometry, FAB-MS) or Bruker Daltonics Ultraflex III TOF/TOF (MALDI TOF-MS) with 9-nitroanthracene as matrix. Melting points were measured on a MPA100 Optimelt automated melting point system. Nuclear magnetic resonance (NMR) spectra were recorded on JEOL JNM-ECA-600 (^{1}H 600 MHz, ^{13}C 150 MHz) spectrometer. Chemical shifts for ^{1}H NMR are expressed in parts per million (ppm) relative to $CHCl_3$ (δ 7.26 ppm) or $CHDCl_2$ (δ 5.32 ppm). Chemical shifts for ^{13}C NMR are expressed in ppm relative to $CDCl_3$ (δ 77.0 ppm) or CD_2Cl_2 (δ 53.8 ppm). Data are reported as follows: chemical shift, multiplicity (s = singlet, d = doublet, m = multiplet, br = broad signal), coupling constant (Hz), and integration.

UV/Vis absorption spectrum of **5** was recorded on a Shimadzu UV-3510 spectrometer with a resolution of 0.5 nm. Emission spectrum of **5** was measured with an F-4500 Hitachi spectrometer with a resolution of 0.4 nm upon excitation at 343 nm. Dilute solution in degassed spectral grade chloroform in a 1 cm square quartz cell was used for measurements. Absolute fluorescence quantum yield was determined with a Hamamatsu C9920-02 calibrated integrating sphere system upon excitation at 343 nm. Fluorescence lifetimes were measured with a

Hamamatsu Picosecond Fluorescence Measurement System C4780 equipped with a USHO pulsed nitrogen laser (excitation wavelength 337 nm with a repetition rate of 10 Hz).

Synthesis of 3

To a 100-mL round-bottom glass flask containing a magnetic stirring bar were added **1** (11.4 g, 22.2 mmol), **2** (1.99 g, 4.39 mmol), $Pd(PPh_3)_4$ (508 mg, 439 μmol), Ag_2O (3.61 g, 15.8 mmol), and dry THF (44 mL). The resultant mixture was heated to reflux for 15 h. After the reaction mixture was cooled down to room temperature, the mixture was passed through short silica gel column chromatography ($CHCl_3$). The crude product was purified by the silica gel column chromatography (hexane/EtOAc = 6:1 to $CHCl_3$/EtOAc = 1:1) to afford **3** (3.23 g, 69%) as a colorless solid. Unreacted **1** (7.07 g) was also recovered by the silica gel column chromatography.

^{1}H NMR (600 MHz, $CDCl_3$) δ 2.15 (brs, 8H), 2.33–2.47 (m, 8H), 3.43 (s, 6H), 3.46 (s, 6H), 4.46 (s, 4H), 4.53 (s, 4H), 7.35 (d, *J* = 8.2 Hz, 4H), 7.47 (d, *J* = 8.2 Hz, 4H), 7.62 (d, *J* = 8.2 Hz, 4H), 7.86 (d, *J* = 8.2 Hz, 4H), 8.13 (s, 4H), 8.38 (s, 4H); ^{13}C NMR (150 MHz, $CDCl_3$) δ 33.2 (CH_2), 56.2 (CH_3), 78.1 (4º), 78.3 (4º), 92.3 (CH_2), 92.5 (CH_2), 121.8 (4º), 123.9 (CH), 124.0 (4º), 127.7 (4º), 128.1 (CH), 128.8 (4º), 131.7 (CH), 131.7 (4º), 138.4 (4º), 140.8 (4º); HRMS (FAB) *m/z* calcd for $C_{60}H_{60}Br_2NaO_{12}$ $[M \cdot Na]^+$: 1089.2553, found: 1089.2582; mp: 121.4–123.3 ºC.

Synthesis of 4

To a 20-mL Schlenk tube containing a magnetic stirring bar were added **3** (336 mg, 315 μmol), nickelbis(1,5-cyclooctadiene) ($Ni(cod)_2$, 176 mg, 692 μmol), 2,2'-bipyridyl (104 mg, 692 μmol), and dry 1,4-dioxane (160 mL). The reaction mixture was stirred at 90 ºC for 24 h. After cooled down to room temperature, the mixture was concentrated under reduced pressure. The mixture was extracted with $CHCl_3$. The combined organic phase was dried over Na_2SO_4 and concentrated under reduced pressure. The crude product was purified by GPC and washed with EtOAc to afford **4** (48.3 mg, 17%) as a white solid.

^{1}H NMR (600 MHz, $CDCl_3$) δ 2.21 (brs, 16H), 2.43 (brs, 16H), 3.45 (s, 12H), 3.47 (s, 12H), 4.49 (s, 8H), 4.54 (s, 8H), 7.47–7.60 (m, 16H), 7.60–7.72 (m, 8H), 7.83 (d, *J* = 7.8 Hz, 8H), 8.08 (s, 8H), 8.34 (s, 8H); ^{13}C NMR (150 MHz, $CDCl_3$) δ 33.6 (CH_2), 56.6 (CH_3), 78.7 (4º), 78.8 (4º), 92.8 (CH_2), 92.9 (CH_2), 124.3 (CH), 124.4 (4°), 127.4 (CH), 128.0 (CH), 128.5 (CH),

132.1 (4°), 138.9 (4º), 140.1 (4º), 141.2 (4º); HRMS (FAB) *m/z* calcd for $C_{120}H_{120}NaO_{16}$ $[M \cdot Na]^+$: 1839.8474, found 1839.8465; mp: 265–300 ºC (dec.).

Synthesis of [12,2]CPPyr 5

To a screw-top test tube containing a magnetic stirring bar were added **4** (10.0 mg, 5.4 μmol), $NaHSO_4 \cdot H_2O$ (15 mg, 108 μmol), and dry 1,2,4-trichlorobenzene (6 mL). The flask was stirred at 150 °C for 40 h. After the reaction mixture was cooled down to room temperature, the mixture was diluted with hexane and passed through a short silica gel column chromatography (hexane to CH_2Cl_2) to remove 1,2,4-trichlorobenzene as the first fraction. The crude product was washed with EtOAc to afford [12,2]CPPyr **5** (1.3 mg, 18%) as a pale yellow solid.

^{1}H NMR (600 MHz, CD_2Cl_2) δ 7.68 (d, *J* = 8.4 Hz, 8H), 7.71 (d, *J* = 8.4 Hz, 8H), 7.72 (s, 16H) 7.76 (d, *J* = 8.4 Hz, 8H), 7.93 (d, *J* = 8.4 Hz, 8H), 8.09 (s, 8H), 8.42 (s, 8H); ^{1}H NMR (600 MHz, $CDCl_3$) δ 7.65 (d, *J* = 8.8 Hz, 8H), 7.68 (d, *J* = 8.8 Hz, 8H), 7.68 (s, 16H) 7.72 (d, *J* = 8.8 Hz, 8H), 7.88 (d, *J* = 8.8 Hz, 8H), 8.06 (s, 8H), 8.36 (s, 8H); ^{13}C NMR (150 MHz, CD_2Cl_2) δ 124.1 (CH), 124.3 (CH), 127.6 (CH), 127.7 (CH), 127.8 (CH), 128.0 (CH), 128.3 (CH), 128.5 (CH), 132.1 (4º), 133.0 (4º), 139.1 (4º), 139.2 (4º), 139.3 (4º), 139.4 (4º), 139.9 (4º),; HRMS (MALDI) *m/z* calcd for $C_{104}H_{64}$ $[M]^+$: 1312.5008, found 1312.5013; mp: >300 ºC.

4-2. Computational Study

The Gaussian 09 program running on a SGI Altix4700 system was used for optimization (B3LYP/6-31G(d)). All structures were optimized without any symmetry assumptions. Zero-point energy, enthalpy, and Gibbs free energy at 298.15 K and 1 atm were estimated from the gas-phase studies. Harmonic vibration frequency calculation at the same level was performed to verify all stationary points as local minima (with no imaginary frequency). Reported energy values were used for biphenyl and *p*-terphenyl. Visualization of the results was performed by use of GaussView 5.0.9 software.

Table 1. Uncorrected and thermal-corrected energies of stationary points (Hartree).[a]

compound	*E*	*E* + *ZPE*	*H*	*G*
2,7-diphenylpyrene	-1077.887431	-1077.517874	-1077.497326	-1077.566676
5	-4000.792025	-4000.445868	-4000.369650	-4000.561771

a) *E*: electronic energy; *ZPE*: zero-point energy; *H* (= $E + ZPE + E_{vib} + E_{rot} + E_{trans} + RT$): sum of

electronic and thermal enthalpies; G (= $H - TS$): sum of electronic and thermal free energies .

Table 2. TD-DFT vertical one-electron excitations (7 states) calculated for the optimized structure of **5**.

	energy	wavelength	Oscillator strength (*f*)	Description
S_3	3.2678 eV	379.41 nm	0.0000	HOMO -> LUMO (0.58653)
S_4	3.4653 eV	357.79 nm	2.9151	HOMO–3 -> LUMO (0.48440) HOMO–1 -> LUMO (0.15985) HOMO -> LUMO+1 (-0.12190) HOMO -> LUMO+3 (0.44413)
S_5	3.5046 eV	353.78 nm	1.3101	HOMO–6 -> LUMO+4 (0.11762) HOMO–4 -> LUMO (0.44700) HOMO–4 -> LUMO+6 (0.10508) HOMO–2 -> LUMO+1 (0.19412) HOMO–1 -> LUMO+2 (0.19141) HOMO -> LUMO+4 (0.43164)
S_9	3.6207 eV	342.43 nm	0.9859	HOMO–5 -> LUMO+1 (0.16553) HOMO–4 -> LUMO (-0.11518) HOMO–3 -> LUMO+2 (0.43718) HOMO–2 -> LUMO+1 (0.22463) HOMO–2 -> LUMO+3 (-0.13415) HOMO–1 -> LUMO+2 (0.39914) HOMO -> LUMO+4 (-0.13483)
S_{11}	3.6737 eV	337.49 nm	1.1748	HOMO–4 -> LUMO (-0.19802) HOMO–3 -> LUMO+2 (-0.40639) HOMO–2 -> LUMO+1 (0.45766) HOMO–2 -> LUMO+3 (-0.20797)
S_{17}	3.7076 eV	334.41 nm	0.5471	HOMO–4 -> LUMO+4 (0.13072) HOMO–3 -> LUMO+2 (-0.27933) HOMO–2 -> LUMO+1 (-0.22407) HOMO–2 -> LUMO+3 (0.31036) HOMO–1 -> LUMO+2 (0.47883)
S_{19}	3.7310 eV	332.31 nm	0.1631	HOMO–3 -> LUMO+2 (0.14207) HOMO–2 -> LUMO+1 (0.33130) HOMO–2 -> LUMO+3 (0.55534) HOMO–1 -> LUMO+2 (-0.18683)

References

1. Vollmann, H.; Becker, H.; Corell, M.; Streeck, H.; Langbein, G. *Liebigs Ann. Chem.* **1937**, *531*, 1.
2. (a) Kuninobu, Y.; Tatsuzaki, T.; Matsuki, T.; Takai, K. *J. Org. Chem.* **2011**, *76*, 7005. (b) Shen, H. -C.; Tang, J. -M.; Chang, H. -K.; Yang, C. -W.; Liu, R. -S. *J. Org. Chem.* **2005**, *70*, 10113.
3. Yagi, A.; Venkataramana, G.: Segawa, Y.; Itami, K. *Chem. Commun.* **2013**, *50*, 957.
4. Omachi, H.; Segawa, Y.; Itami, K. *Acc. Chem. Res.* **2012**, *45*. 1378.
5. (a) Omachi, H.; Matsuura, S.; Segawa, Y.; Itami, K. *Angew. Chem., Int. Ed.* **2010***, 49*, 10202. (b) Ishii, Y.; Nakanishi, Y.; Omachi, H.; Matsuura, S.; Matsui, K.; Shinohara, H. Segawa, Y.; Itami, K. *Chem. Sci.* **2012***, 3*, 2340.
6. Omachi, H.; Segawa, Y.; Itami, K. *Org. Lett.* **2011***, 13*, 2480.
7. Matsui, K.; Segawa, Y.; Itami, K. *Org. Lett.* **2012***, 14*, 1888.
8. Takaba, H.; Omachi, H.; Yamamoto, Y.; Bouffard, J.; Itami, K. *Angew. Chem., Int. Ed.* **2009**, *48*, 6112.
9. Coventry, D. N.; Batsanov, A. S.; Goeta, A. E.; Howard, J. A. K.; Marder T. B.; Perutz, R. N. *Chem. Commun.* **2005**, 2172.
10. (a) Minkin, V. L. *Pure Appl. Chem.* **1999**, *71*, 1919. (b) George, P.; Trachtman, M.; Bock, C. W.; Brett, A. M. *Tetrahedron* **1976**, *32*, 317.
11. Jasti, R.; Bhattacharjee, J.; Neaton, J. B.; Bertozzi, C. R. *J. Am. Chem. Soc.* **2008**, *130*, 17646.
12. Segawa, Y.; Fukazawa, A.; Matsuura, S.; Omachi, H.; Yamaguchi, S.; Irle S.; Itami, K. *Org. Biomol. Chem.* **2012**, *10*, 5979.
13. (a) Mangle, E. A.; Topp, M. R. *J. Phys. Chem.* **1986**, *90*, 802. (b) Baba, M.; Saitoh, M.; Kowaka, Y.; Taguma, K.; Yoshida, K.; Semba, Y.; Kasahara, S.; Yamanaka, T.; Ohshima, Y.; Hsu Y.-C.; Lin, S. H. *J. Phys. Chem.* **2009**, *131*, 224318.
14. (a) Qiao, Y.; Zhang, J.; Xu W.; Zhu, D. *Tetrahedron*, **2011**, *67*, 3395. (b) Crawford, A. G.; Dwyer, A. D.; Liu, Z. Steffen, A.; Beeby, A.; Palsson, L.-O.; Tozer D. J.; Marder, T. B. *J. Am. Chem. Soc*. **2011**, *133*, 13349.

Chapter 2

Synthesis and Properties of [9]Cyclo-1,4-naphthylene

Abstract: The first synthesis of [9]cyclo-1,4-naphthylene ([9]CN), which is a carbon nanoring consisting solely of naphthalene, has been achieved as a part of synthesizing potential precursors for carbon nanobelt. The L-shaped unit, which has a dihydronaphthalene ring as a core part, was prepared to construct a macrocyclic structure of CN. A nickel-mediated coupling of the L-shaped unit produced a less-strained cyclic trimer. Finally, the aromatization of the cyclic trimer afforded [9]CN. Careful structure–property analyses uncovered a number of unique features of [9]CN that are quite different from those of [9]CPP.

1. Introduction

In our campaign to synthesize carbon nanobelts, several carbon nanorings are designed as potential precursors. Chapter 1 described the synthesis of a pyrene-containing carbon nanoring. For the synthesis of highly strained carbon nanobelt, a stepwise construction of belt-like structure on the pyrene-containing carbon nanoring will be promising. On the other hand, a carbon nanoring possessing all carbon components of the carbon nanobelt would become an ideal precursor because it can be straightforwardly transformed to desired carbon nanobelt. Cyclo-1,4-naphthylene (CN) is a carbon nanoring consisting solely of naphthalene rings and one of such ideal precursors for the carbon nanobelt (Figure 1). Cyclodehydrogenation reaction between the *peri* positions of neighboring naphthalene rings constructs a perylene unit in CNs. Therefore, it is expected that the sequential cyclodehydrogenation reactions of CNs finally gives corresponding carbon nanobelts. In this work, CN was selected as a next target of a potential precursor for carbon nanobelt.

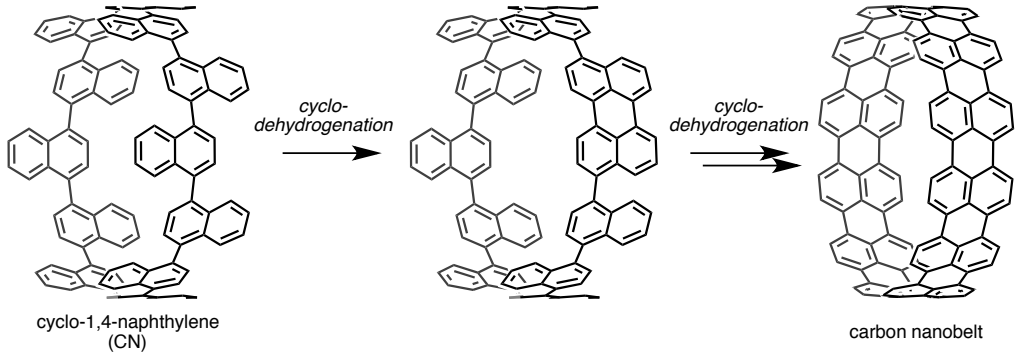

Figure 1. Cyclo-1,4-naphthylenes (CNs) as possible precursors of carbon nanobelts.

The strategy for the synthesis of CN is shown in Figure 2. Encouraged by the synthesis of CPP, [1] a *cis*-1,4-dinaphthyl-1,4-dihydronaphthalene derivative was designed as a ternaphthylene-convertible L-shaped unit in the synthesis of CN. In order to obtain CN in short steps, our "shotgun" synthesis of [9]CPP and [12]CPP was imitated. [2] A nickel complex-mediated homocoupling reaction of the L-shaped units was expected to afford less-strained macrocycles in short steps. Following aromatization reaction of the dihydronaphthalene moieties in the macrocycles would lead to CN. This strategy actually provided only [9]CN, not [12]CN. In this chapter, details for the synthesis of [9]CN are described.[3] In addition, the structural and photophysical properties of [9]CN are also discussed.

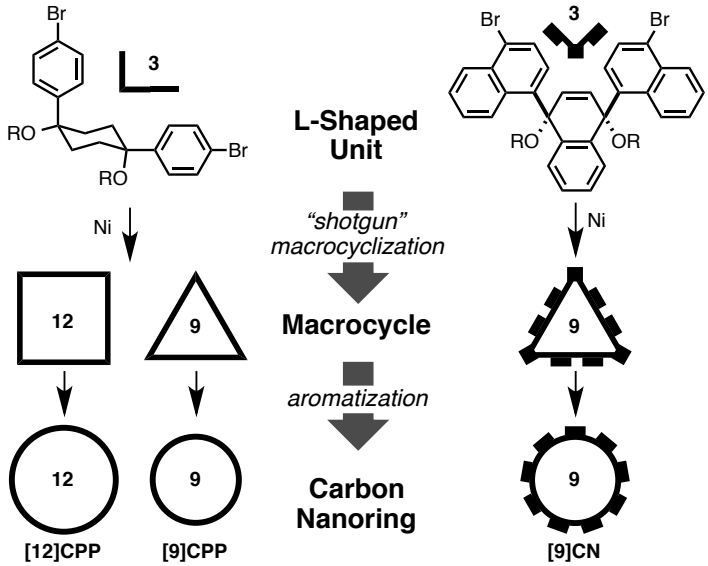

Figure 2. Strategy for the synthesis of [9]CN.

2. Results and discussion

2-1. Synthesis of [9]cyclo-1,4-naphthylenes

2-1-1. Synthesis of L-shaped unit 2

The synthesis of [9]CN began with the preparation of L-shaped unit **2**, which is a ternaphthylene-convertible molecule (Scheme 1). First, 1,4-dibromonaphthalene was treated with *n*-butyllithium to produce 1-bromo-4-lithionaphthalene, which was then reacted with 1,4-naphthoquinone. This double nucleophilic addition yielded the desired *cis*-configurated diol (***cis*-1**) in 36% yield, along with undesired ***trans*-1** (13%). The stereoselectivity of double-addition was determined to be 3:1 (*cis*/*trans*) by ^{1}H NMR spectroscopy. It was reported that *cis*-addition was favored on the addition of two 1-iodo-4-lithiobenzenes to benzoquinone.[4] In these previous works, it was proposed that *syn*-stereochemistry was due to electrostatic interactions of 1-iodo-4-lithiobenzene and lithium alkoxide of *mono*-adduct in the transition state in the second carbonyl addition. Next, ***cis*-1** was treated with MeI and NaH to give L-shaped unit **2** to facilitate further synthetic operations. The configurations of these molecules were confirmed by X-ray crystallography. A suitable single crystal was obtained by slow vapor diffusion of *n*-pentane into a THF solution of **2** at room temperature. In the solid state, the included angle between the two 1-(4-bromo)naphthyl groups of **2** is ca. 71° (Figure 3). This value is somewhat smaller than that of the cyclohexane-based L-shaped unit used in the synthesis of CPPs by our group (ca. 80°).[2a]

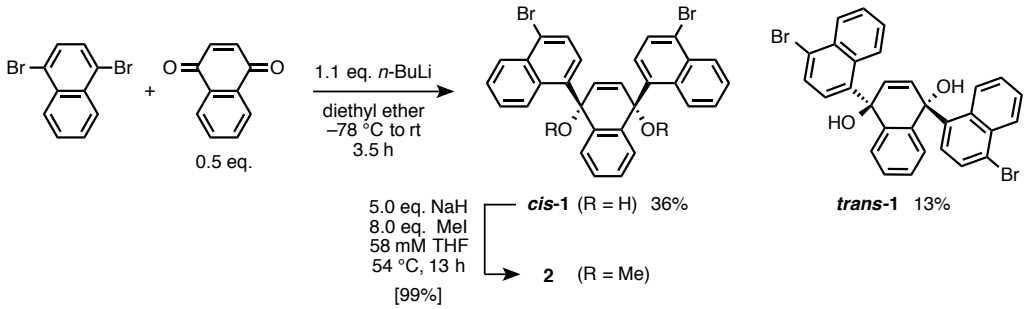

Scheme 1. Synthesis of L-shaped unit **2**.

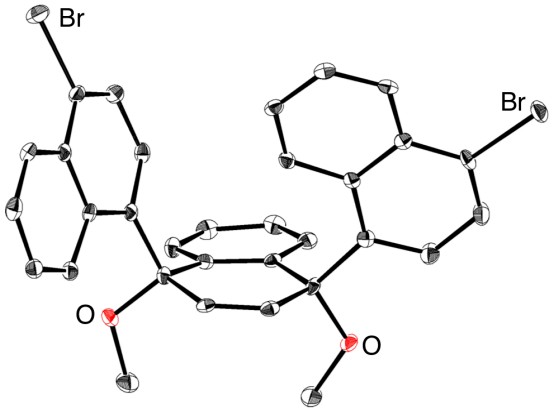

Figure 3. ORTEP drawing of **2** with 50% thermal ellipsoid. All hydrogen atoms are omitted for clarity.

2-1-2. Synthesis of macrocycle 3

With L-shaped unit **2** in hand, the nickel-mediated macrocyclization of **2** was investigated to produce the macrocycle in a single operation (Scheme 2).[5,6] The treatment of **2** (1.0 equiv, 8.3 mM) with $Ni(cod)_2$ (2.2 equiv) and 2,2'-bipyridyl (2.2 equiv) in DMF at 85 °C furnished the cyclic trimer **3** in 2% isolated yield after extensive purification using preparative recycling gel permeation chromatography and preparative thin-layer silica-gel chromatography. It should be noted that no other macrocyclic compound such as cyclic tetramer was identified, although many linear oligomers were generated. The coupling of **2** might prefer forming cyclic trimer to cyclic tetramer due to its included angle. No reaction occurred under more diluted conditions (1.0 mM of **2**), and the polymerization became predominant at higher concentrations (64 mM of **2**). In the similar synthesis of CPP analogues, the nickel-mediated macrocyclization furnished two macrocycles of different ring size (the precursors for [9]CPP and [12]CPP) in 23% and 32% yield, respectively.[2b] The yield of **3** is quite low compared to that of the macrocyclic precursor for [9]CPP. The homocoupling reaction on 1-positions of naphthalene rings might not proceed well due to the steric repulsion of hydrogen atoms on the *peri*-position (5- and 8-position).

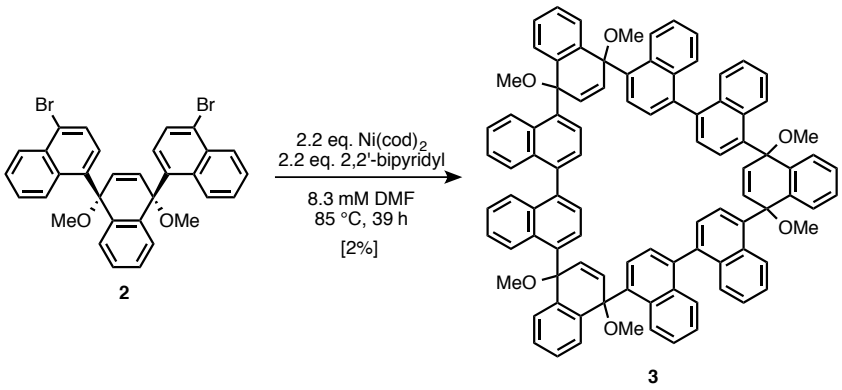

Scheme 2. Cyclotrimerization of **2** by a homocoupling reaction.

2-1-3. Synthesis of [9]cyclo-1,4-naphthylene ([9]CN)

The reductive aromatization of macrocycle **3** was investigated to obtain [9]cyclo-1,4-naphthylene ([9]CN) (Scheme 3). In CPP synthesis by Bertozzi and Jasti, lithium naphthalenide was employed as reductant at low temperature (–78 °C).[4] They also proposed a plausible mechanism for the reductive aromatization of dimethoxycyclohexadiene moieties as shown in Scheme 4. The reductive aromatization of the dihydronaphthalene moieties in **3** should proceed as well. Although a number of reductive conditions such as the use of $SnCl_2$, lithium naphthalenide, or a lithium dispersion were applied to **3**, simple treatment with granular lithium in THF at room temperature afforded [9]CN in the highest yield of 59%. The color of reaction mixture was dark purple probably derived from generated radical anion species. [9]CN shows bright yellow color in the solid state and greenish yellow color in chloroform solution.

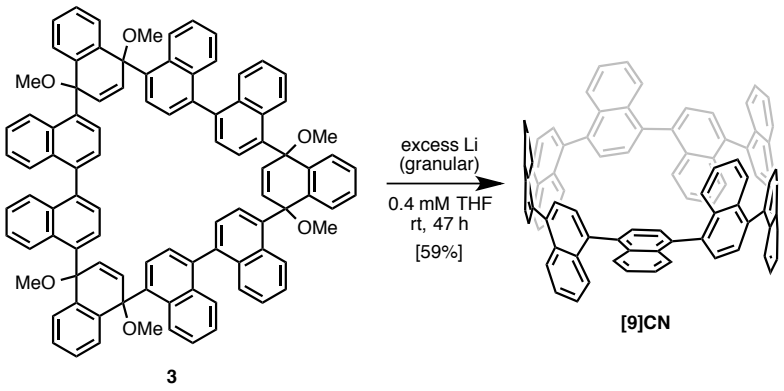

Scheme 3. Reductive aromatization of **3**.

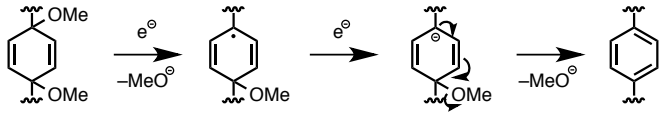

Scheme 4. Plausible mechanism for reductive aromatization of dimethoxycyclohexadiene moiety.

2-2. Structural features of [9]cyclo-1,4-naphthylene

The ^{1}H NMR spectrum of [9]CN in THF-d_8 is shown in Figure 4b. Contrary to simple ^{1}H NMR spectra of CPPs, many signals appeared in aromatic region with one characteristic singlet in a high magnetic field (δ = 6.28 ppm). These signals coalesced to three broadened signals (δ = 7.03, 7.66, 8.47 ppm) when a DMSO-d_6 solution of [9]CN was heated to 150 °C (Figure 5). When the heated sample was cooled back to room temperature, a spectrum identical to that acquired before heating was observed. These measurements indicated that the ground-state structure of [9]CN has low symmetry and the dynamic conformational change (arene rotation) of [9]CN is sufficiently slow with respect to the NMR timescale at room temperature. Furthermore, the assignment of these groups of signals to the 2,3- (red), 5,8- (green), and 6,7-positions (blue) of naphthalene units (Figure 4a) was enabled by using HH COSY, NOESY, and HMQC methods.

To gain insight into the structural properties of [9]CN, the structure optimization as well as GIAO calculations of [9]CN were performed. The most stable conformation of [9]CN (**A**) is shown in Figure 4a. Since **A** has C_2 symmetry, 27 hydrogen atoms of [9]CN are magnetically non-equivalent. The result of the GIAO calculation of **A** by B3LYP/6-311+G(2d,p)//B3LYP/6-31G(d) in THF with $SiMe_4$ (δ = 0.0 ppm) as a reference is shown in Figure 4c, where hydrogen atoms on 2,3-positions, 5,8-positions, and 6,7-positions on naphthalene units are colored in red, green, and blue, respectively. Although all the calculated chemical shifts were higher than those observed, the three sets of signals corresponding to these positions (8:18:1) were reproduced quite accurately. The characteristic high-field-shifted singlet signal is assigned to the hydrogens at 2- and 3-positions indicated by red diamonds in Figure 4a. The upfield shift of these inner hydrogen atoms should be ascribed to the ring current of the neighboring naphthalene rings.

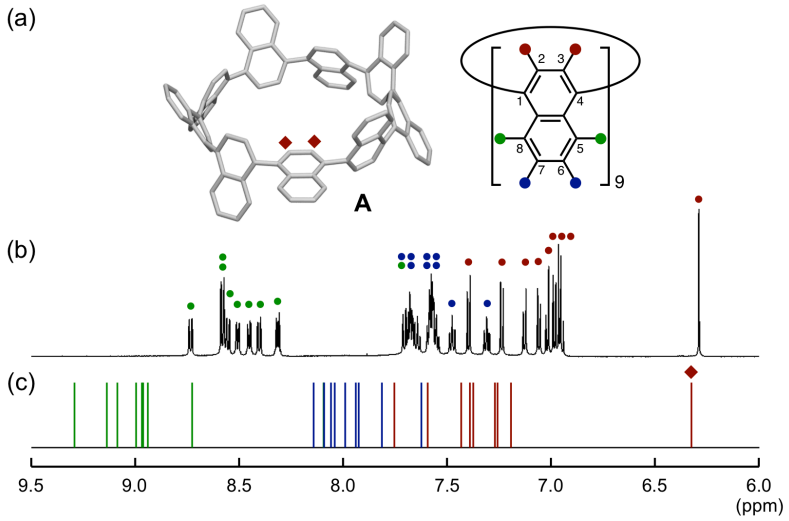

Figure 4. (a) Optimized structure of [9]CN. (b) ^{1}H NMR spectrum of [9]CN in THF-d_8. (c) Calculated ^{1}H NMR chemical shifts of [9]CN at B3LYP/6-311+G(2d,p)//B3LYP/6-31G(d) level in THF with $SiMe_4$ (δ = 0.0 ppm) as a reference.

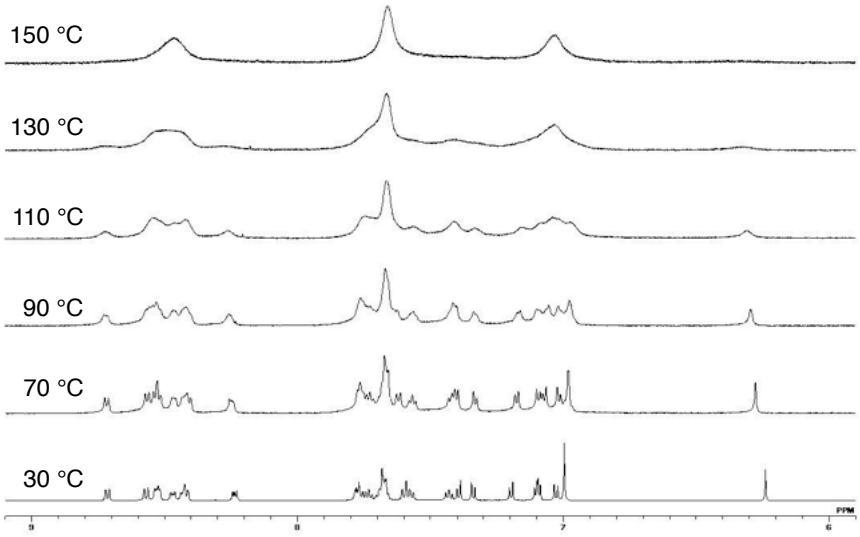

Figure 5. VT NMR of [9]CN in DMSO-d_6.

Optimized structure of [9]CN also revealed the striking structural difference between [9]CN and [9]CPP (Figure 6). Due to the sterically demanding naphthyl groups, the average dihedral angle between neighboring naphthalene rings in [9]CN is considerably larger (ca. 60°) than that of [9]CPP (ca. 30°).[2b] Moreover, because these nanorings are both odd-numbered cycloarylenes, it is not possible for all arene rings to be alternately twisted; one helical moiety has to be generated in the structure. As a result, one benzene ring in [9]CPP aligns perpendicular to the

plane of nanoring. In contrast, one naphthalene ring in [9]CN is parallel to the nanoring plane due to the larger dihedral angles.

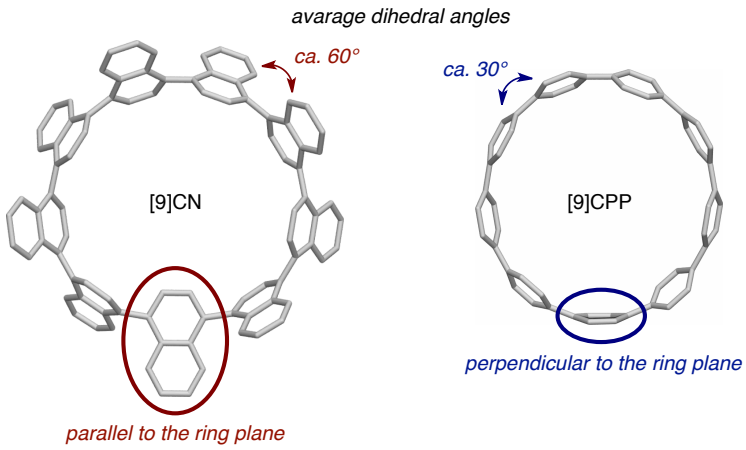

Figure 6. Comparison of optimized structures of [9]CN and [9]CPP.

It was also revealed that [9]CN is inherently a unique chiral molecule according these structural features. Investigation of the racemization pathway and the activation energy for racemization was conducted by the DFT calculations (B3LYP/6-31G(d)) to uncover the dynamic behavior of [9]CN (Figure 7). For comparison, the racemization process of 1,1'-binaphthyl was also calculated at the same level of calculation.[7] As shown in Figure 7, there are two twisting modes of racemization for 1,1'-binaphthyl between the ground state **C** and its enantiomer **C***: the higher transition state (**TS1**) where 4- and 4'-hydrogens come close and the lower transition state (**TS2**) where 2- and 4'-hydrogens come close. In the case of [9]CN, the transition states with similar rotation modes were also identified. One is the transition state for the racemization of [9]CN between the most stable conformation **A** and its enantiomer **A*** ($\mathbf{TS_{rac}}$) and the other is that for the isomerization of **A** to the conformation **B** ($\mathbf{TS_{AB}}$). Counterintuitively, it was found that these barriers to interconversion are lower for [9]CN (19.9/21.4 kcal·mol^{-1}) than for 1,1'-binaphthyl (34.3/25.4 kcal·mol^{-1}). These relatively lower barriers to arene rotation most likely stem from the ring strain of [9]CN. Due to the ring strain, the ground state energy of [9]CN becomes relatively higher in energy, thereby getting closer to the transition-state structure. Although the experimental determination of racemization barrier by using chiral HPLC or NMR spectroscopy was unsuccessful, a unique effect of ring strain to the rotation mode of 1,1'-binaphthyl moiety was uncovered from these studies.

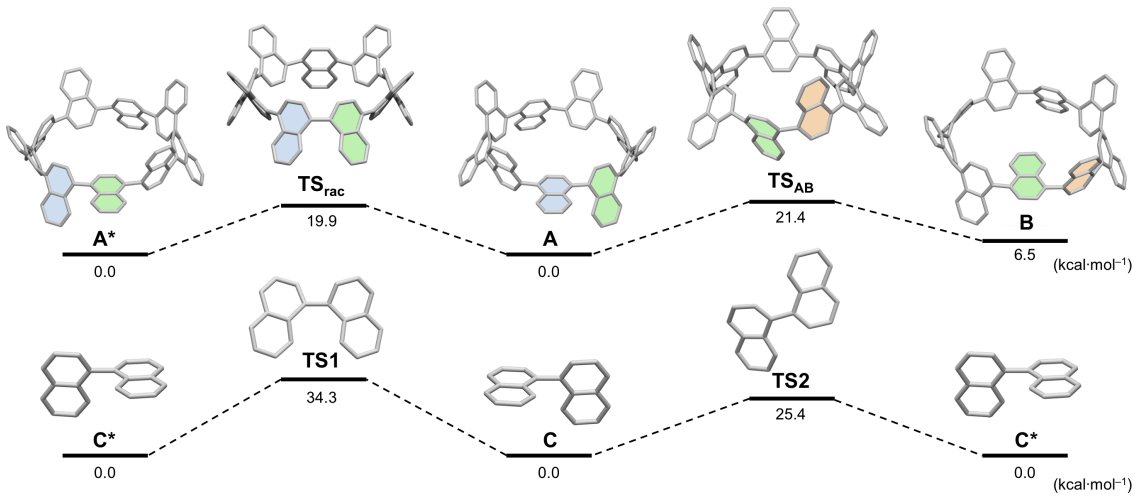

Figure 7. Rotation pathways of [9]CN and 1,1'-binaphthyl. Values are relative Gibbs free energies (ΔG) calculated at B3LYP/6-31G(d) level of theory. The symbol * represents the enantiomer of corresponding structure.

2-3. Photophisical properties of [9]cyclo-1,4-naphthylene

The photophysical properties (UV-vis absorption and fluorescence) of [9]CN in chloroform were measured (Figure 8, green lines). For comparison, the spectra of [9]CPP (gray lines) are also depicted in Figure 8.[2b] In the UV–vis spectrum of [9]CN, the absorption maximum (λ_{abs}) was observed at 378 nm with the molecular absorption coefficient (ε) of 6.8×10^4 M^{-1} cm^{-1}. The shape of the spectrum implies that several distinct electronic transitions overlap in the higher wavelength region above 378 nm. In order to determine the nature of excitation of [9]CN, a TD-DFT study was performed at the B3LYP/6-31G(d) level. The molecular structure, the spatial distribution, and the energy of representative frontier molecular orbitals of [9]CN are shown in Figure 9. It was found that λ_{abs} corresponds to the HOMO-1→LUMO and HOMO→LUMO+1 π-π* transitions (431 nm, f_{calc} = 0.823), whereas the HOMO→LUMO transition occurs at a longer wavelength (472 nm) with weak oscillator strength (f_{calc} = 0.165). There is a clear red-shift in the absorption of [9]CN in comparison with that of [9]CPP, which should be ascribed to the π-extension of arene units. Nevertheless, the fluorescence maxima (λ_{em}) of [9]CN (491 nm) and [9]CPP (494 nm) were found to be quite similar. The absolute fluorescence quantum yield (Φ_F) of [9]CN was determined to be 0.35 using a calibrated integrating sphere (average of 7 measurements).

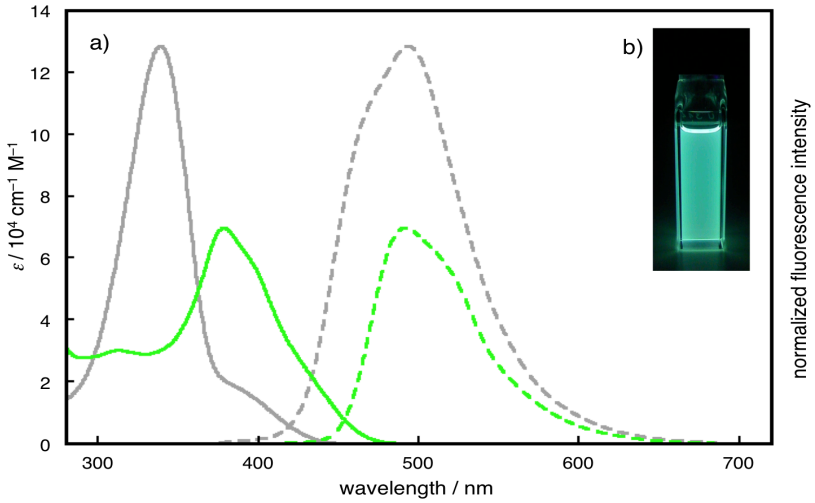

Figure 8. (a) UV-vis absorption (solid lines) and fluorescence spectra (broken lines) of [9]CN (green lines) and [9]CPP (gray lines). (b) Green fluorescence emission of [9]CN (1.12×10^{-6} M in chloroform solution).

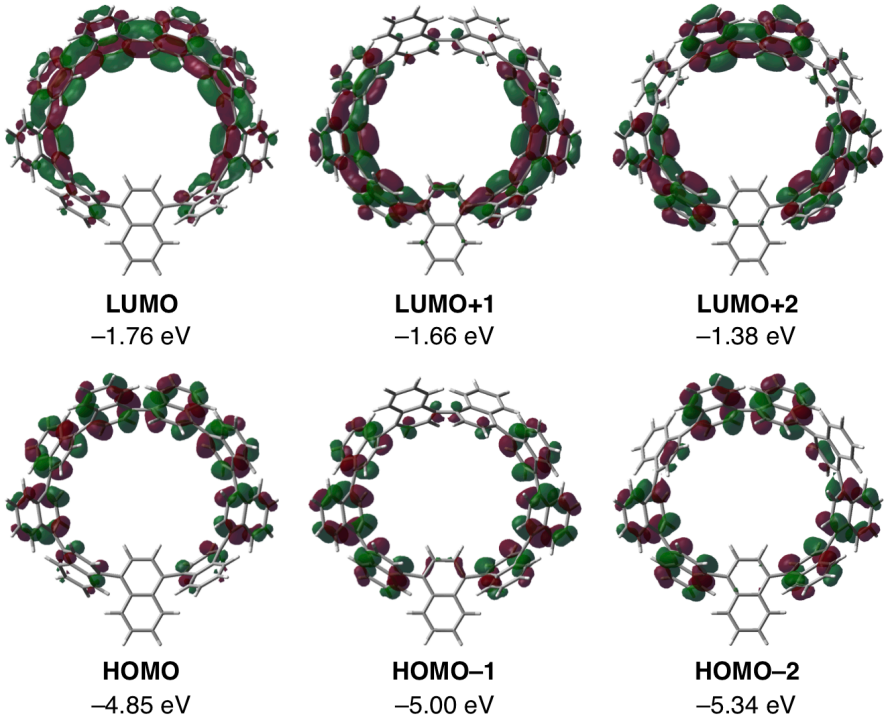

Figure 9. The molecular structure, the spatial distribution, and the energy of representative frontier molecular orbitals of [9]CN.

3. Conclusion

In conclusion, the synthesis of all-naphthalene carbon nanoring [9]CN has been achieved. A nickel-mediated cyclotrimerization of L-shaped unit successfully provided the macrocycle, which was transformed to [9]CN by reductive aromatization. Careful structure analysis uncovered a number of unique structural features of [9]CN, such as large dihedral angles, slow arene rotation, chirality, and a racemization process, that are quite different from those of [9]CPP. Due in part to the π-extension of arene unit, [9]CN has an absorption maximum at a longer wavelength, and luminesces with smaller Stokes shift in comparison with [9]CPP.

[9]CN is the first carbon nanoring consisting solely of fused arene rings. Uncovered unique features of [9]CN certainly triggered the following synthesis of other carbon nanorings.[8] Most importantly, the synthesis of a precursor that has a potential to be straightforwardly transformed to carbon nanobelt should become a significant progress in the history of synthetic studies of belt-shaped aromatic hydrocarbons. Since the sequential cyclodehydrogenation reaction in [9]CN can lead to the carbon nanobelt, it can be said that our synthetic campaign will reach its goal within several steps. The synthesis of [9]CN also showed the possibility for synthesis of other sizes of CNs (Chapter 3).

4. Experimental section

4-1. General

Unless otherwise noted, all materials including dry solvents (dimethylformamide (DMF)) were obtained from commercial suppliers and used without further purification. Tetrahydrofuran (THF) and diethyl ether were purified by passing through a solvent purification system (Glass Contour). All reactions were performed using standard vacuum-line and Schlenk techniques. Work-up and purification procedures were carried out with reagent-grade solvents under air. 1,4-Dibromonaphthalene[9] and $Ni(cod)_2$[10] were prepared according to procedures reported in the literatures.

Analytical thin-layer chromatography (TLC) was performed using E. Merck silica gel 60 F254 precoated plates (0.25 mm). The developed chromatogram was analyzed by UV lamp (254 nm and 365 nm). Flash column chromatography was performed with E. Merck silica gel 60 (230–400 mesh). Preparative thin-layer chromatography (PTLC) was performed using Wako-gel® B5-F silica coated plates (0.75 mm) prepared in our laboratory. Preparative gel permeation chromatography (GPC) was performed with a JAI LC-9204 instrument equipped with JAIGEL-1H/JAIGEL-2H columns using chloroform as an eluent. High-resolution mass spectra (HRMS) were obtained from a JEOL JMS700 (fast atom bombardment mass spectrometry, FAB MS) or a Bruker Daltonics Ultraflex III TOF/TOF (MALDI-TOF MS) with 9-nitroanthracene as matrix. Melting points were measured on a MPA100 Optimelt automated melting point system. Nuclear magnetic resonance (NMR) spectra were recorded on a JEOL JNM-ECA-600 (^{1}H 600 MHz, ^{13}C 150 MHz) spectrometer. Chemical shifts for ^{1}H NMR are expressed in parts per million (ppm) relative to $CHCl_3$ (δ 7.26 ppm), $CHDCl_2$ (δ 5.32 ppm), DMSO-d_5 (δ 2.50 ppm) and THF-d_7 (δ 1.72 ppm). Chemical shifts for ^{13}C NMR are expressed in ppm relative to $CDCl_3$ (δ 77.0 ppm), CD_2Cl_2 (δ 53.8 ppm), DMSO-d_6 (δ 39.5 ppm) and THF-d_8 (δ 67.2 ppm). Data are reported as follows: chemical shift, multiplicity (s = singlet, d = doublet, dd = doublet of doublets, ddd = doublet of doublets of doublets, t = triplet, m = multiplet), coupling constant (Hz), and integration.

UV/Vis absorption spectrum of [9]CN was recorded on a Shimadzu UV-3510 spectrometer with a resolution of 0.5 nm. Emission spectrum of [9]CN was measured with an F-4500 Hitachi spectrometer with a resolution of 0.4 nm upon excitation at 390 nm. Dilute solution in degassed spectral grade chloroform in a 1 cm square quartz cell was used for measurements. Absolute

fluorescence quantum yield was determined with a Hamamatsu C9920-02 calibrated integrating sphere system upon excitation at 390 nm.

Synthesis of *cis*-1 and *trans*-1

A three-necked 1-L glass round bottom flask containing a magnetic stirring bar was dried under vacuum and filled with argon after cooling to room temperature. A hexane solution *n*-butyllithium (1.6 M, 18.0 mL, 28.9 mmol) was added slowly to a solution of 1,4-dibromonaphthalene (7.50 g, 26.3 mmol) in dry diethyl ether (450 mL) at –78 °C under argon atmosphere. The reaction mixture was stirred at –78 °C for 1 h. The solution of 1,4-naphthoquinone (1.66 g, 10.5 mmol) in dry diethyl ether (120 mL) was added and the mixture was stirred for 1.5 h at –78 °C and for 1 h at room temperature. The reaction mixture was quenched with water, extracted with EtOAc (100 mL × 3), dried over Na_2SO_4, and concentrated under reduced pressure. ^{1}H NMR of the residue was taken to determine *cis*/*trans* ratio. The crude product was purified by silica gel column chromatography ($CHCl_3$/hexane = 3:1) and by reprecipitation (THF/hexane) to obtain *cis*-**1** (2.15 g, 36%) and *trans*-**1** (736 mg, 13%) as white solids.

cis-**1**: ^{1}H NMR (600 MHz, 150 °C, DMSO-d_6) δ 5.67 (s, 2H), 6.39 (s, 2H), 7.13 (dd, J = 6, 4 Hz, 2H), 7.17 (dd, J = 6, 4 Hz, 2H), 7.44 (ddd, J = 9, 7, 1 Hz, 2H), 7.62 (ddd, J = 9, 7, 1 Hz, 2H), 7.79 (d, J = 8 Hz, 2H), 7.93 (d, J = 8 Hz, 2H), 8.26 (dd, J = 8, 1 Hz, 2H), 8.42 (d, J = 9 Hz, 2H); ^{13}C NMR (150 MHz, 120 °C, DMSO-d_6) δ 71.1 (4°), 121.6 (4°), 125.4 (CH), 125.6 (CH), 126.3 (CH), 126.4 (CH), 126.7 (CH), 127.1 (CH), 127.6 (CH), 128.5 (CH), 131.3 (4°), 131.5 (4°), 132.8 (CH), 140.4 (4°), 140.9 (4°); HRMS (FAB) *m/z* calcd for $C_{30}H_{20}NaO_2Br_2$ $[M{\cdot}Na]^+$: 594.9702, found: 594.9719; mp: 175.3–177.3 °C.

trans-**1**: ^{1}H NMR (600 MHz, 100 °C, DMSO-d_6) δ 6.12 (s, 2H), 6.19 (s, 2H), 7.09 (dd, J = 6, 3 Hz, 2H), 7.13 (dd, J = 6, 3 Hz, 2H), 7.40 (t, J = 8 Hz, 2H), 7.57 (t, J = 7 Hz, 2H), 7.94 (d, J = 8 Hz, 2H), 7.99 (d, J = 8 Hz, 2H), 8.19 (d, J = 8 Hz, 2H), 8.65 (d, J = 9 Hz, 2H); ^{13}C NMR (150 MHz, 100 °C, DMSO-d_6) δ 71.1 (4°), 121.5 (4°), 125.1 (CH), 125.5 (CH), 126.2 (CH), 126.3 (CH), 126.9 (CH), 127.1 (CH), 127.2 (CH), 128.6 (CH), 131.1 (4°), 131.2 (4°), 131.3 (CH), 139.6 (4°), 143.0 (4°); HRMS (FAB) *m/z* calcd for $C_{30}H_{20}NaO_2Br_2$ $[M{\cdot}Na]^+$: 594.9702, found: 594.9766; mp: 158.0–160.0 °C.

Synthesis of L-shaped unit 2

A two-necked 200-mL glass round bottom flask containing a magnetic stirring bar was dried under vacuum and filled with argon after cooling to room temperature. A solution of *cis*-**1** (1.00 g, 1.74 mmol) in dry THF (15 mL) was added slowly to a suspension of sodium hydride (60% oil suspension, 367 mg, 8.74 mmol) in dry THF (30 mL) at 0 °C. Methyl iodide (800 μL, 12.9 mmol) was added dropwisely at 0 °C and the reaction mixture was stirred at 54 °C for 13 h. The reaction mixture was quenched with water and extracted with EtOAc (30 mL × 3), and the combined organic phase was dried over Na_2SO_4 and concentrated under reduced pressure. The crude product was purified by short column chromatography (hexane/EtOAc = 3:1) and follow-up reprecipitation (THF/hexane). The product **2** (1.06 g, 99%) was obtained as a white solid.

^{1}H NMR (600 MHz, $CDCl_3$) δ 3.35 (s, 6H), 6.74 (s, 2H), 6.94 (d, *J* = 8 Hz, 2H), 7.44 (t, *J* = 8 Hz, 2H), 7.47 (dd, *J* = 6, 3 Hz, 2H), 7.54 (t, *J* = 8 Hz, 2H), 7.57 (d, *J* = 8 Hz, 2H), 7.63 (dd, *J* = 6, 3 Hz, 2H) 8.28 (d, *J* = 8 Hz, 2H), 8.85 (d, *J* = 9 Hz, 2H); ^{13}C NMR (150 MHz, $CDCl_3$) δ 51.6 (CH_3), 79.3 (4°), 124.2 (4°), 126.4 (CH), 126.9 (CH), 127.2 (CH), 127.5 (CH), 128.4 (CH), 128.8 (CH), 128.9 (CH), 129.2 (CH), 132.8 (CH), 132.9 (4°), 133.1 (4°), 138.9 (4°), 140.1 (4°); HRMS (FAB) *m/z* calcd for $C_{32}H_{24}NaO_2Br_2$ $[M{\cdot}Na]^+$: 623.0015, found: 623.0018; mp: 190.6–192.6 °C.

Synthesis of cyclic trimer 3 by Ni-mediated "shortgun" macrocyclization of 2

To a Schlenk tube containing a magnetic stirring bar were added **2** (100 mg, 166 μmol), $Ni(cod)_2$ (101 mg, 367 μmol) and 2,2'-bipyridyl (57.2 mg, 366 μmol). After dry DMF (20 mL) was added via syringe through septum, the septum was replaced with oven-dried and argon-balloon-equipped condenser. The resultant mixture was stirred at 85 °C for 39 h. After the reaction mixture was cooled to room temperature, brine (ca. 100 mL) was added to the mixture. The mixture was extracted with EtOAc (50 mL × 3). The combined organic phase was subjected to preparative recycling gel permeation chromatography ($CHCl_3$) and then purified by PTLC (CH_2Cl_2/hexane = 4:1) to afford compound **3** (3.8 mg, 2%) as a white solid.

^{1}H NMR (600 MHz, CD_2Cl_2) δ 3.34 (s, 3H), 3.35 (s, 3H), 3.37 (s, 3H), 3.40 (s, 3H), 3.40 (s, 3H), 3.46 (s, 3H), 6.52 (d, *J* = 10 Hz, 1H), 6.72 (d, *J* = 8 Hz, 1H), 6.86 (s, 1H), 6.87 (d, *J* = 3 Hz, 1H), 6.96 (d, *J* = 8 Hz, 1H), 6.97–7.01 (m, 3H), 7.02–7.10 (m, 7H), 7.10–7.33 (m, 16H), 7.37 (t, *J* = 7 Hz, 1H), 7.41 (t, *J* = 7 Hz, 1H), 7.45–7.58 (m, 7H), 7.60 (dd, *J* = 6, 3 Hz, 2H),

7.63 (d, J = 8 Hz, 1H), 7.69 (d, J = 8 Hz, 1H), 7.76 (dd, J = 6, 3 Hz, 2H), 7.78 (d, J = 7Hz, 1H), 8.08 (d, J = 8 Hz, 1H), 8.76 (d, J = 9 Hz, 1H), 9.10 (d, J = 9 Hz, 1H), 9.13 (d, J = 9 Hz, 1H), 9.19 (t, J = 9 Hz, 2H), 9.78 (d, J = 9 Hz, 1H); ^{13}C NMR (150 MHz, CD_2Cl_2) δ 51.4 (CH_3), 51.5 (CH_3), 51.6 (CH_3), 51.7 (CH_3), 51.8 (CH_3), 79.3 (4°), 80.5 (4°), 80.5 (4°), 80.7 (4°), 81.1 (4°), 81.8 (4°), 125.4 (CH), 125.4 (CH), 125.6 (CH), 125.6 (CH), 125.7 (CH), 125.7 (CH), 125.9 (CH), 126.1 (CH), 126.1 (CH), 126.4 (CH), 126.5 (CH), 126.5 (CH), 126.6 (CH), 126.8 (CH), 126.9 (CH), 127.6 (CH), 127.9 (CH), 127.9 (CH), 128.1 (CH), 128.6 (CH), 128.8 (CH), 128.9 (CH), 129.0 (CH), 129.8 (CH), 129.9 (CH), 130.0 (CH), 130.5 (CH), 131.6 (4°), 132.0 (4°), 132.1 (CH), 132.1 (4°), 132.2 (4°), 132.2 (CH), 132.3 (4°), 132.5 (CH), 132.9 (CH), 134.6 (CH), 134.9 (4°), 135.0 (4°), 135.0 (4°), 135.1 (4°), 138.4 (4°), 139.1 (4°), 139.4 (4°), 139.5 (4°), 139.5 (4°), 139.8 (4°), 139.9 (4°), 140.2 (4°), 140.3 (4°), 140.8 (4°), 140.9 (4°), 140.9 (4°), 141.3 (4°), 141.7 (4°); HRMS (FAB) *m/z* calcd. for $C_{96}H_{72}NaO_6$ $[M{\cdot}Na]^+$: 1344.5255, found: 1344.5240; mp: 235.5–245.5 °C (dec.).

Synthesis of [9]cyclo-1,4-naphthylene ([9]CN)

A 50-mL flask containing glass-coated magnetic stirring bar was dried under vacuum and filled with argon after cooling to room temperature. In a glovebox, the compound **3** (8.0 mg, 3.7 μmol), lithium granular (20 mg, 2.9 mmol), and dry THF (10 mL) were added to this flask. The reaction mixture was stirred at room temperature for 47 h. The residue was diluted with hexane and quenched with methanol. After evaporated, the reaction mixture was passed through a short silica gel pad ($CHCl_3$). The filtrate was evaporated and purified by PTLC (CH_2Cl_2/hexane = 1:1) to obtain **[9]CN** (4.0 mg, 59%) as a yellow solid.

^{1}H NMR (600 MHz, THF-d_8) δ 6.28 (s, 2H), 6.95 (d, J = 8 Hz, 2H), 6.97 (d, J = 8 Hz, 2H), 6.99 (d, J = 8 Hz, 2H), 7.01 (d, J = 8 Hz, 2H), 7.06 (d, J = 8 Hz, 2H), 7.12 (d, J = 8 Hz, 2H), 7.24 (d, J = 8 Hz, 2H), 7.31 (ddd, J = 8, 7, 1 Hz, 2H), 7.40 (d, J = 8 Hz, 2H), 7.48 (ddd, J = 8, 7, 1 Hz, 2H), 7.51–7.61 (m, 8H), 7.61–7.73 (m, 8H), 8.32 (dd, J = 6, 3 Hz, 2H), 8.40 (dd, J = 8, 1 Hz, 2H), 8.45 (dd, J = 7, 2 Hz, 2H), 8.51 (dd, J = 7, 2 Hz, 2H), 8.55 (d, J = 8, 1 Hz, 2H), 8.58 (d, J = 8 Hz, 2H), 8.74 (d, J = 8 Hz, 2H); ^{13}C NMR (150 MHz, THF-d_8) δ 126.1 (CH), 126.5 (CH), 126.7 (CH), 126.9 (CH), 127.0 (CH), 127.0 (CH), 127.0 (CH), 127.1 (CH), 127.2 (CH), 127.4 (CH), 127.5 (CH), 127.5 (CH), 127.6 (CH), 127.7 (CH), 128.1 (CH), 128.3 (CH), 129.3 (CH), 129.3 (CH), 129.4 (CH), 129.5 (CH), 129.8 (CH), 130.0 (CH), 130.3 (CH), 130.3 (CH), 132.3 (CH), 132.6 (4°), 132.6 (4°), 133.9 (4°), 134.1(4°), 134.5 (4°), 134.8 (4°), 135.2 (4°), 136.5 (4°),

138.7 (4°), 138.9 (4°), 139.0 (4°), 139.1 (4°), 139.3 (4°), 139.5 (4°), 140.6 (4°), 140.9 (4°); HRMS (MALDI-TOF MS) *m/z* calcd. for $C_{90}H_{54}$ $[M]^+$: 1134.4226, found: 1134.4233; mp: partial decomposition at 300 °C.

4-2. X-ray Crystallography

Details of the crystal data and a summary of the intensity data collection parameters for *trans*-**1**·EtOAc and **2** are listed in Table 1. In each case, a suitable crystal was mounted with mineral oil on a glass fiber and transferred to the goniometer of a Rigaku Saturn CCD diffractometer. Graphite-monochromated Mo Kα radiation (λ = 0.71070 Å) was used. The structures were solved by direct methods with (SIR-97) [11] and refined by full-matrix least-squares techniques against F^2 (SHELXL-97).[12] The intensities were corrected for Lorentz and polarization effects. The non-hydrogen atoms were refined anisotropically. Hydrogen atoms were placed using AFIX instructions.

Table 1. Crystallographic data and structure refinement details for *trans*-**1** and **2**.

	trans-**1**·EtOAc	**2**
formula	$C_{34}H_{28}Br_2O_4$	$C_{32}H_{24}Br_2O_2$
fw	660.38	600.33
T (K)	103(2)	103(2)
λ (Å)	0.71070	0.71070
cryst syst	Monoclinic	Triclinic
space group	$P2_1/c$	P-1
a, (Å)	6.9781(14)	7.5571(11)
b, (Å)	18.955(4)	12.8797(16)
c, (Å)	21.355(4)	14.111(2)
α, (deg)	90	68.140(5)
β, (deg)	96.569(3)	83.629(6)
γ, (deg)	90	76.933(6)
V, (Å^3)	2806.1(9)	1241.2(3)
Z	4	2
D_{calc}, (g / cm^3)	1.563	1.606

μ (mm^{-1})	2.928	3.295
F(000)	1336	604
cryst size (mm)	0.15 × 0.03 × 0.01	0.15 × 0.15 × 0.10
2θ range, (deg)	3.07–25.00	3.11-25.00
reflns collected	18674	8344
indep reflns/R_{int}	4935/0.0425	4263/0.0239
params	365	327
GOF on F^2	1.066	1.031
R_1, wR_2 [I>2σ(I)]	0.0408, 0.0903	0.0244, 0.0561
R_1, wR_2 (all data)	0.0527, 0.0976	0.0322, 0.0588

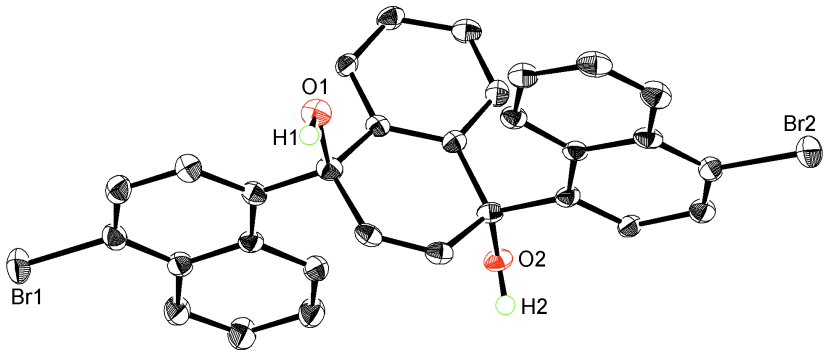

Figure 10. ORTEP drawing of *trans*-**1**·EtOAc with 50% thermal ellipsoid. All hydrogen atoms (except OH) and EtOAc molecule are omitted for clarity.

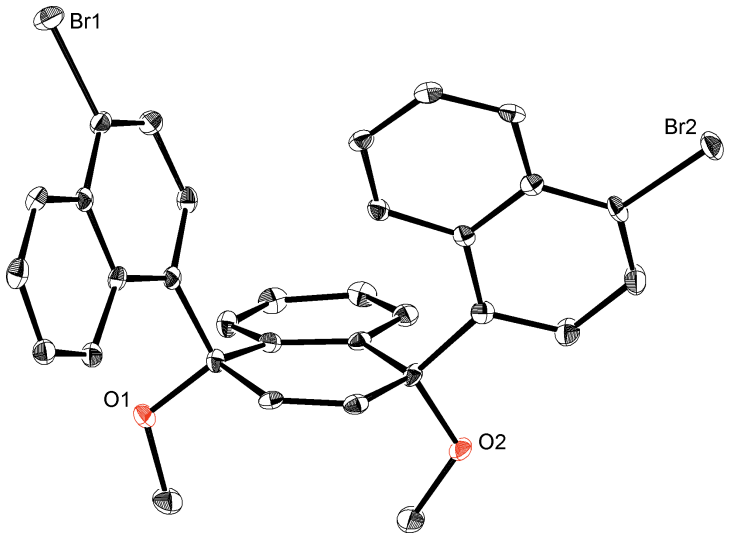

Figure 11. ORTEP drawing of **2** with 50% thermal ellipsoid. All hydrogen atoms are omitted for clarity.

4-3. Computational Study

The Gaussian 09 program running on a SGI Altix4700 system was used for optimization (B3LYP/6-31G(d)). All structures were optimized without any symmetry assumptions. Zero-point energy, enthalpy, and Gibbs free energy at 298.15 K and 1 atm were estimated from the gas-phase studies unless otherwise noted. Harmonic vibration frequency calculations at the same level were performed to verify all stationary points as local minima (with no imaginary frequency) or transition states (with one imaginary frequency). IRC calculations were also performed to check transition states. Visualization of the results was performed by use of POV-Ray for Windows v3.5 software.

Table 2. TD-DFT vertical one-electron excitations (6 states) calculated for the conformation **A** of [9]CN.

energy	wavelength	Oscillator strength (*f*)	Description
2.6281 eV	471.77 nm	0.1653	HOMO -> LUMO (0.65816) HOMO–1 -> LUMO+1 (0.23881)
2.8763 eV	431.05 nm	0.8226	HOMO–1 -> LUMO (0.19078) HOMO -> LUMO+1 (0.67369)
2.9299 eV	423.17 nm	0.2564	HOMO–1 -> LUMO (0.67223) HOMO -> LUMO+1 (-0.18410)
3.0127 eV	411.53 nm	0.2202	HOMO–1 -> LUMO+1 (0.65159) HOMO -> LUMO (-0.23999)
3.1337 eV	395.64 nm	0.1271	HOMO -> LUMO+2 (0.65639) HOMO–2 -> LUMO (-0.18011)
3.2484 eV	381.68 nm	0.3391	HOMO–2 -> LUMO (0.66426) HOMO -> LUMO+2 (0.19699)

Table 3. Uncorrected and thermal-corrected (298K) energies of stationary points (Hartree).[a]

compound	E	E + ZPE	H	G
[9]CN (A)	-3462.16886695	-3461.019367	-3460.954276	-3461.117841
[9]CN (B)	-3462.15892837	-3461.009337	-3460.944387	-3461.108107
[9]CN (TS_{AB})	-3462.13578458	-3460.986469	-3460.922092	-3461.084452
[9]CN (TS_{rac})	-3462.13793163	-3460.988718	-3460.924328	-3461.086813
1,1'-binaphtyl (C)	-770.587625051	-770.311952	-770.296834	-770.354150
1,1'-binaphtyl (TS1)	-770.536568946	-770.260617	-770.246495	-770.299540
1,1'-binaphtyl (TS2)	-770.538606528	-770.263546	-770.249675	-770.302349

a) E: electronic energy; ZPE: zero-point energy; H (=E+ZPE+E_{vib}+E_{rot}+E_{trans}+RT): sum of electronic and themal enthalpies; G (=H–TS): sum of electronic and thermal free energies.

References

1. (a) Omachi, H.; Segawa, Y.; Itami, K. *Acc. Chem. Res.* **2012**, *45*. 1378. (b) Sisto, T. J.; Jasti, R. *Synlett* **2012**, *23*, 483. (c) Yamago, S.; Kayahara, E.; Iwamoto, T. *Chem. Rec.* **2014**, *14*, 84. (d) Lewis, S. E. *Chem. Soc. Rev.* **2015**, *44*, 2221. (e) Darzi, E. R.; Jasti, R. *Chem. Soc. Rev.* **2015**, *44*, 6401. (f) Evans, P.; Jasti, R. in *Polyarenes I, Vol. 349* (Eds.: J. S. Siegel, Y.-T. Wu), Springer Berlin Heidelberg, **2014**, pp. 249.
2. (a) Segawa, Y.; Miyamoto, S.; Omachi, H.; Matsuura, S.; Šenel, P.; Sasamori, T.; Tokitoh, N.; Itami, K. *Angew. Chem., Int. Ed.* **2011***, 50*, 3244. (b) Segawa, Y.; Šenel, P.; Matsuura, S.; Omachi, H.; Itami, K. *Chem. Lett.* **2011***, 40*, 423.
3. Yagi, A.; Segawa, Y.; Itami, K. *J. Am. Chem. Soc.* **2012***, 134*, 2962.
4. Jasti, R.; Bhattacharjee, J.; Neaton, J. B.; Bertozzi, C. R. *J. Am. Chem. Soc.* **2008**, *130*, 17646.
5. For a review of nickel-mediated biaryl coupling of aryl halides, see: (a) Nelson, T. D.; Crouch, R. D. *Org. React.* **2004**, *63*, 265. For the mechanism see: (b) Tsou, T. T.; Kochi, J. K. *J. Am. Chem. Soc.* **1979**, *101*, 7547. Application to polymer synthesis: (c) Yamamoto, T.; Ito, T.; Kubota, K. *Chem. Lett.* **1988**, 153.
6. For nickel-based synthesis of cyclic ortho-arylenes, see: (a) Chao, C. S.; Chang, C. H.; Chang, C. T. *J. Org. Chem.* **1983**, *48*, 4904. (b) Zhou, Z.; Yamamoto, T. *J. Organomet. Chem.* **1991**, *414*, 119.
7. Theoretical study of 1,1'-binaphthyl with HF, AM3, and B3LYP methods with 6-31G(d,p) basis set: (a) Meca, L.; Řeha, D.; Havlas, Z. *J. Org. Chem.* **2003**, *68*, 5677. Experimental studies of 1,1'-binaphthyl: (b) Colter, A. K.; Clemens, L. M. *J. Phys. Chem.* **1964**, *68*, 651. (c) Cooke, A. S.; Harris, M. M. *J. Chem. Soc.* **1963**, 2365.
8. The carbon nanorings that include naphthalene rings: (a) Batson J. M.; Swager, T. M. *Synlett*, **2013**, *24*, 2545. (b) Huang, C.; Huang, Y.; Akhmedov, N. G.; Popp, B. V.; Peterson J. L.; Wang, K. K. *Org. Lett.,* **2014**, *16*, 2672.
9. Horgen, S. T.; Procopiou, P. A.; Vinader Brugarolas, M. V. PCT Int. Appl. WO 2007071691 May 28, 2007.
10. Krysan, D. J.; Macknzie, P. B. *J. Org. Chem*. **1990**, *55*, 4229.
11. Altomare, A.; Burla, M. C.; Camalli, M.; Cascarano, G. L.; Giacovazzo, C.; Guagliardi, A.; Moliterni, A. G. G.; Polidori, G.; Spagna, R. *J. Appl. Crystallogr.* **1999**, *32,* 115.
12. G. M. Sheldrick, University of Göttingen: Göttingen, Germany, 1997.

Chapter 3

Synthesis and Properties of [8]-, [10]-, [12]-, and [16]Cyclo-1,4-naphthylenes

Abstract: To obtain diverse sizes of potential precursors for carbon nanobelts, [8]-, [10]-, [12]-, and [16]CNs were synthesized. Novel extended L-shaped units, quaternaphthylene- or quinquenaphthylene-convertible molecules, were firstly prepared. The nickel- or palladium-mediated couplings of the extended L-shaped units followed by the aromatization of the coupling products afforded [8]-, [10]-, [12]-, and [16]CNs. The size-dependent properties of these CNs were confirmed by measuring their UV–vis absorption and fluorescence. The theoretical studies also indicated the unique effects of the number of naphthalene rings on the structural and photophysical properties of CNs.

1. Introduction

After the successful synthesis of [9]cyclo-1,4-naphthylene ([9]CN) described in Chapter 2,[1] other sizes of CNs have also received much attention as potential precursors of carbon nanobelts. According to our synthetic strategy, carbon nanobelts would be obtained by multiple cyclodehydrogenation reactions of CNs. The reactivity of CNs may differ depending on their ring size. Because the strain energy decreases as the ring size increases, large CNs are better precursors than small CNs (Figure 1). On the other hand, large CNs requires many bond formation reactions for the transformation to carbon nanobelts than small CNs. As the best ring size of CN is unpredictable, the author attempted the synthesis of several sizes of CNs.

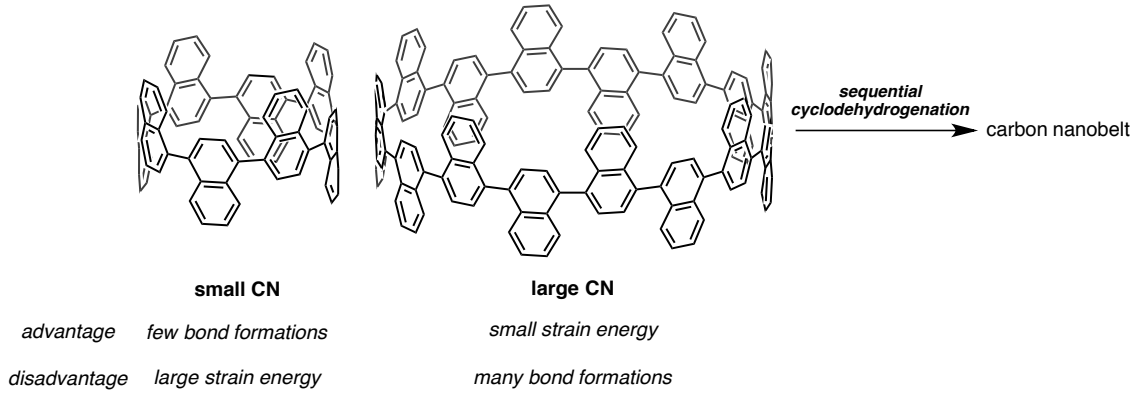

Figure 1. Small and large CNs as precursors of carbon nanobelts.

To obtain various sizes of CNs, the synthetic strategy yielding various sizes of cycloparaphenylenes (CPPs) was applied.[2] Previously, the groups of Jasti, Itami, and Yamago have succeeded in the syntheses of several sizes of CPPs in a modular fashion (Figure 2). The coupling reactions of the L-shaped units with the linear units afforded various unstrained macrocycles, which were transformed to the corresponding CPPs by aromatization. To date, [5]–[16]CPP and [18]CPP have been synthesized using this strategy. Thus, the author envisioned that several sizes of CNs should also be synthesized using the L-shaped and linear naphthylene units.

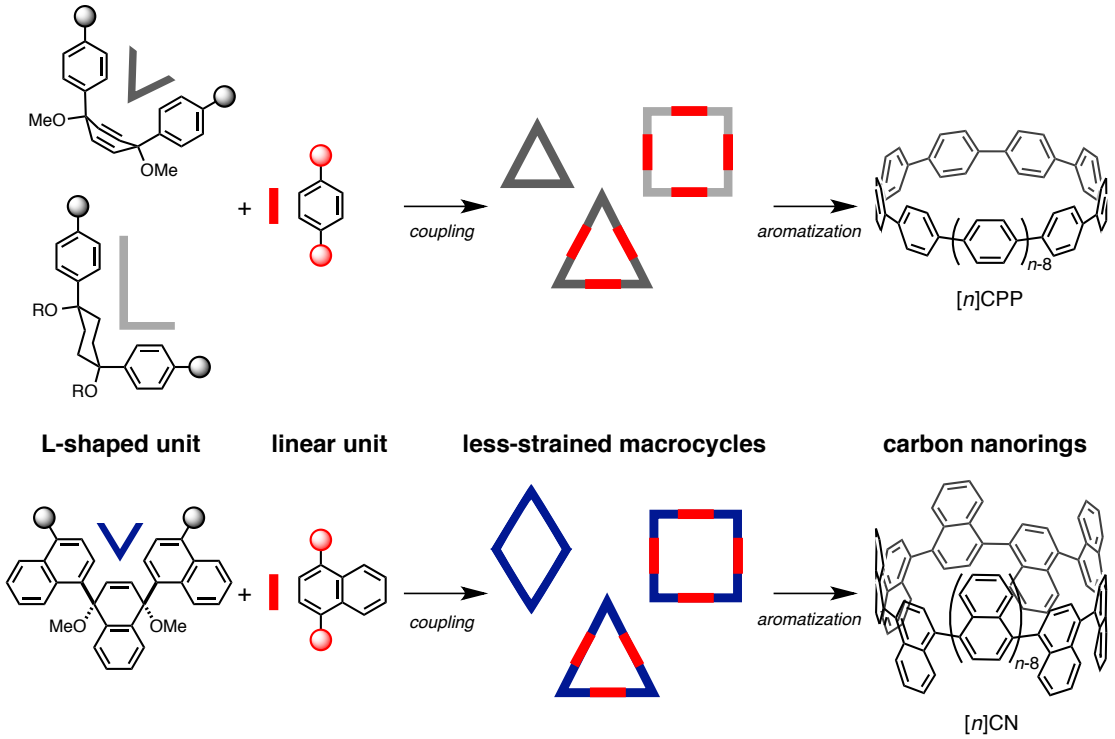

Figure 2. Synthetic strategy for several sizes of CNs.

In this chapter, the syntheses of [8]-, [10]-, [12]-, and [16]CNs are described (Figure 3). The above-mentioned synthetic strategy successfully afforded these four sizes of CNs. The structural and photophysical properties of these CNs were also investigated, and unique effects generated by different numbers of naphthalene rings were observed. In the final part, theoretical studies of [6]–[16]CNs were performed, and the size-dependencies on the structures, strain energies, and molecular orbitals are discussed.

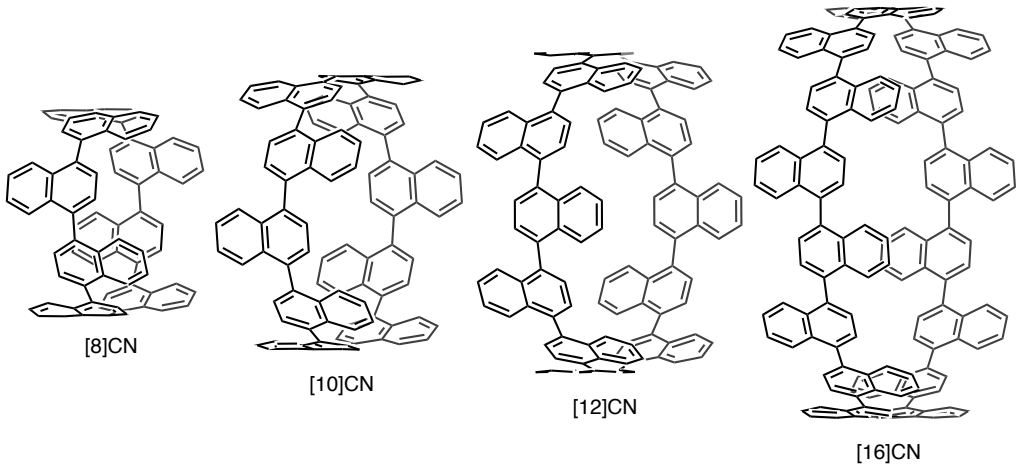

Figure 3. Structures of [8]-, [10]-, [12]-, and [16]CNs.

2. Results and discussion

2-1. Synthesis of [8]-, [10]-, [12]-, and [16]CNs

2-1-1. Synthesis of L-shaped units 5 and 6

As noted in Chapter 2, the cyclization of **2** afforded only [9]CN. To synthesize several sizes of CNs, other L-shaped units are required. Therefore, novel L-shaped units **5** or **6** were synthesized (Scheme 1). First, bis(pinacolato)diboronate **4** was synthesized by the Miyaura borylation reaction of dibromide **2** in 58% yield.[3] Next, the Suzuki–Miyaura cross-coupling reaction of **4** with 2.5 equiv of 1,4-dibromonaphthalene furnished **5**, a quaternaphthylene-convertible unit, in 34% yield.[4] The reaction with an excess amount of 1,4-dibromonaphthalene (5.0 equiv of **4**) afforded **6**, a quinquenaphthylene-convertible unit, in 71% yield.

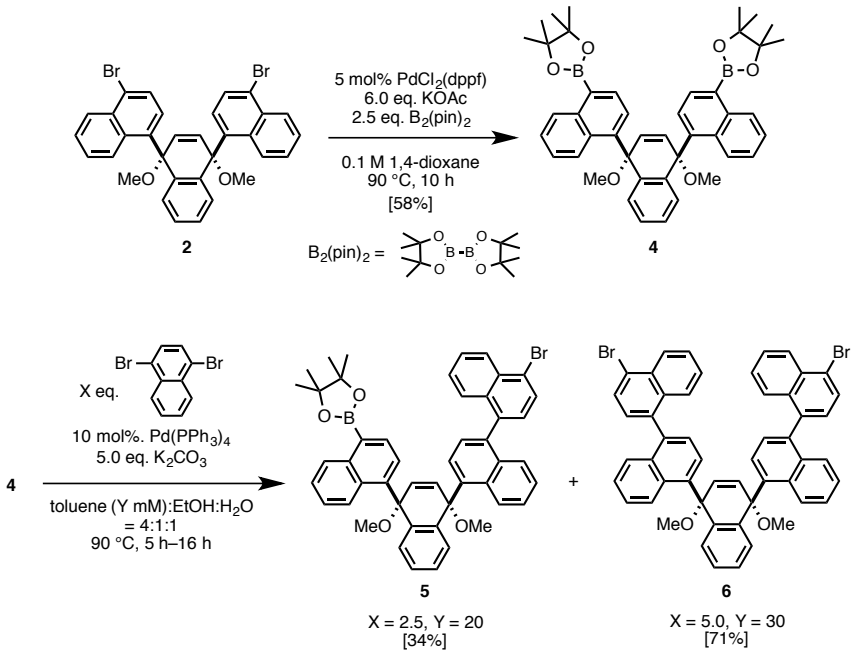

Scheme 1. Synthesis of **5** and **6**.

2-1-2. Synthesis of [8]-, [12]-, and [16]CNs

To obtain cyclic oligomers, **5** was subjected to Suzuki–Miyaura cross-coupling reaction (Scheme 2). The products were purified by preparative recycling gel permeation chromatography (GPC). In the GPC chart, some products were detected whose molecular weights were higher than cyclic trimer **3**. However, the products could not be identified by ^{1}H NMR and mass spectrometry because of complicated spectra. Therefore, the coupling product mixtures were subjected to reductive aromatization using granular lithium. As a result, [8]-, [12]-, and [16]CNs were successfully isolated in 0.3%, 1.5%, and 0.4% yields over two steps, respectively. This result indicates that the cross-coupling reaction of **5** produced the corresponding cyclic dimer, trimer, and tetramer, whereas the homocoupling of **2** only afforded a cyclic trimer. This is probably because of the flexibility of large L-shaped unit **5**, generating the unfavorable cyclic dimer and tetramer in addition to the favorable cyclic trimer.

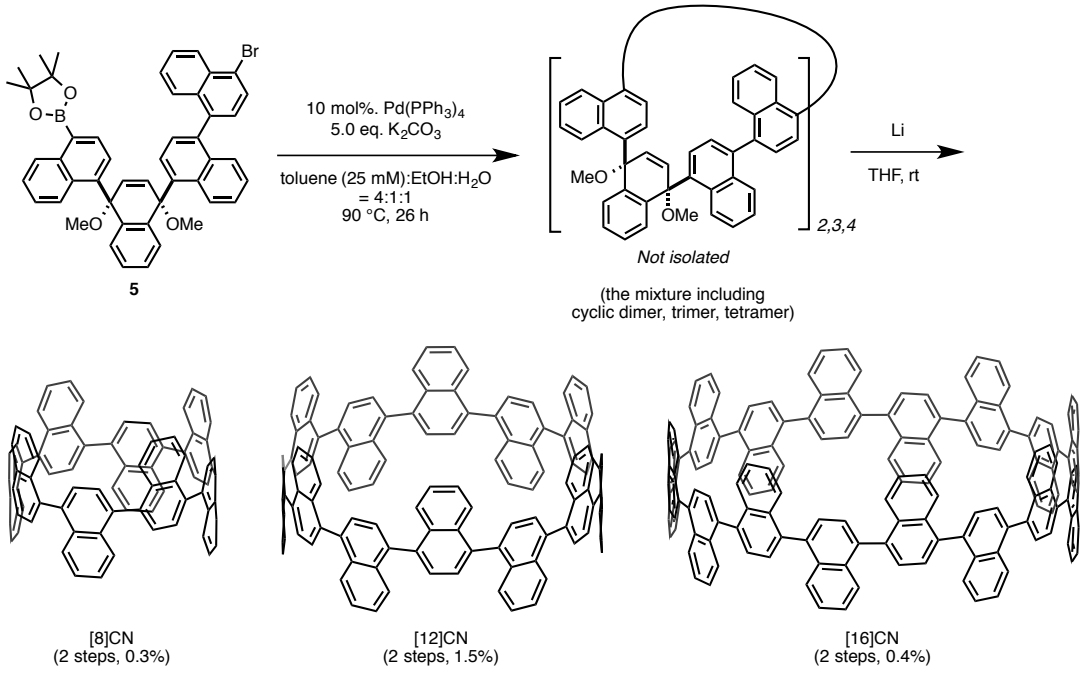

Scheme 2. Synthesis of [8]CN, [12]CN, and [16]CN.

2-1-3. Synthesis of [10]cyclo-1,4-naphthylene ([10]CN)

The other L-shaped unit **6** is also a possible precursor of CNs. The treatment of **6** (1.0 equiv, 1.0 mM) with $Ni(cod)_2$ (2.2 equiv) and 2,2′-bipyridyl (2.2 equiv) in DMF at 85 °C furnished a mixture of coupling products (Scheme 3). After the following reductive aromatization, [10]CN was isolated in 0.5 % yield over two steps. This indicates that the mixture of coupling products contained a cyclic dimer. [15]CN, which can be obtained from a cyclic trimer, was also detected, but not isolated yet. [20]CN was not detected by the mass analysis of the aromatization product, presumably because the precursor (cyclic tetramer) or [20]CN did not dissolve in normal organic solvents and was lost during the purification.

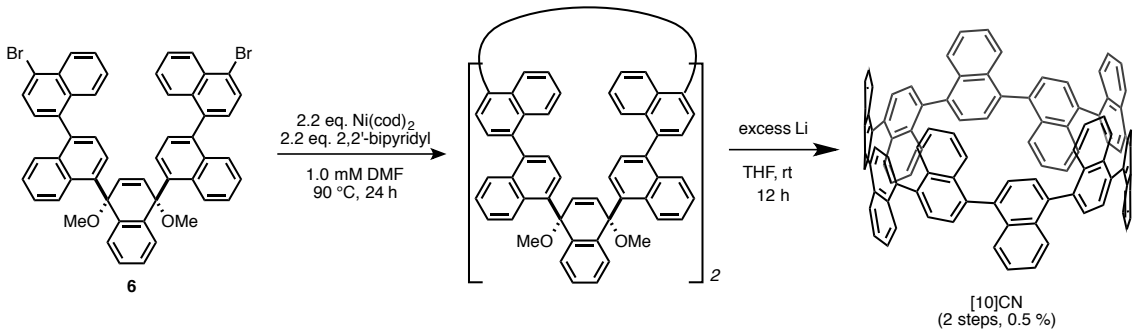

Scheme 3. Synthesis of [10]CN.

2-2. Properties of [8]-, [10]-, [12]-, and [16]CNs

2-2-1. Structural features of [8]-, [10]-, [12]-, and [16]CNs

Here, the structural features of [8]-, [10]-, [12]-, and [16]CNs are discussed. The ^{1}H NMR spectra of [8]-, [10]-, [12]-, and [16]CNs in CD_2Cl_2 are shown in Figure 4. These even-numbered CNs showed simple spectra with three types of proton signals assigned to the 2,3- (red), 5,8- (green), and 6,7-positions (blue) of naphthalene units. These spectra indicated highly symmetric structures of [8]-, [10]-, [12]-, and [16]CNs in solutions in contrast to that of [9]CN (Figure 4, Chapter 2). The NMR signals of the hydrogen atoms on the 2,3-positions (red) of naphthalene units shifted upfield as the (n) value in [n]CN decreased (Table 1). To determine the main effect on the chemical shifts that is dependent on the ring size, e.g., through-bond (e.g., C2–C3 bond orders, hybridization) or through-space interactions, the structural and magnetic properties are discussed below along with DFT calculations.

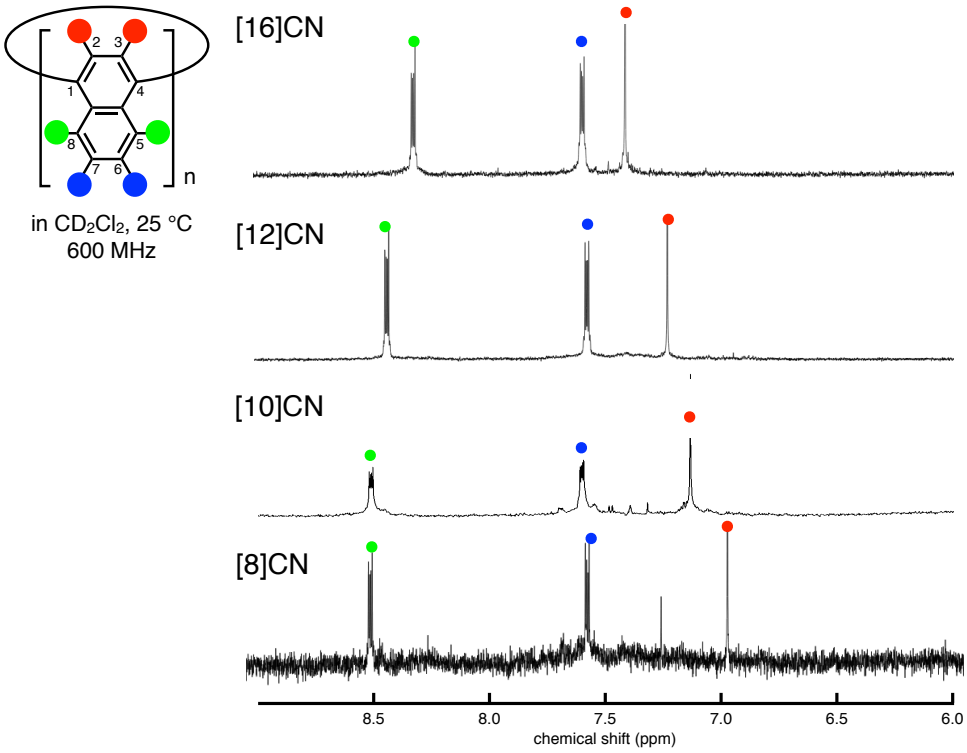

Figure 4. ^{1}H NMR spectra of [8]-, [10]-, [12]-, and [16]CNs.

Table 1. Chemical shifts (δ ppm) of CNs in CD_2Cl_2.

n in [*n*]CN	8	10	12	16
2,3-position	6.98	7.14	7.27	7.43
5,8-position	8.52	8.51	8.48	8.34
6,7-position	7.59	7.61	7.61	7.61

To clarify the differences in chemical shifts, structure optimization and GIAO calculations were performed for CNs at the B3LYP/6-31G(d) level. The optimized structures are shown in Figure 5, and the structural data are summarized in Table 2. The highly symmetric structures (D_{4d} for [8]CN, D_{5d} for [10]CN, D_{6d} for [12]CN, and D_{8d} for [16]CN) were the most stable, which are consistent with their simple ^{1}H NMR spectra. The GIAO calculations of the optimized structures afforded their chemical shifts, which well corresponded to the measured chemical shift values. The bent angles (α, β (°)) of CNs were also estimated.[5] Both the α and β in [8]CN were larger than those in [16]CN by ca. 6°, i.e., the naphthalene rings became distorted as the ring size of CN decreased, indicating the presence of through-bond electronic influence on the corresponding hydrogen atoms. Then, the carbon–carbon bond length (*a*, *b*) and NICS(0) values for six-membered rings attached with corresponding hydrogen atoms were estimated. These values indicated no significant difference in the aromaticity of the naphthalene rings in each CN. Thus, the through-bond electronic influence seems to be small. Next, the through-space magnetic shielding effects of the neighboring naphthalene rings on the hydrogen atoms at the 2,3-positions were investigated. The corresponding hydrogen atom and neighboring naphthalene ring were extracted from the optimized structure. The hydrogen atom was set to a dummy atom, and its shielding constant was calculated for each CN. The shielding constant increased as the (*n*) value in [*n*]CN decreased, corresponding to the observed upfield chemical shifts. This result shows that the through-space magnetic shielding by the neighboring naphthalene rings caused the upfield chemical shifts of the protons at the 2,3-positions. As shown in Figure 4 of Chapter 2, the shielding of neighboring naphthalene rings caused the upfield shift of the NMR signals of the hydrogen atoms of [9]CN. A similar effect was observed in [8]-, [10]-, [12]-, and [16]CNs. It is also reasonable that the larger the bent angles become, the stronger the shielding effects become on the hydrogen atoms at the 2,3-positions. Therefore, the NMR signals of the hydrogen atoms at the 2,3-positions shifted upfield as the (*n*) value in [*n*]CN decreased.

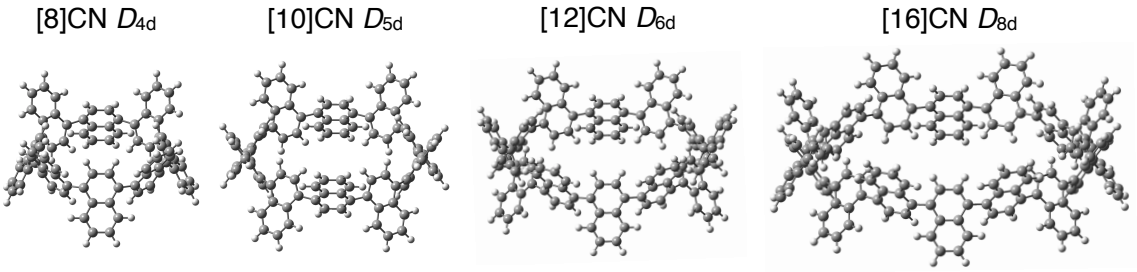

Figure 5. Optimized structures of [8]-, [10]-, [12]-, and [16]CNs.

Table 2. Structural data of optimized structures of [8]-, [10]-, [12]-, and [16]CNs. Estimated chemical shifts (ppm), bond lengths (*a*, *b* (Å)), NICS(0) (ppm), averaged bent angles (α, β (°)), and the shielding constant of the dummy atom (ppm).

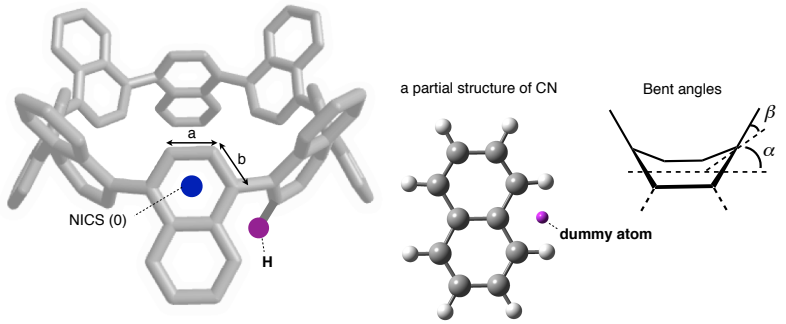

n in [*n*]CN	8	10	12	16
(2,3-position) (ppm)	6.93	7.04	7.18	7.33
(5,8-position) (ppm)	8.30	8.32	7.53	8.25
(6,7-position) (ppm)	7.48	7.51	8.30	7.54
a (Å)	1.406	1.406	1.406	1.407
b (Å)	1.388	1.387	1.386	1.385
NICS(0) (ppm)	–8.00	–8.08	–8.09	–8.11
Bent angle α (°)	11.6	8.4	7.1	5.5
Bent angle β (°)	12.5	10.2	8.5	6.4
Shielding constant (ppm)	–0.61	–0.51	–0.43	–0.31

2-2-2. Photophysical properties of [8]-, [10]-, [12]-, and [16]CNs

The photophysical properties including UV–vis absorption and fluorescence of [8]-, [10]-, [12]-, and [16]CNs were investigated. The spectra of these CNs in dichloromethane are depicted in Figure 6, and the photophysical data are lined in Table 2. In the UV–vis absorption spectra, the absorption bands with the maximum absorption wavelength (λ_{abs1}) shifted to shorter wavelengths as the (n) value in [n]CN increased. This tendency is opposite to that of linear polyarylenes, which are known for shifting absorption bands to longer wavelengths with increasing (n) in [n]polyarylenes.[6] By using a peak deconvolution program, the maximum absorption wavelengths of the shoulder-shaped absorption bands (λ_{abs2}) were determined. As depicted in Table 2, λ_{abs2} and λ_{abs1} shifted to shorter wavelengths as the (n) value in [n]CN increased. Intense photoluminescence was observed in solutions of all the CNs, and their emission wavelength depended on the ring size similar to the UV–vis absorption. Namely, the emission maxima blue-shifted with the increase in the (n) values in [n]CN. The shapes of the fluorescence spectra of all the CNs were not depended on the excitation wavelength, indicating that these peaks in the emission spectra originated from one excited state. The absolute fluorescence quantum yields (Φ_F) of the CNs in dichloromethane were measured (Table 3). The Φ_F values of the CNs increased as the (n) value in [n]CN increased, similar to CPPs.[5]

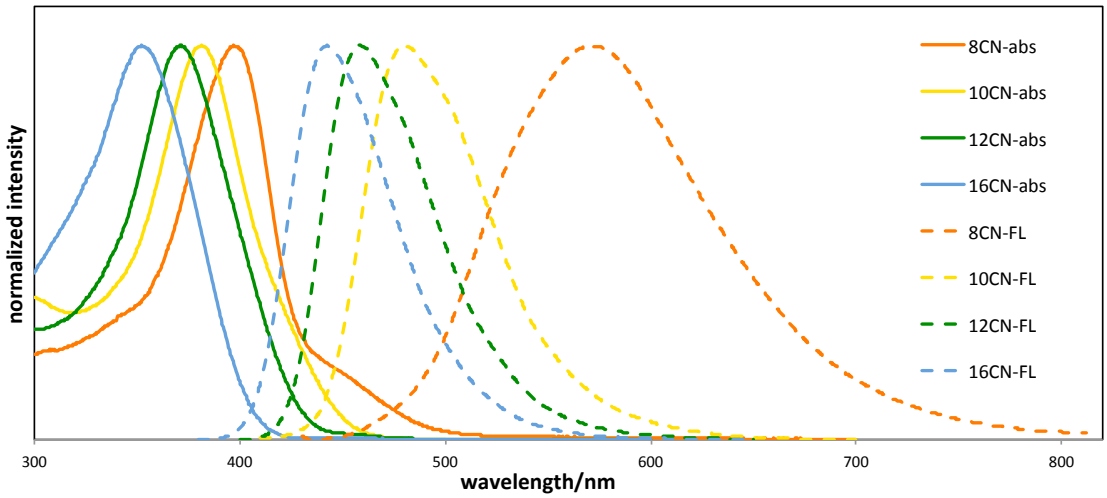

Figure 6. UV–vis absorption spectra (solid line) and fluorescence spectra (broken line) of [8]-, [9]-, [10]-, [12]-, and [16]CNs in dichloromethane. Absorption and fluorescence spectra were normalized.

Table 2. Photophysical data for [*n*]CNs.[a]

Compound	Absorption		Fluorescence	
	λ_{abs1} [nm][b]	λ_{abs2} [nm][c]	λ_{em} [nm]	Φ_F
[8]CN	397	447	580	0.23
[10]CN	381	424	480	0.37
[12]CN	371	406	458	0.40
[16]CN	350	378	442	0.43

[a]In dichloromethane. [b]The highest absorption maxima are given. [c]The longest absorption maxima determined by a peak separation method are given. [d]Emission maxima upon excitation at the excitation maxima λ_{abs1} [e]Absolute fluorescence quantum yields determined by a calibrated integrating sphere system within 3% error.

To investigate the photophysical properties deeply, particularly the size-dependency of the MOs, TD-DFT calculations of [8]-, [10]-, [12]-, and [16]CNs were performed at the B3LYP/6-31G(d) level. It was found that the shapes of the orbitals, degeneracy features, and transitions were identical and irrespective of the ring size. The energy diagrams of six frontier molecular orbitals from HOMO–2 to LUMO+2 and pictorial representations of these six orbitals of [12]CN are shown in Figure 7. In the MOs of [12]CN with a D_{6d} symmetry, the HOMO and LUMO are delocalized over the ring, whereas HOMO–1, HOMO–2, LUMO+1, and LUMO+2 are delocalized to two opposite sides with a C_s symmetry. In the energy levels, the degeneracy was seen in the pairs of frontier orbitals, HOMO–1/HOMO–2 (–5.07 eV) and LUMO+1/LUMO+2 (–1.57 eV). Judging from the shape of each orbital, the occupied and unoccupied orbitals represent the π and π* frontier orbitals of conjugated poly-1,4-naphthylenes. The TD-DFT calculations indicates that two energetically low-lying characteristic transitions originate from the set of six orbitals: one of the transitions is a forbidden HOMO→LUMO transition with an oscillator strength (*f*) of 0.00 (excites state 1); the other transition is a degenerate transition in which both the HOMO–1→LUMO and HOMO→LUMO+1 excitations are mixed with a high *f* value of 1.216 for [12]CN (excited states 2 and 3). These transitions are all π–π* transitions. Compared to the absorption spectrum of [12]CN, excited states 2 and 3 should correspond to λ_{abs1}, and the shoulder peak λ_{abs2} should correspond to excited state 1. The deformation away from a high symmetry owing to a dynamic conformational change might be responsible for the forbidden transition.

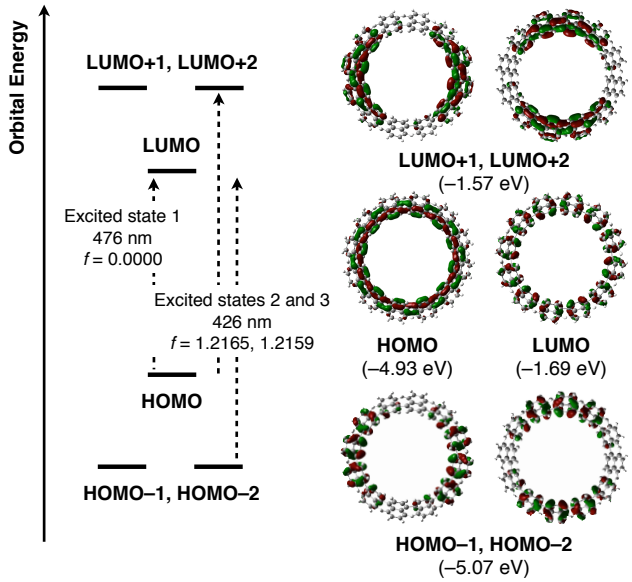

Figure 7. Energy diagrams and pictorial representations of the frontier MOs for [12]CN, calculated at the B3LYP/6-31G(d) level of theory. Excitation energies were computed using TD-DFT at the same level.

Figure 8 shows the molecular orbital energies for [8]-, [10]-, [12]-, and [16]CNs. The HOMO level increased and the LUMO level decreased with the increase in the (*n*) value in [*n*]CN. On the other hand, the energies of HOMO–1 and LUMO+1 did not change significantly with the (*n*) value in [*n*]CN. The observed red-shift of λ_{abs1}, λ_{abs2}, and λ_{em} with the decrease in the (*n*) value in [*n*]CN can be explained by the transitions and plots shown in Figure 8. The HOMO and LUMO behaviors were similar to those of CPPs,[5] opposite to those of linear polyarylenes.[6] The origin of this behavior can be ascribed to the lack of energy dependence of frontier MOs on the conjugation length and the significant effects of bending and twisting naphthalene rings on the orbital energies, as in the case of CPPs.

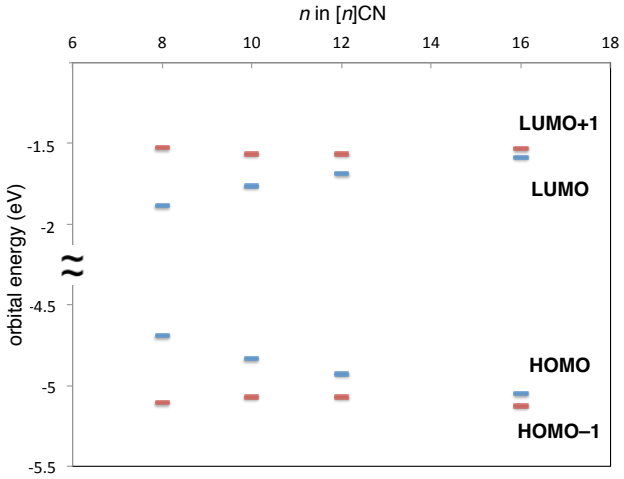

Figure 8. Molecular orbital energies for [8]-, [10]-, [12]-, and [16]CNs.

2-3. Theoretical studies of [6]–[16]CNs

2-3-1. Optimized structures of CNs

For a better understanding of the size-dependency of CNs, the DFT calculations were conducted for all [6]–[16]CNs at the B3LYP/6-31G(d) level. First, the most stable conformation of each CN was estimated (Figure 9). The calculations showed that the structures of even-numbered CNs have high symmetries, whereas those of all the odd-numbered CNs have low symmetries. As already described, [8]-, [10]-, [12]-, and [16]CNs have a D_{md} symmetry for [n]CN where $m = n/2$. [14]CN also has a highly symmetric structure (D_{7d}). The most stable conformation of [6]CN was also highly symmetric, estimated as S_6. On the other hand, the structure of [9]CN has a low symmetry of C_2 (Chapter 2). It was found that [11]-, [13]-, and [15]CN have a C_2 symmetry as well. For [7]CN, only the conformation with a C_1 symmetry was observed.

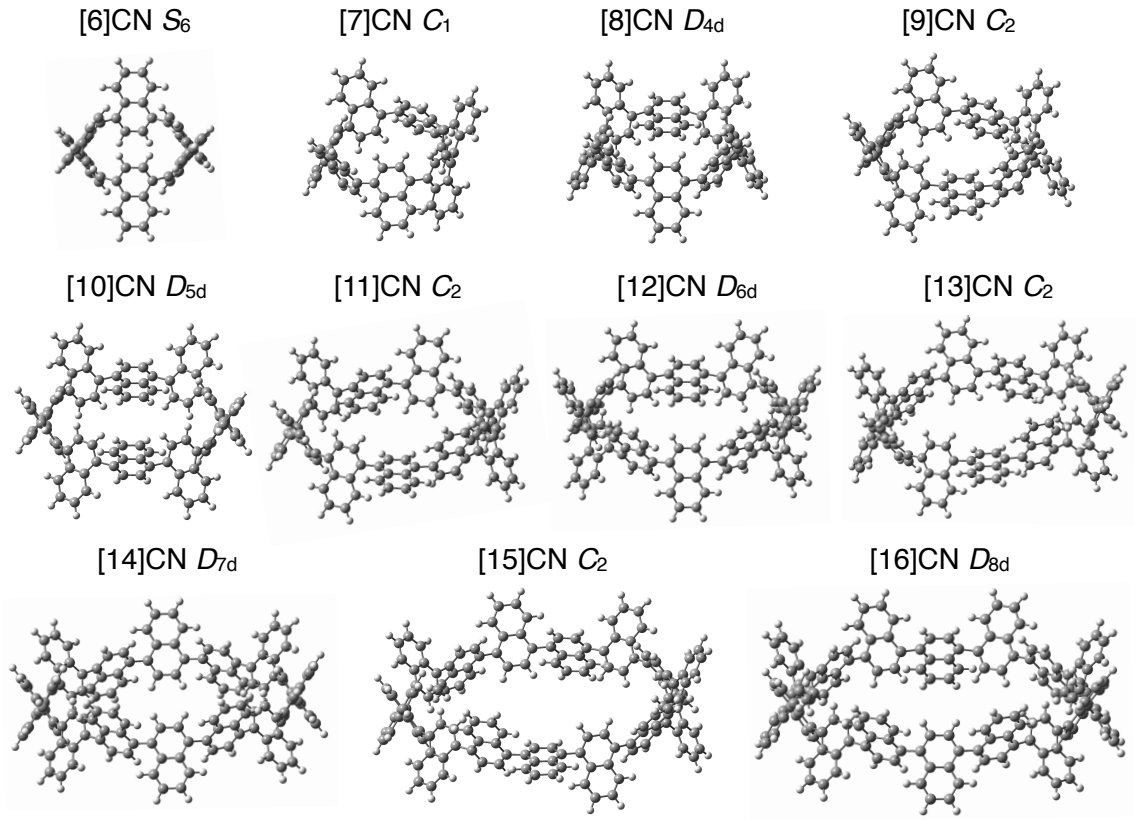

Figure 9. Optimized structures of [6]–[16]CNs.

2-3-2. Strain energies of CNs

The optimization of the structures of CNs enabled the estimation of the strain energies of the CNs using DFT calculations.[7] Hypothetical homodesmotic reactions, where the *n* number of ternaphthyl is produced from [*n*]CN and the *n* number of binaphthyl, were utilized. The heat of formation (ΔH) of the optimized structures of these molecules was applied to the reaction formula to obtain the strain energies (Scheme 4). As expected, the strain energy decreased as the diameter of CN increased (Table 3). Compared to CPPs, the strain energies of CNs are lower than those of CPPs, whereas the diameters of [*n*]CN and [*n*]CPP are similar. Because of the relatively low aromaticity of a naphthalene ring than a benzene ring, CNs would need low energies to bend the arenes.

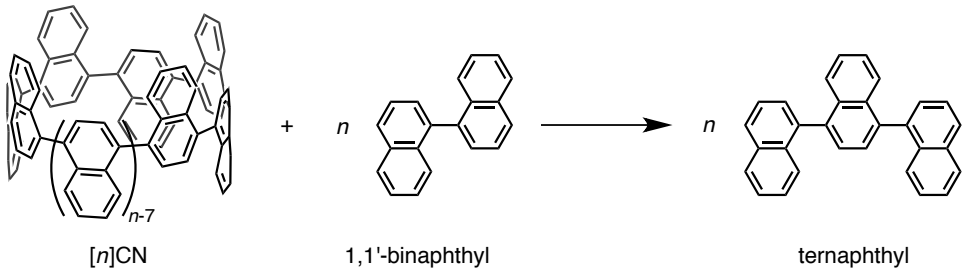

Scheme 4. Hypothetic homodesmotic reactions for the estimation of strain energies of CNs.

Table 3. Strain energies and diameters of [*n*]CN and [*n*]CPP.

n in [*n*]CN or [*n*]CPP	strain energy of CN (kcal·mol^{-1})[a]	diameter of CN (Å)[b]	strain energy of CPP (kcal·mol^{-1})	diameter of CPP (Å)
6	73.3	8.4	96.0	8.4
7	71.4	–	84.0	9.5
8	50.6	11.2	72.2	11.1
9	50.4	–	65.6	12.3
10	37.0	13.9	57.7	13.9
11	36.9	–	53.7	15.1
12	27.8	16.7	48.1	16.6
13	27.8	–	45.5	17.9
14	–	19.4	41.0	19.4
15	21.4	–	39.2	20.6
16	–	22.2	35.6	22.1

(a) For [14]CN and [16]CN, the energies were not able to be estimated. (b) The diameters of odd-numbered CNs could not be estimated due to their elliptical shapes.

2-3-3. Molecular orbitals of CNs

In addition to [8]-, [9]-, [10]-, [12]-, and [16]CNs, the TD-DFT calculations for the other CNs from [6]CN to [15]CN were performed. The plots for the molecular orbital energies of the CNs and CPPs are shown in Figure 10. Notably, the energy profiles of the odd-numbered CNs do not follow the tendency of those of even-numbered CNs unlike those of CPPs. This is probably because the π-conjugation is not connected circularly in the odd-numbered CNs as shown for [9]CN in Chapter 2.

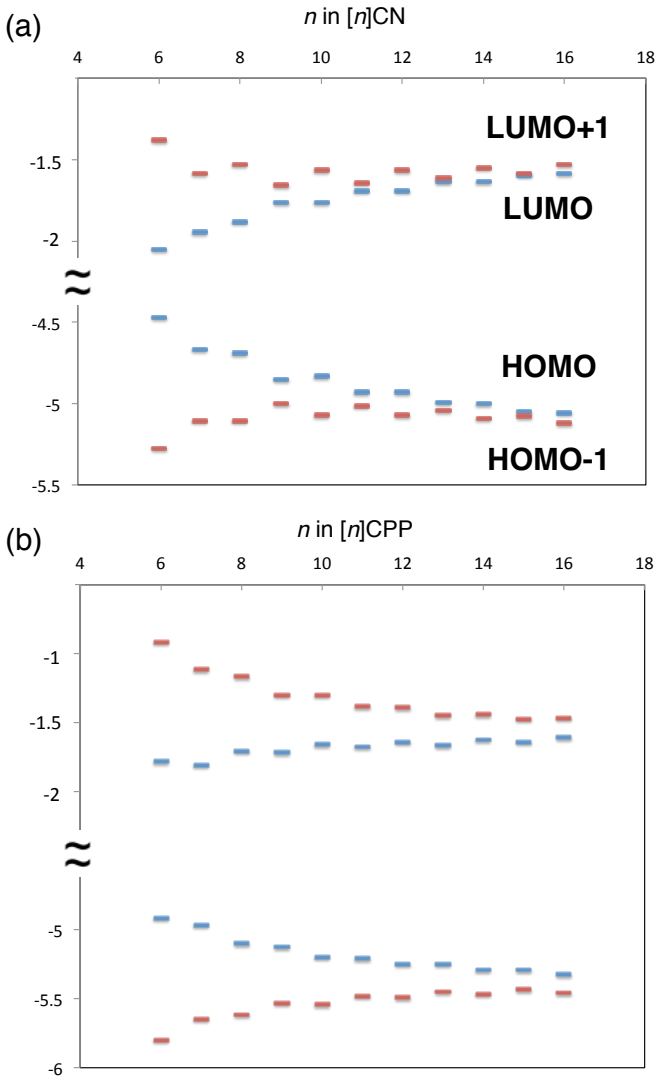

Figure 10. Molecular orbital energies for (a) [*n*]CN and (b) [*n*]CPP.

3. Conclusion

In conclusion, [8]-, [10]-, [12]-, and [16]CNs were synthesized using the modular synthesis methods for CPPs. Unlike the complicated ^{1}H NMR spectrum of [9]CN, [8]-, [10]-, [12]-, and [16]CNs showed simple ^{1}H NMR spectra, indicating the presence of highly symmetric structures in solutions. The size-dependent electronic properties of CNs were confirmed from the UV–vis absorption and fluorescence spectra. The structural and electronic features of CNs were better understood by the theoretical studies of [6]–[16]CNs. The developed method in this chapter can be used to synthesize other sizes of CNs as well. The synthesis of precursors with diverse sizes represents a significant step towards the synthesis of carbon nanobelts.

4. Experimental section

4-1. General

Unless otherwise noted, all materials including dry solvents (1,4-dioxane and *N,N'*-dimethyformamide) were obtained from commercial suppliers and used without further purification. Tetrahydrofuran (THF) and toluene were purified by passing through a solvent purification system (Glass Contour). All reactions were performed using standard vacuum-line and Schlenk techniques. Work-up and purification procedures were carried out with reagent-grade solvents under air unless otherwise noted. 1,4-Dibromonaphthalene was prepared according to procedures reported in the literatures.[8]

Analytical thin-layer chromatography (TLC) was performed using E. Merck silica gel 60 F254 precoated plates (0.25 mm). The developed chromatogram was analyzed by UV lamp (254 nm and 365 nm). Flash column chromatography was performed with E. Merck silica gel 60 (230–400 mesh). Preparative thin-layer chromatography (PTLC) was performed using Wako-gel® B5-F silica coated plates (0.75 mm) prepared in our laboratory. Preparative gel permeation chromatography (GPC) was performed with a JAI LC-9204 instrument equipped with JAIGEL-2H/JAIGEL-2H columns using chloroform as an eluent. High-resolution mass spectra (HRMS) were obtained from a JEOL JMS700 (fast atom bombardment mass spectrometry, FAB MS) or a JEOL JMS-S3000 SpiralTOF (MALDI-TOF MS) with *trans*-2-[3-(4-tert-Butylphenyl)-2-methyl-2-propenylidene]malononitrile as matrix. Nuclear magnetic resonance (NMR) spectra were recorded on a JEOL JNM-ECA-600 (^{1}H 600 MHz, ^{13}C 150 MHz) spectrometer. Chemical shifts for ^{1}H NMR are expressed in parts per million (ppm) relative to $CHCl_3$ (δ 7.26 ppm) and $CHDCl_2$ (δ 5.32 ppm). Chemical shifts for ^{13}C NMR are expressed in ppm relative to $CDCl_3$ (δ 77.0 ppm) and CD_2Cl_2 (δ 53.8 ppm). Data are reported as follows: chemical shift, multiplicity (s = singlet, d = doublet, dd = doublet of doublets, ddd = doublet of doublets of doublets, t = triplet, m = multiplet), coupling constant (Hz), and integration.

UV/Vis absorption spectra of CNs were recorded on a Shimadzu UV-3510 spectrometer with a resolution of 0.5 nm. Emission spectra of CNs was measured with an F-4500 Hitachi spectrometer with a resolution of 0.4 nm upon excitation at each absorption maximum wavelength. Dilute solution in degassed spectral grade dichloromethane in a 1 cm square quartz cell was used for measurements. Absolute fluorescence quantum yield was determined with a

Hamamatsu C9920-02 calibrated integrating sphere system upon excitation at each absorption maximum wavelength.

Synthesis of L-shaped unit 4 by Miyaura-borylation of 2

To a two-necked 100 mL glass round bottom flask containing a magnetic stirring bar were added **2** (2.50 g, 4.16 mmol), $PdCl_2$(dppf) (170 mg, 208 μmol), dried KOAc (2.45 g, 25.0 mmol), and bis(pinacolate)diboron (2.67 g, 10.4 mmol), and the flask was evacuated and backfilled with argon three times. Then, dry 1,4-dioxane (42 mL) was added via syringe. After stirring at 90 °C for 10 h, the mixture was passed through a short pad of silica gel (EtOAc) and the solvent was removed under reduced pressure. The crude product was subjected to preparative recycling gel permeation chromatography to afford **4** (1.68 g, 58%) as a white solid.

^{1}H NMR (600 MHz, $CDCl_3$) δ 1.39 (s, 12H), 1.40 (s, 12H), 3.36 (s, 6H), 6.74 (s, 2H), 7.10–7.21 (bs, 2H), 7.31–7.42 (m, 4H), 7.45 (ddd, *J* = 8.4, 6.6, 1.2 Hz, 2H), 7.56 (dd, *J* = 6.0, 3.6 Hz, 2H), 7.88 (d, *J* = 7.2 Hz, 2H), 8.75 (d, *J* = 7.2 Hz, 2H), 8.77–8.87 (bs, 2H); ^{13}C NMR (150 MHz, CD_2Cl_2) δ 25.0 (CH_3), 25.1 (CH_3), 51.6 (CH_3), 79.8 (4°), 84.2 (4°), 125.2 (CH), 125.7 (CH), 126.3 (CH), 127.7 (CH), 128.7 (CH), 129.4 (CH), 129.6 (CH), 131.6 (4°), 132.9 (CH), 134.6 (CH), 138.6 (4°), 139.5 (4°), 143.5 (4°); HRMS (FAB) *m/z* calcd. for $C_{44}H_{48}NaO_6B_2$ $[M\cdot Na]^+$: 717.3535, found: 717.3539.

Synthesis of L-shaped unit 5 by Suzuki–Miyaura cross coupling of 4 and 1,4-dibromonaphthalene

To a two-necked 100 mL glass round bottom flask containing a magnetic stirring bar were added **4** (400 mg, 576 μmol), K_2CO_3 (398 mg, 2.88 mmol), and 1,4-dibromonaphthalene (416 mg, 1.44 mmol), and the flask was evacuated and backfilled with argon three times. Then, dry toluene (29 mL, 20 mM) was added via syringe. Subsequently, degassed EtOH (7 mL) and degassed distilled water (7 mL) were added. Then, $Pd(PPh_3)_4$ (66.6 mg, 57.6 μmol) was added under argon flow, and the mixture was stirred at 90 °C for 5 h. After the reaction mixture was cooled to room temperature, brine (ca. 50 mL) was added to the mixture. The mixture was extracted with EtOAc (50 mL × 3). The combined organic phase was then purified by silica chromatography (hexane:EtOAc=30:1–>20:1) and preparative recycling gel permeation chromatography ($CHCl_3$) to afford compound **5** (150 mg, 34%) as a white solid.

^{1}H NMR (600 MHz, CD_2Cl_2) δ 1.33 (s, 6H), 1.34 (s, 6H), 1.37 (s, 12H), 3.36 (s, 6H), 3.41 (s, 6H), 6.77 (d, *J* = 10.1 Hz, 1H), 6.77 (d, *J* = 10.7 Hz, 1H), 6.92 (d, *J* = 10.7 Hz, 1H), 6.94 (d, 10.7 Hz, 1H), 7.12 (d, *J* = 7.4 Hz, 1H), 7.15 (d, *J* = 7.4 Hz, 1H), 7.18 (d, *J* = 7.7 Hz, 1H) 7.21-7.64 (m, 27H) 7.73 (d, *J* = 7.9 Hz, 1H), 7.78 (d, *J* = 9.3 Hz, 1H), 7.79 (d, *J* = 7.2 Hz, 1H), 7.80 (d, *J* = 7.3 Hz, 1H), 7.87 (d, *J* = 7.6 Hz, 1H), 7.90 (d, *J* = 7.6 Hz, 1H), 8.32 (d, *J* = 6.2 Hz, 1H) 8.32 (d, *J* = 8.4 Hz, 1H), 8.74 (d, *J* = 8.5 Hz, 2H), 8.85 (d, *J* = 7.9 Hz, 2H), 9.02 (d, *J* = 8.4 Hz, 1H); ^{13}C NMR (150 MHz, CD_2Cl_2) δ 25.0 (CH_3), 25.0 (CH_3), 25.1 (CH_3), 51.6 (CH_3), 51.6 (CH_3), 51.8 (CH_3), 51.8 (CH_3), 79.6 (4°), 79.6 (4°), 80.0 (4°) 80.1 (4°), 84.2 (4°), 84.2 (4°), 122.8 (CH), 125.3 (CH), 125.7 (CH), 125.7 (CH), 125.7 (CH), 125.8 (CH), 125.8 (CH), 125.8 (CH), 126.2 (CH), 126.2 (CH), 126.9 (CH), 126.9 (CH), 127.2 (CH), 127.2 (CH), 127.6 (CH), 127.6 (CH), 127.7 (CH), 127.7 (CH), 127.9 (CH), 128.0 (CH), 128.5 (CH), 128.8 (CH), 128.8 (CH), 128.9 (CH), 128.9 (CH), 129.4 (CH), 129.4 (CH), 129.5 (CH), 129.6 (CH), 129.6 (CH), 129.9 (CH), 131.4 (CH), 131.5 (CH), 132.1 (CH), 132.2 (CH), 133.0 (CH), 133.1 (CH), 133.1 (CH), 133.2 (CH), 134.3 (CH), 134.4 (CH), 134.5 (CH), 134.7 (CH), 138.5 (CH), 138.5 (CH), 138.6 (CH), 139.1 (CH), 139.3 (CH), 139.4 (CH), 139.8 (CH), 139.8 (CH), 140.5 (CH), 140.6 (CH), 143.6 (CH), 143.6 (CH); HRMS (FAB) *m/z* calcd. for $C_{48}H_{42}BrO_4BNa$ $[M{\cdot}Na]^+$: 795.2257, found: 795.2232.

Synthesis of L-shaped unit 6 by Suzuki–Miyaura cross coupling of 4 and 1,4-dibromonaphthalene

To a two-necked 200-mL glass round bottom flask containing a magnetic stirring bar were added **4** (802 mg, 1.15 mmol), K_2CO_3 (796 mg, 5.76 mmol), and 1,4-dibromonaphthalene (1.67 g, 5.76 mmol), and the flask was evacuated and backfilled with argon three times. Then, dry toluene (38 mL, 30 mM) was added via syringe. Subsequently, degassed EtOH (9 mL) and degassed distilled water (9 mL) were added. Then, $Pd(PPh_3)_4$ (133 mg, 115 μmol) was added under argon flow, and the mixture was stirred at 90 °C for 16 h. After the reaction mixture was cooled to room temperature, brine (ca. 100 mL) was added to the mixture. The mixture was extracted with EtOAc (100 mL × 3). The combined organic phase was then purified by silica chromatography (hexane: EtOAc = 20:1) and preparative recycling gel permeation chromatography ($CHCl_3$) to afford compound **6** (633 mg, 71%) as a white solid.

^{1}H NMR (600 MHz, CD_2Cl_2) δ 3.43 (s, 3H), 3.43 (s, 6H), 3.44 (s, 3H), 6.95 (d, *J* = 6.0 Hz, 4H), 7.06 (t, *J* = 7.2 Hz, 1H), 7.14 (d, *J* = 7.8 Hz, 1H), 7.16-7.25 (m, 14H), 7.27-7.34 (m, 11H),

7.36-7.45 (m, 4H), 7.48 (t, *J* = 7.2 Hz, 1H), 7.51-7.60 (m, 8H), 7.72-7.82 (m, 5H), 7.86 (d, *J* = 7.2 Hz, 1H), 7.86 (d, *J* = 7.8 Hz, 1H), 7.88 (d, *J* = 7.8 Hz, 1H), 8.28 (d, *J* = 8.4 Hz, 1H), 8.29 (d, *J* = 9.0 Hz, 1H), 8.31 (d, *J* = 8.4 Hz, 1H), 8.32 (d, *J* = 8.5 Hz, 1H), 8.98 (d, *J* = 8.4 Hz, 1H), 9.00 (d, *J* = 8.4 Hz, 1H), 9.01(d, *J* = 6.5 Hz, 1H), 9.02 (d, *J* = 8.4 Hz, 1H); ^{15}C NMR (150 MHz, CD_2Cl_2) δ 51.8 (CH_3), 51.8 (CH_3), 79.8 (4°), 79.9 (4°), 80.0 (4°), 80.0 (4°), 122.8 (CH), 122.8 (CH), 122.8 (CH), 125.7 (CH), 125.7 (CH), 125.8 (CH), 125.8 (CH), 125.8 (CH), 126.8 (CH), 126.9 (CH), 127.0 (CH), 127.1 (CH), 127.3 (CH), 127.5 (CH), 127.5 (CH), 127.6 (CH), 127.7 (CH), 127.7 (CH), 127.8 (CH), 127.9 (CH), 127.9 (CH), 127.9 (CH), 128.5 (CH), 128.5 (CH), 128.6 (CH), 128.9 (CH), 128.9 (CH), 129.0 (CH), 129.5 (CH), 129.6 (CH), 129.6 (CH), 129.8 (CH), 129.9 (CH), 129.9 (CH), 129.9 (CH), 132.0 (CH), 132.0 (CH), 132.2 (CH), 133.1 (CH), 133.2 (CH), 133.4 (CH), 133.4 (CH), 134.4 (CH), 134.4 (CH), 134.4 (CH), 138.5 (CH), 138.6 (CH), 138.6 (CH), 139.0 (CH), 139.1 (CH), 139.1 (CH), 139.6 (CH), 139.7 (CH), 139.7 (CH), 140.6 (CH), 140.6 (CH), 140.7 (CH); HRMS (FAB) *m/z* calcd. for $C_{52}H_{36}Br_2O_2Na$ $[M{\cdot}Na]^+$: 873.0980, found: 873.0966.

Synthesis of [8]-, [12]-, and [16]CN

To a two-necked 500 mL glass round bottom flask containing a magnetic stirring bar were added **5** (580 mg, 750 mmol), and the flask was evacuated and backfilled with argon three times. Then, dry toluene (290 mL, 25 mM) was added via syringe. Subsequently, K_2CO_3 (518 mg, 3.75 mmol), degassed EtOH (70 mL) and degassed distilled water (70 mL) were added. Then, $Pd(PPh_3)_4$ (86.6 mg, 75.0 μmol) was added under argon flow, and the mixture was stirred at 90 °C for 26 h. After the reaction mixture was cooled to room temperature, brine (ca. 200 mL) was added to the mixture. The mixture was extracted with EtOAc (200 mL × 3). The combined organic phase was then purified by preparative recycling gel permeation chromatography ($CHCl_3$). The purified products were subjected to the next aromatization step directly. A 30 mL vials containing glass-coated magnetic stirring bars and cyclization products were dried under vacuum and filled with argon after cooling to room temperature. In a glove box, lithium granular (20–30 mg, 2.9–4.3 mmol) and dry THF (3 mL) were added to the vials. The reaction mixtures were stirred at room temperature for 8–12 h. The residues were diluted with hexane and quenched with methanol. After evaporated, the reaction mixtures were passed through a short silica gel pad (CH_2Cl_2). The filtrates were evaporated and respectively purified by PTLC (CH_2Cl_2/hexane = 2:3) to obtain **[8]CN** (1.5 mg, 0.3% over 2 steps) as a orange solid, **[12]CN**

(5.7 mg, 1.5% over 2 steps) as a yellow solid, and **[16]CN** (1.6 mg, 0.4% over 2 steps) as a white solid.

[8]CN: ^{1}H NMR (600 MHz, CD_2Cl_2) δ 6.98 (s, 16H), 7.59 (dd, *J* = 6.6, 3.0 Hz, 16H), 8.52 (dd, *J* = 6.6, 3.0 Hz, 16H). HRMS (MALDI-TOF MS) *m/z* calcd. for $C_{80}H_{48}$ $[M]^+$: 1008.3756, found: 1008.3.

[12]CN: ^{1}H NMR (600 MHz, CD_2Cl_2) δ 7.27 (s, 24H), 7.61 (dd, *J* = 6.6, 3.0 Hz, 24H), 8.48 (dd, *J* = 7.8, 3.6 Hz, 24H); ^{13}C NMR (150 MHz, CD_2Cl_2) δ 126.6 (CH), 127.2 (CH), 129.2 (CH), 134.2 (4°), 138.4 (4°). HRMS (MALDI-TOF MS) *m/z* calcd. for $C_{120}H_{72}$ $[M]^+$: 1512.5634, found: 1512.6.

[16]CN: ^{1}H NMR (600 MHz, CD_2Cl_2) δ 7.43 (s, 32H), 7.61 (dd, *J* = 6.6, 3.6 Hz, 32H), 8.34 (dd, *J* = 6.0, 3.6 Hz, 32H); ^{13}C NMR (150 MHz, CD_2Cl_2) δ 126.6 (CH), 127.3 (CH), 129.1 (CH), 134.0 (4°), 138.6 (4°). HRMS (MALDI-TOF MS) *m/z* calcd. for $C_{160}H_{96}$ $[M]^+$: 2016.7512, found: 2016.7.

Synthesis of [10]CN

To a two-necked 300 mL glass round bottom flask containing a magnetic stirring bar were added **6** ((150 mg, 176 μmol) for A, (120 mg, 141 μmol) for B) and 2,2'-bipyridyl ((60.5 mg, 387 μmol) for A, (48.4 mg, 310 μmol) for B), then the flask was evacuated and backfilled with argon three times. In a glove box, $Ni(cod)_2$ ((107 mg, 387 μmol) for A, (85.1 mg, 310 μmol) for B) was added. Subsequently, dry *N,N'*-dimethylformamide (150 mL, 1 mM) were added via syringe. Then, the mixtures A and B were stirred at 90 °C for 24 h. After the reaction mixtures were cooled to room temperature, brine (ca. 200 mL) was added. The mixtures A and B were combined and extracted with EtOAc (400 mL × 3). The combined organic phase was then purified by preparative recycling gel permeation chromatography ($CHCl_3$) and PTLC (CH_2Cl_2:hexane=2:1). The purified products were subjected to the next aromatization step directly. A 30 mL vial containing glass-coated magnetic stirring bars and cyclization products was dried under vacuum and filled with argon after cooling to room temperature. In a glove box, lithium granular (20 mg, 2.9 mmol) and dry THF (3 mL) were added to the vial. The reaction mixture was stirred at room temperature for 7 h. The residues were diluted with hexane and quenched with methanol. After evaporated, the reaction mixtures were passed through a short silica gel pad (CH_2Cl_2). The filtrates were evaporated and respectively purified by PTLC (CH_2Cl_2/hexane = 2:3) to obtain **[10]CN** (1.5 mg, 0.5% over 2 steps) as a yellow solid.

^{1}H NMR (600 MHz, CD_2Cl_2) δ 7.14 (s, 20H), 7.61 (dd, J = 6.6, 3.0 Hz, 20H), 8.51 (dd, J = 6.6, 3.6 Hz, 20H); ^{13}C NMR (150 MHz, CD_2Cl_2) δ 126.6 (CH), 127.2 (CH), 129.3 (CH), 134.2 (4°), 138.5 (4°). HRMS (MALDI-TOF MS) m/z calcd. for $C_{100}H_{60}$ $[M]^+$: 1260.4695, found: 1260.5.

4-2. Computational Study

The Gaussian 09 program running on a SGI Altix4700 system was used for optimization (B3LYP/6-31G(d)). All structures were optimized without any symmetry assumptions. Zero-point energy, enthalpy, and Gibbs free energy at 298.15 K and 1 atm were estimated from the gas-phase studies unless otherwise noted. Harmonic vibration frequency calculations at the same level were performed to verify all stationary points as local minima (with no imaginary frequency) or transition states (with one imaginary frequency).

Table 4. TD-DFT vertical one-electron excitations (6 states) calculated for [8]CN.

energy	wavelength	Oscillator strength (*f*)	Description
2.3244 eV	533.40 nm	0.0000	HOMO -> LUMO (0.69301)
2.8300 eV	438.11 nm	0.2890	HOMO–2 -> LUMO (-0.17133) HOMO -> LUMO+1 (0.67601)
2.8300 eV	438.10 nm	0.2889	HOMO–1 -> LUMO (-0.17144) HOMO -> LUMO+2 (0.67598)
2.9069 eV	426.51 nm	0.7969	HOMO–2 -> LUMO (0.65159) HOMO-1 -> LUMO (-0.23999) HOMO -> LUMO+2 (0.67601)
2.9069 eV	426.51 nm	0.7968	HOMO–2 -> LUMO (0.66975) HOMO-1 -> LUMO (0.10078) HOMO -> LUMO+1 (0.18323)
3.1279 eV	396.38 nm	0.0000	HOMO–2 -> LUMO+1 (-0.20852) HOMO–2 -> LUMO+2 (-0.44951) HOMO–1 -> LUMO+1 (0.44966) HOMO–1 -> LUMO+2 (-0.20848)

Table 5. TD-DFT vertical one-electron excitations (6 states) calculated for [10]CN.

energy	wavelength	Oscillator strength (*f*)	Description

2.6021 eV	476.47 nm	0.0000	HOMO–2 ->LUMO+2 (0.17227) HOMO–1 ->LUMO+1 (-0.17257) HOMO -> LUMO (0.66061)
2.9135 eV	425.56 nm	1.2165	HOMO–1 -> LUMO (-0.37106) HOMO -> LUMO+1 (0.59277)
2.9139 eV	425.49 nm	1.2159	HOMO–2 -> LUMO (0.36972) HOMO -> LUMO+2 (0.59352)
3.0020 eV	413.01 nm	0.0488	HOMO–1 -> LUMO (0.59231) HOMO -> LUMO+1 (0.36345)
3.0024 eV	412.95 nm	0.0499	HOMO–2 -> LUMO (0.48729) HOMO -> LUMO+2 (0.48880)
3.1377 eV	395.14 nm	0.0000	HOMO–2 -> LUMO+2 (-0.45757) HOMO–1 -> LUMO+1 (0.46242) HOMO-> LUMO (-0.25046)

Table 6. TD-DFT vertical one-electron excitations (6 states) calculated for [12]CN.

energy	wavelength	Oscillator strength (*f*)	Description
2.7819 eV	445.68 nm	0.0000	HOMO–2 ->LUMO+2 (-0.24408) HOMO–1 ->LUMO+1 (-0.24408) HOMO -> LUMO (0.60812)
2.9801 eV	416.04 nm	1.4624	HOMO–1 -> LUMO (-0.43393) HOMO -> LUMO+1 (0.52861)
2.9801 eV	416.04 nm	1.4624	HOMO–2 -> LUMO (-0.43393) HOMO -> LUMO+2 (0.52861)
3.1317 eV	395.90 nm	0.0051	HOMO–1 -> LUMO (0.52236) HOMO -> LUMO+1 (0.41590) HOMO -> LUMO+2 (0.12603)
3.1317 eV	395.90 nm	0.0051	HOMO–1 -> LUMO (0.52236) HOMO -> LUMO+1 (-0.12603) HOMO -> LUMO+2 (0.41590)
3.1840 eV	389.39 nm	0.0000	HOMO–2 -> LUMO+1 (-0.45757) HOMO–1 -> LUMO+2 (0.46242)

Table 7. TD-DFT vertical one-electron excitations (6 states) calculated for [16]CN.

energy	wavelength	Oscillator strength (*f*)	Description

2.9992 eV	413.39 nm	0.0000	HOMO -> LUMO (0.50414) HOMO–1 -> LUMO+1 (0.32129) HOMO–2 -> LUMO+2 (0.32129) HOMO–3 -> LUMO+3 (0.12822) HOMO–4 -> LUMO+4 (0.12822)
3.1057 eV	399.22 nm	1.9499	HOMO -> LUMO+1 (0.47204) HOMO–1 -> LUMO+4 (-0.14530) HOMO–1 -> LUMO (0.44016) HOMO–2 -> LUMO+2 (0.14531) HOMO–3 -> LUMO+2 (0.12343) HOMO–4 -> LUMO+1 (-0.12343)
3.1057 eV	399.22 nm	1.9501	HOMO -> LUMO+2 (0.47204) HOMO–1 -> LUMO+3 (0.14530) HOMO–2 -> LUMO+4 (0.14530) HOMO–2 -> LUMO (0.44016) HOMO–3 -> LUMO+1 (0.12343) HOMO–4 -> LUMO+2 (0.12343)
3.2595 eV	380.38 nm	0.0000	HOMO–3 -> LUMO (0.24847) HOMO–2 -> LUMO+1 (0.38120) HOMO–1 -> LUMO+2 (0.38120) HOMO -> LUMO+3 (0.35211)
3.2595 eV	380.38 nm	0.0000	HOMO–4 -> LUMO (-0.24847) HOMO–2 -> LUMO+2 (-0.38120) HOMO–1 -> LUMO+1 (0.38120) HOMO -> LUMO+4 (-0.35211)
3.3290 eV	372.44 nm	0.0000	HOMO–4 -> LUMO+1 (-0.14606) HOMO–3 -> LUMO+2 (0.14606) HOMO–2 -> LUMO+3 (-0.15531) HOMO–1 -> LUMO (0.46885) HOMO–1 -> LUMO+4 (0.15531) HOMO -> LUMO+2 (-0.41360)

Table 8. Uncorrected and thermal-corrected (298K) energies of stationary points (Hartree).[a]

compound	E	E + ZPE	H	G
[8]CN	-3077.47382346	-3076.452172	-3076.394634	-3076.539354
[10]CN	-3846.88569576	-3845.607310	-3845.535005	-3845.712075
1,1'-binaphtyl	-770.587625051	-770.311952	-770.296834	-770.354150
ternaphtyl	-1155.28226017	-1154.878843	-1154.856237	-1154.931792

a) E: electronic energy; ZPE: zero-point energy; H (=E+ZPE+E_{vib}+E_{rot}+E_{trans}+RT): sum of electronic and themal enthalpies; G (=H–TS): sum of electronic and thermal free energies.

References

1. Yagi, A.; Segawa, Y.; Itami, K. *J. Am. Chem. Soc.* **2012***, 134*, 2962.
2. (a) Omachi, H.; Segawa, Y.; Itami, K. *Acc. Chem. Res.* **2012**, *45*. 1378. (b) Sisto, T. J.; Jasti, R. *Synlett* **2012**, *23*, 483. (c) Yamago, S.; Kayahara, E.; Iwamoto, T. *Chem. Rec.* **2014**, *14*, 84. (d) Lewis, S. E. *Chem. Soc. Rev.* **2015**, *44*, 2221. (e) Darzi, E. R.; Jasti, R. *Chem. Soc. Rev.* **2015**, *44*, 6401. (f) Evans, P.; Jasti, R. in *Polyarenes I, Vol. 349* (Eds.: J. S. Siegel, Y.-T. Wu), Springer Berlin Heidelberg, **2014**, pp. 249.
3. Ishiyama, T.; Murata, M.; Miyaura, N. *J. Org. Chem.* **1995**, *95*, 2457.
4. Nagarajian, S.; Barthes, C.; Girdhar, N. K.; Dang, T. T.; Gourdon, A. *Tetrahedron* **2012**, *68*, 9371.
5. Segawa, Y.; Fukazawa, A.; Matsuura, S.; Omachi, H.; Yamaguchi, S.; Irle, S.; Itami, K. *Org. Biomol. Chem.* **2012**, *10*, 5979.
6. Koch, K.-H.; Müllen, K. *Chem. Ber.* **1991**, *124*, 2091.
7. Segawa, Y.; Omachi, H.; Itami, K. *Org. Lett.* **2010**, *12*, 2262.
8. Horgen, S. T.; Procopiou, P. A.; Vinader Brugarolas, M. V. PCT Int. Appl. WO 2007071691 May 28, 2007.

Chapter 4

Cyclodehydrogenation of cyclo-1,4-naphthylenes: A final step towards carbon nanobelts

Abstract: The synthesis of carbon nanobelts was challenged by using of cyclo-1,4-naphthylenes (CNs) as precursors. Prior to the synthetic investigation, theoretical studies were conducted to predict the structural and electronic features of carbon nanobelts. The cyclodehydrogenation of [9]CN, [12]CN, and [16]CN was attempted, and a possible way for efficient cyclodehydrogenation was identified. This work would contribute to achieve the synthesis of carbon nanobelt by further investigation in the future.

1. Introduction

The author has achieved the synthesis of potential precursors for carbon nanobelts as shown in Chapter 1 to 3. In this chapter, the synthesis of carbon nanobelts was attempted together with the understanding the properties of carbon nanobelts.

To date, the structure, reactivity, and aromaticity of belt-shaped aromatic hydrocarbons have been predicted.[1] However, theoretical studies specific to carbon nanobelts have not been reported yet. Therefore, prior to their synthetic studies, the structural and electronic properties of carbon nanobelts were estimated by calculation at the B3LYP/6-31G(d) level (Table 1 and Figure 1). By the TD-DFT calculation, the absorption maxima of [8]-, [9]-, [10]-, [12]-, and [16]carbon nanobelts were predicted. The absorption maximum shifts to long wavelength as the ring size increases. As for the HOMO levels of these carbon nanobelts, the energy level increases as (n) in [n]carbon nanobelt increases. On the other hand, the LUMO levels behave oppositely. These behaviors are similar to those of linear polyrylenes.[2] The red-shift of the absorption maximum should be reflected by the behaviors of the frontier orbitals. The Raman spectra were also estimated by calculation (Figure 1). Intense peaks around 1250 cm^{-1} and 1600 cm^{-1}, which are derived from C–H bending vibration and in-plane vibration of benzene rings respectively, were estimated in all the carbon nanobelts. For the radial breathing mode, which is observed in the low frequency area (100–300 cm^{-1}), no notable peaks were estimated unlike carbon nanotubes.[3] These predictions should be useful for the identification of carbon nanobelts. Recently, our group developed a general method to estimate the strain energies of belt-shaped aromatic hydrocarbons.[4] Their strain energies are inversely proportional to the ring size (n), as estimated by the formula (a) in Table 1. The strain energies are higher than those of the same sizes of cyclo-1,4-naphthylenes (CNs) by ca. 50 $kcal \cdot mol^{-1}$, and similar to those of previously synthesized small CPPs (117 $kcal \cdot mol^{-1}$ for [5]CPP, and the strain energies for other CPPs are in Table 3 of Chapter 3).

Table 1. Properties of carbon nanobelts estimated at the B3LYP/6-31G(d) level.

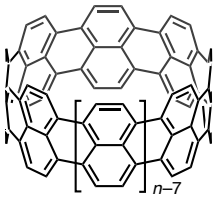

[*n*]carbon nanobelt

n	absorption maxima (nm)	HOMO energy (eV)	LUMO energy (eV)	strain energy (kcal·mol^{-1})
8	549	–4.17	–2.62	109.0
9	589	–4.13	–2.69	96.9
10	628	–4.10	–2.75	87.2
12	700	–4.07	–2.83	72.7
16	832	–4.06	–2.92	54.5

strain energy (kcal·mol^{-1}) = 872.3 · n^{-1} ··· (a)

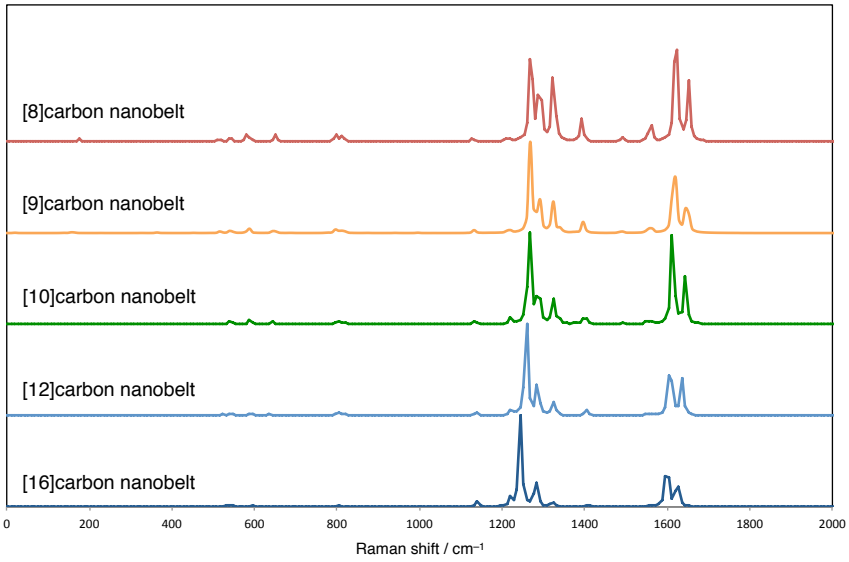

Figure 1. Estimated Raman spectra for [8]-, [9]-, [10]-, [12]-, and [16]carbon nanobelts.

Chapter 2 and 3 described the successful synthesis of [8]-, [9]-, [10]-, [12]-, and [16]CNs. The sequential intramolecular cyclodehydrogenation reaction of CNs is the most straightforward transformation to carbon nanobelts (Figure 2a). Many methods for cyclodehydrogenation of arenes have been reported to date (Figure 2b).[5] In 1910, Scholl and co-workers found that aluminum chloride (III) oxidatively fused 5-, and 5'-positions of 1,1'-binaphthyl at 140 °C.[6] This intramolecular Friedel–Crafts type reaction of 1,1'-binaphthyl first furnished perylene, albeit in low yield. The reactions using oxidants such as iron chloride

(III), copper chloride (II), and 2,3-dichloro-5,6-dicyano-*p*-benzoquinone (DDQ) were also found to afford the cyclodehydrogenated products.[5a] Although the mechanisms for these cationic cyclodehydrogenations are still unclear, it was proposed that electron-oxidation of the arene rings triggers their coupling and following dehydrogenation.[7] Recently, thermal cyclodehydrogenations have been employed to synthesize several oligorylenes.[8] Meanwhile, the anionic cyclodehydrogenation of 1,1'-binaphthyl by potassium metal was discovered in 1967 by Solodovnikov and co-workers.[9] This anionic cyclodehydrogenation of 1,1'-binaphthyl is realized by lithium metal as well, and known for the method to produce less byproducts.[10] The group of Müllen has often employed this method to achieve the synthesis of many kinds of oligorylenes.[2] This reaction includes the both processes of electron-reduction and oxidation, albeit oxidative pathway totally. In 2010, the group of Scott reinvestigated the detail on the anionic cyclodehydrogenation of 1,1'-binaphthyl, and gained mechanistic insight into the reaction.[11] They proposed that the electron-reduction causes the coupling in 1,1'-binaphthyl, and a hydrogen molecule eliminates to form anionic perylene. The yield of perylene was drastically improved, which is the highest in all conditions for the cyclodehydrogenation of 1,1'-binaphthyl reported to date. This Scott's condition seems to be the most effective for cyclodehydrogenation of CNs.

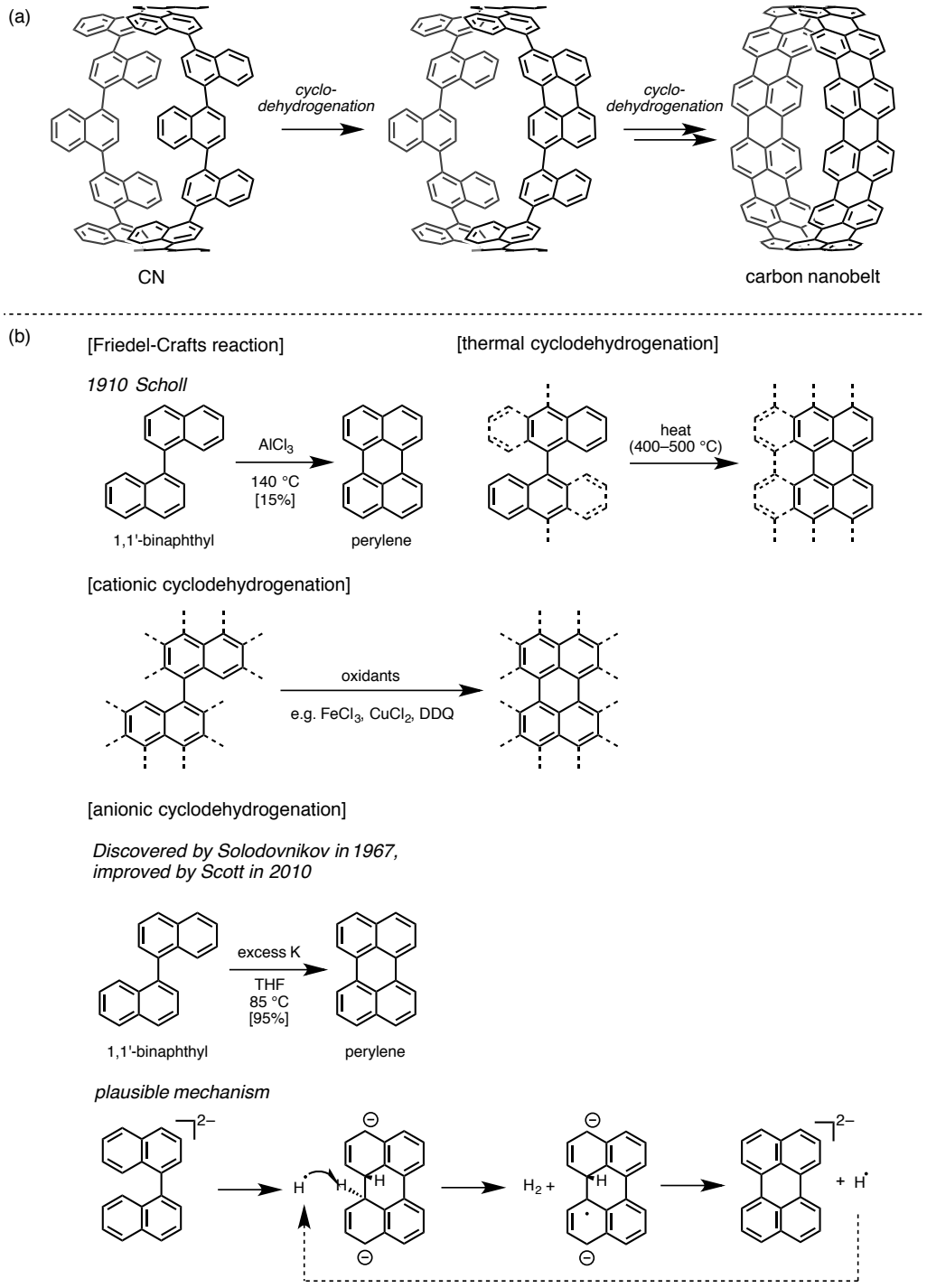

Figure 2. Cyclodehydrogenation of (a) CNs and (b) 1,1'-binaphthyl derivatives.

Based on these backgrounds, the author challenged the synthesis of carbon nanobelts by anionic cyclodehydrogenation of CNs (Figure 3). Prior to the extensive investigation of the reaction conditions, the relationship between reactivity and the ring size of CNs were examined by using [9]CN, [12]CN, and [16]CN. Following optimization of the reaction conditions

afforded the products expected as highly cyclodehydrogenated nanorings. Taking the results, some ideas are also suggested to successfully obtain desired carbon nanobelts.

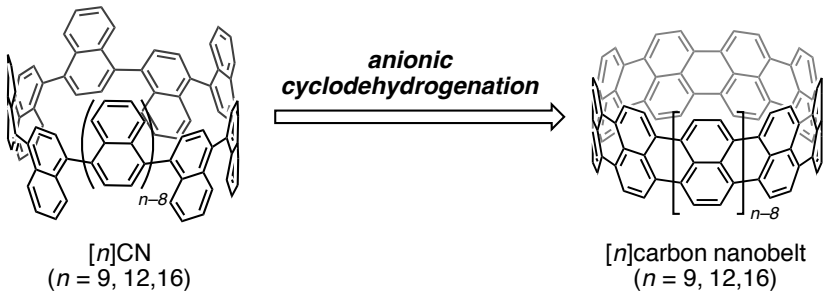

Figure 3. Survey of this chapter.

2. Results and discussion

2-1. Anionic cyclodehydrogenation of [9]CN, [12]CN, and [16]CN in Scott's condition

[9]CN, [12]CN, and [16]CN were first subjected to Scott's condition for the anionic cyclodehydrogenation. These CNs were treated with excess amount of potassium metal in THF at 85 °C for 48 h. In all cases, the color of the reaction solution turned to dark green initially and then dark purple, which is typical color change for the generation of metal naphthalenide.[11] In such kind of reduction, oxygen gas or iodine is generally used to oxidize the anionic products after the metal is removed. When oxygen gas was used, mass peaks of oxygen adducts were detected by MALDI-TOF MS, in addition to those of neutralized products. In order to avoid such addition of oxygen atoms, the anion species were first reacted with degassed methanol for protonation, and then the protonated products were treated with DDQ for oxidation and re-aromatization. This treatment was tried in the reaction of 1,1'-binaphthyl in advance of CNs. It was confirmed that the protonated products were obtained and were successfully re-aromatized by DDQ. After these procedures, the products by the reactions of CNs were analyzed by MALDI-TOF MS (Table 2). In the product mixture from the reaction of [9]CN, the mass peaks of *m/z* = 1122 (–12H from [9]CN), 1124 (–10H), 1126 (–8H), 1128 (–6H), and 1130 (–4H) were detected. In the reaction of [12]CN, the product mixture with the mass peaks of *m/z* = 1492 (–20H from [12]CN), 1494 (–18H), 1496 (–16H), 1498 (–14H), 1500 (–12H), 1502 (–10H) and 1504 (–8H) were obtained. The products by the reaction of [16]CN contained the compounds with *m/z* = 2002 (–14H from [16]CN) and 2004 (–12H). Firstly in the purification, the dichloromethane solution of the products and the precipitate were separated. Detected mass peaks from the solution were listed in Table 2. It was found that far dehydrogenated products were contained in the precipitate of the three CNs. Although the isolation of the soluble products was attempted by gel permeation chromatography, silica chromatography, aluminum oxide chromatography and crystallization, it has not been successful due probably to the similarities in their structure and polarity. To get further structural information of the products, the UV–vis absorption spectra of the dichloromethane solution were measured (Figure 4). The absorption maxima of the products were observed around 460 nm, which was longer wavelength than those of [9]CN, [12]CN, and [16]CN. The insoluble compounds were analyzed by the Raman spectroscopy (Figure 5). In common to all the compounds, the Raman peaks were observed in 1270 cm^{-1}, 1360 cm^{-1}, and 1560 cm^{-1} excited by the laser of 532 nm.

The mass analysis, absorption spectra, and Raman spectra showed that the Scott's anionic condition converted [9]CN, [12]CN, and [16]CN into some compounds, but carbon nanobelts were not contained. The decreases of molecular weights and their degree indicate that sequential cyclodehydrogenation reactions successfully proceeded in the CNs. Furthermore, according to the mass analysis, highly dehydrogenated products had poor solubility. This is the typical behavior of π-extended aromatic hydrocarbons. The red-shifts observed in the absorption spectra also supported the extension of π-conjugation by cyclodehydrogenation. Judging from estimated absorption maxima for carbon nanobelts (Table 1), the solutions seem not to contain the carbon nanobelts. The Raman spectra of the three products were similar to each other. This suggests that they might have similar structures. Compared to the estimated Raman spectra for [9]-, [12]-, and [16]carbon nanobelts (Figure 1), the additional peaks around 1350 cm^{-1} were observed. The origin of these additional peaks has not been cleared.

Table 2. Cyclodehydrogenation of [9]CN, [12]CN, and [16]CN in the Scott's condition.

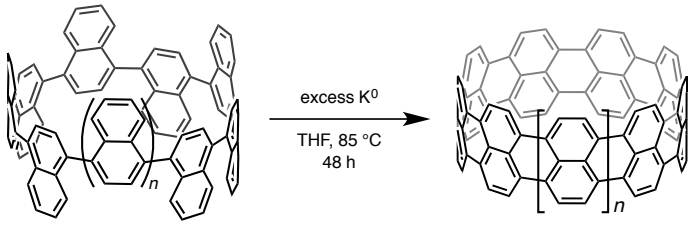

n = 1: [9]CN *m/z* = 1134
n = 4: [12]CN *m/z* = 1513
n = 8: [16]CN *m/z* = 2017

n = 1: [9]carbon nanobelt *m/z* = 1116 ([9]CN –18H)
n = 4: [12]carbon nanobelt *m/z* = 1488 ([12]CN –24H)
n = 8: [16]carbon nanobelt *m/z* = 1985 ([16]CN –32H)

		detected mass peaks by MALDI-TOF MS (*m/z*)	
entry	CN	reaction mixture	dichloromethane solution
1	[9]CN	1122 (–12H), 1124 (–10H), 1126 (–8H), 1128 (–6H), 1130 (–4H), 1132 (–2H)	1128 (–6H), 1130 (–4H), 1132(–2H)
2	[12]CN	1492 (–20H), 1494 (–18H), 1496 (–16H), 1498 (–14H), 1500 (–12H), 1502 (–10H), 1504 (–8 H)	1502 (–10H), 1504 (–8H)
3	[16]CN	2002 (–14H), 2004 (–12H)	2002 (–14H), 2004 (–12H)

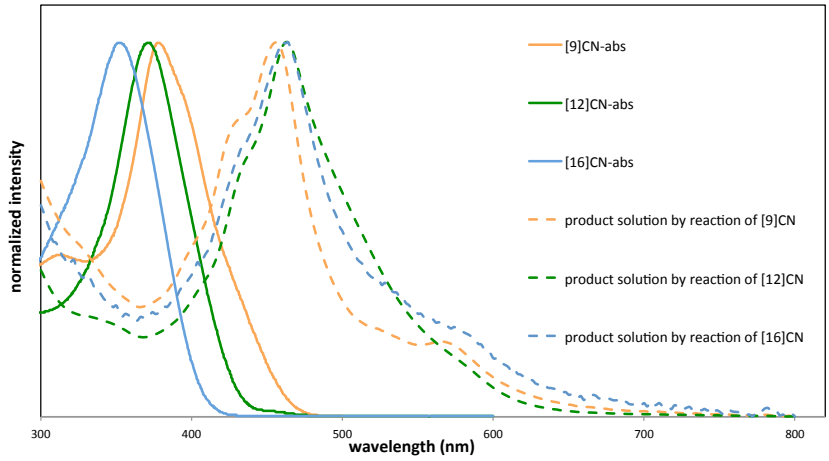

Figure 4. UV–vis absorption spectra of the dichloromethane solutions and [9]CN, [12]CN, and [16]CN.

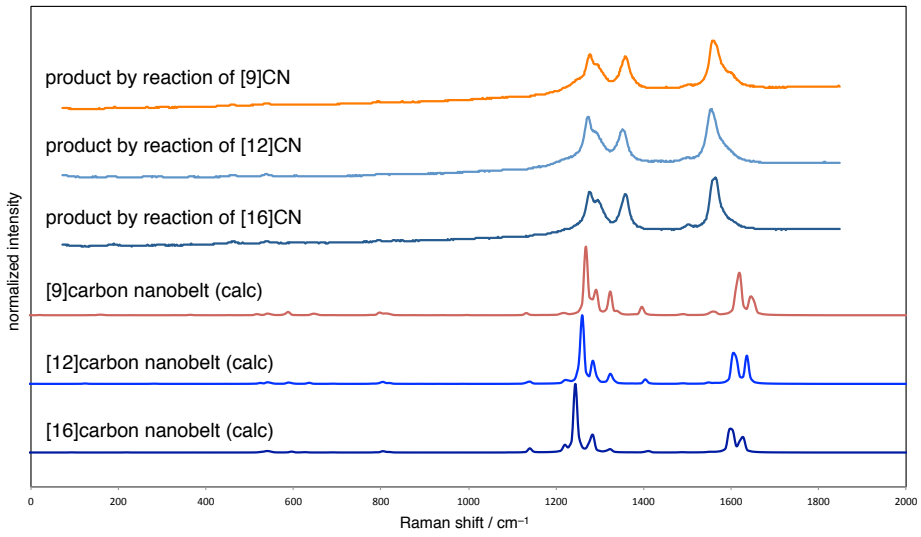

Figure 5. Raman spectra of the products insoluble to dichloromethane excited at 532 nm laser.

To discuss the structures of the products, computational studies on the partially cyclodehydrogenated nanorings were conducted. Since the sequential cyclodehydrogenation of CNs should include a number of possible pathways, it is impossible to explore the all possible pathways of the cyclodehydrogenation of CNs. Thus, the discussion was attempted for only the early stage of the cyclodehydrogenation by using the measured absorption spectra and estimated ones for possible structures. In 1991, Müllen found that the anionic cyclodehydrogenation in the quaternaphthylene- and the quinquenaphthylene derivatives were converted into only small rylenes such as perylene and terrylene, not larger rylenes (Scheme 1).[2b] Namely, the formation

of small rylenes was prior to large ones in such oligonaphthylenes. The TD-DFT calculations were performed for several kinds of nanorings, which can be obtained from [12]CN (Figure 6). When one perylene unit is formed in the CN (A), the estimated absorption maximum is shifted to longer wavelength (435 nm). The formation of another perylene unit triggers further redshift (417, 496, 616 nm for B, 382, 523 nm for C). Subsequently, the absorption spectrum was estimated for the nanoring with one terrylene unit (D), which is generated by cyclodehydrogenation of the perylene unit with neighboring naphthalene unit. As a result, the intense absorption in 661 nm was estimated in addition to the absorption maximum of 424 nm. According to these calculations, the formation of a few terrylene units would cause much longer wavelength absorption than the formation of more perylene units. Considering the measured results (absorption spectrum and the degree of dehydrogenation (–8H and –10H)) together, it would be reasonable to assume that several perylene units were formed prior to terrylene unit in the early stage of sequential cyclodehydrogenation in [12]CN.

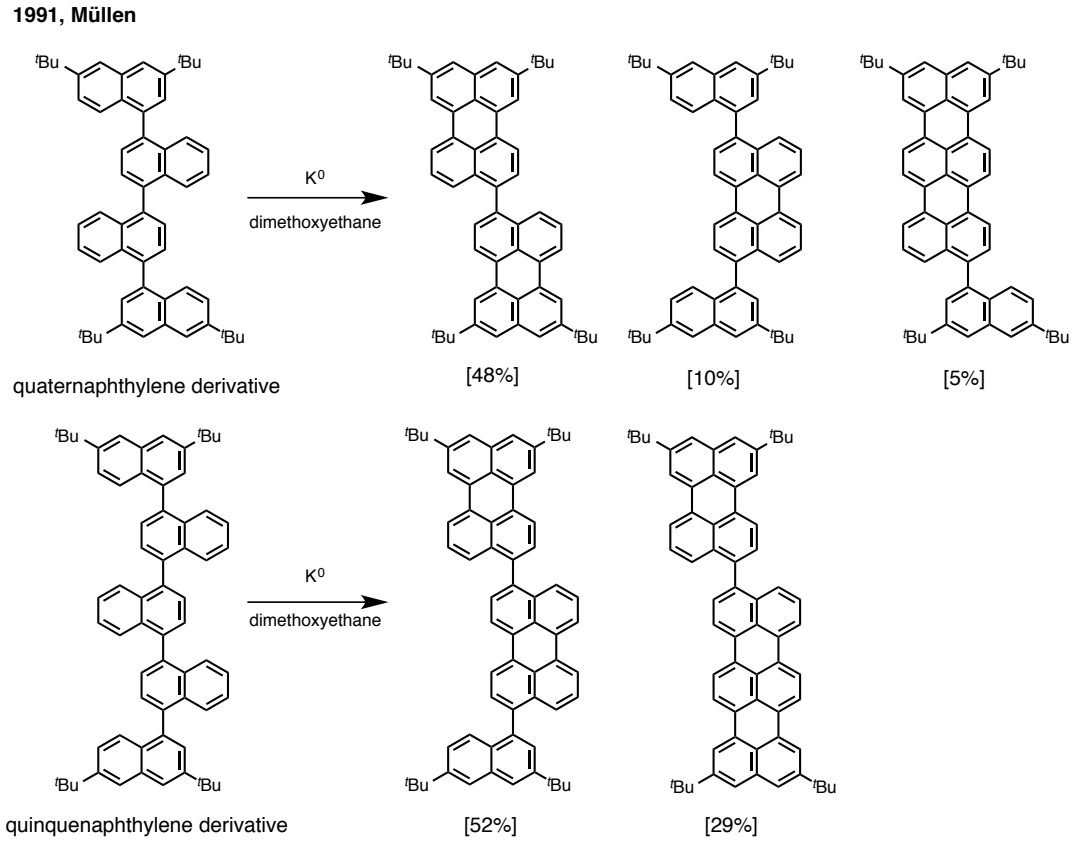

Scheme 1. Cyclodehydrogenation of oligonaphthylenes by Müllen.

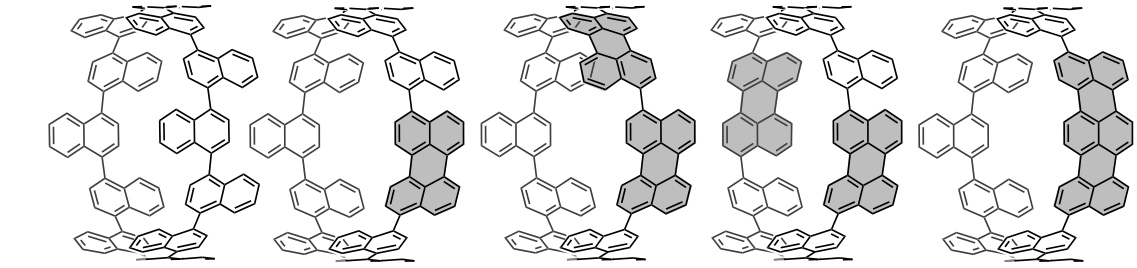

Figure 6. Cyclodehydrogenated nanorings and their estimated absorption maxima. Optimized structures were obtained at the B3LYP/6-31G(d) level.

2-2. Anionic cyclodehydrogenation of [12]CN

2-2-1. Effects of alkali metals

By the preliminary investigation above, it was found that sequential cyclodehydrogenation in [9]CN, [12]CN, and [16]CN can proceed to afford fused nanorings. Thus, further investigation of the reaction conditions was conducted. First, the effect of alkali metals was examined with [12]CN because the cyclodehydrogenation of [12]CN proceeded well as shown above. Products were analyzed by MALDI-TOF MS (Table 3). In the condition with lithium metal, the addition or substitution of THF (*m/z* = 1582, 1654, 1724) seemed to proceed rather than the cyclodehydrogenation (entry 1). No reaction occurred by using sodium metal (entry 2). The use of NaK alloy is also effective for the cyclodehydrogenation as well as potassium metal (entries 3 and 4). The differences in the reduction potentials of lithium, sodium, and potassium metals are small (–3.04 eV, –2.71 eV and –2.93 eV, respectively). Previously, Rabinovitz and co-workers reported the THF addition to pyrene and curved pyrene derivatives by using lithium metal (Scheme 2).[12] Taking their results into consideration, the result in entry 1 is probably caused by the instability of the ion pair, *i.e.* the anionic nanoring and lithium ion. The difference in the reactivity among sodium metal, NaK alloy, and potassium metal can be attributed to their surface areas in the reactions derived from their melting points (sodium: 98 °C, NaK alloy: 19 °C, potassium: 63 °C).

Table 3. Effects of alkali metals in cyclodehydrogenation of [12]CN.

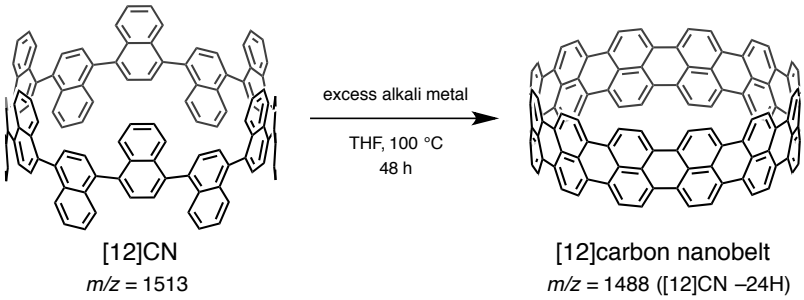

entry	alkali metal	detected mass peaks by MALDI-TOF MS (*m/z*)
1	Li	1509 (–4H), 1511 (–2H), 1582,1654,1725
2	Na	1513 ([12]CN)
3	K	1492 (–20H), 1494 (–18H), 1496 (–16H), 1498 (–14H), 1500 (–12H), 1502 (–10H), 1504 (–8H), 1506 (–6H), 1508 (–4H)
4	NaK	1492 (–20H), 1494 (–18H), 1496 (–16H), 1498 (–14H)

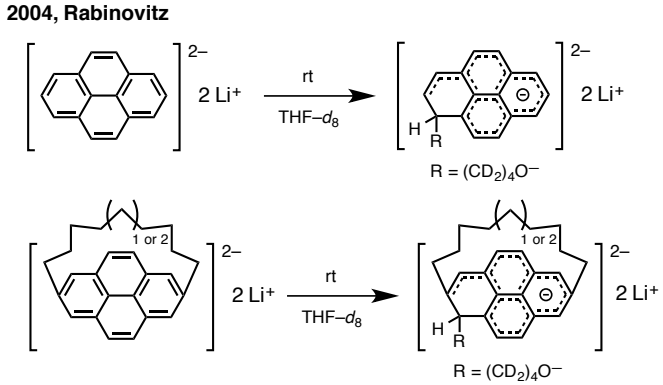

Scheme 2. THF addition to pyrene and curved pyrene derivatives by lithium metal.

2-2-2. Effect of reaction temperature and time

Subsequently, the appropriate reaction temperature and time were investigated (Table 4). The cyclodehydrogenation of [12]CN proceeded even at lower temperature than that in Scott's condition (50 °C, entry 1). Extending the reaction time allowed further cyclodehydrogenation (entries 2 and 3). Though the condition at high temperature afforded further cyclodehydrogenated products (entries 4 and 5), the mass peaks that correspond to rylenes (*m/z* = 624, 748, 872, 996) were also detected (entry 6). Representative structures of rylenes are shown in Figure 7. The generation of rylenes indicates the decomposition of the nanoring. Thus,

all detected mass peaks might be those of decomposed products as well, not of nanorings. The decomposition of the nanorings could be triggered by the instability of the anionic nanoring at high temperature. Rabinovitz and co-workers previously reported that the strained carbon–carbon bond in the anionic curved pyrene dimer was cleaved by electron-reduction (Scheme 3).[12] They explained that two anionic species were generated by the bond cleavage, which repulsed each other. Judging from this previous work, the author presumed that the nanorings were decomposed by the excess electron-reduction at high temperature. The conditions for efficient cyclodehydrogenation where the excess electron-reduction is avoided were examined in the next section.

Table 4. Effects of reaction temperature and time.

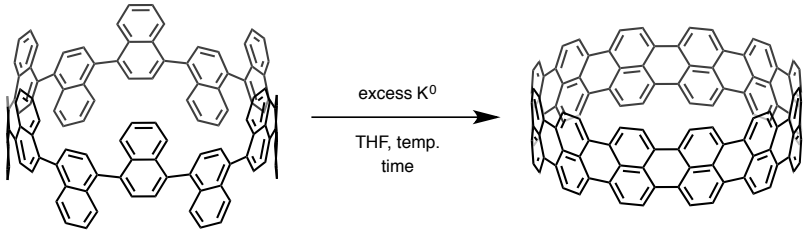

[12]CN
m/z = 1513

[12]carbon nanobelt
m/z = 1488 ([12]CN –24H)

entry	temp. (°C)	time (h)	detected mass peaks by MALDI-TOF MS (*m/z*)
1	50	48	1504 (–8H)
2	50	120	1492 (–20H), 1494 (–18H), 1496 (–16H),1498 (–14H)
3	50	168	1492 (–20H), 1494 (–18H), 1496 (–16H),1498 (–14H), 1502 (–10H), 1504 (–8H), 1506 (–6H)
4	70	48	1492 (–20H), 1494 (–18H), 1496 (–16H),1498 (–14H)
5	70	96	1492 (–20H), 1494 (–18H), 1496 (–16H),1498 (–14H), 1502 (–10H), 1504 (–8H)
6	120	48	1492 (–20H), 1494 (–18H), 1496 (–16H), 1498 (–14H) 624, 748, 872, 996

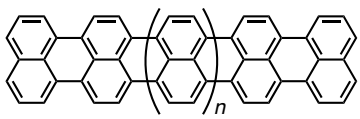

m/z = 624 (*n* = 1), 748 (*n* = 2), 872 (*n* = 3), 996 (*n* = 4),

Figure 7. Representative structures of rylenes and their exact mass.

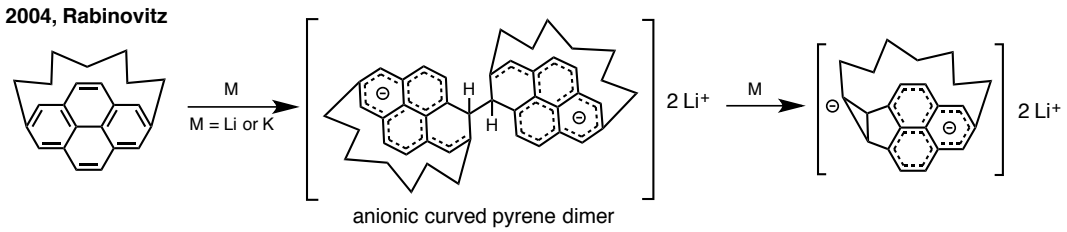

Scheme 3. Decomposition of curved pyrene dimer induced by electron repulsion.

2-2-3. Anionic cyclodehydrogenation of nanorings after removing alkali metal

By the investigation above, it was suggested that the excess electron-reduction triggered the generation of multianionic nanorings. To gain insight into the valence of anionic nanorings, "potassium [12]cyclo-1,4-naphthalenide (nK$^+$·[12]CN^{n-})", which is the species generated firstly in the cyclodehydrogenation of [12]CN with potassium metal, was formed then protonated with degassed methanol (Scheme 4). The mass peaks for multiprotonated products (*m/z* = 1515 ([12]CN +2H), 1517 (+4H) and 1519 (+6H)) were detected, indicating that multianionic species were generated. Not only [12]CN, but also the cyclodehydrogenated nanorings could become multianionic species. Based on these findings, the reactions were then attempted under the conditions where the excess electron-reduction can be avoided. Since controlling the equivalent of potassium metal was difficult, the reaction conditions were arranged in two ways. In the first way, after nK$^+$·[12]CN^{n-} was formed as above, the potassium metal was removed from the reaction. The resulting solution was then reacted at 120 °C (Scheme 5). Whereas the nanorings were not decomposed, the cyclodehydrogenation did not proceed better than the case with potassium metal *in situ*. In addition, many mass peaks were detected. The mass analysis showed that this reaction, where excess electron-reduction can be prevented, made the sequential cyclodehydrogenation of [12]CN inefficient. One of the possible factors for this is that electrons were lost from the anionic nanorings. Controlling the valence of anionic species seems to be important. When comparing the LUMO levels of fused nanorings, the more fused (cyclodehydrogenated) structures are constructed, the lower the LUMO level gets. Therefore, in the second way, alkali metals were removed after cyclodehydrogenation of [12]CN partially proceeded to inhibit the loss of electrons. The reaction of [12]CN was performed with potassium metal at 50 °C for 48 h, then the metal was removed (Scheme 6). When removing the metal, the absence of the decomposed fragments (rylenes) was confirmed. The solution of anionic cyclodehydrogenated nanorings was next heated to 150 °C for 288 h. As a result, deep

blue solid with the mass peak of *m/z* = 1492 (–20H), which hardly dissolves in common organic solvents, was obtained. The Raman spectrum of the blue solid was similar to that obtained by the Scott's conditions, which is somewhat different from that of [12]carbon nanobelt (Figure 8). Though the absorption spectrum has not been obtained yet, the color of the solid indicated the absorption in long wavelength. Taking the detected mass peak into consideration together, the sequential cyclodehydrogenation of anionic nanorings proceeded efficiently and without decomposition.

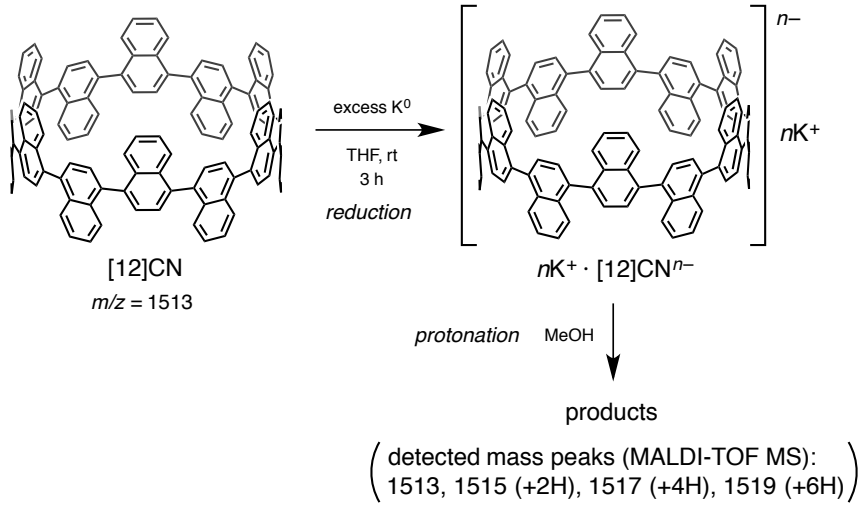

Scheme 4. Protonation of potassium [12]cyclo-1,4-naphthalenide.

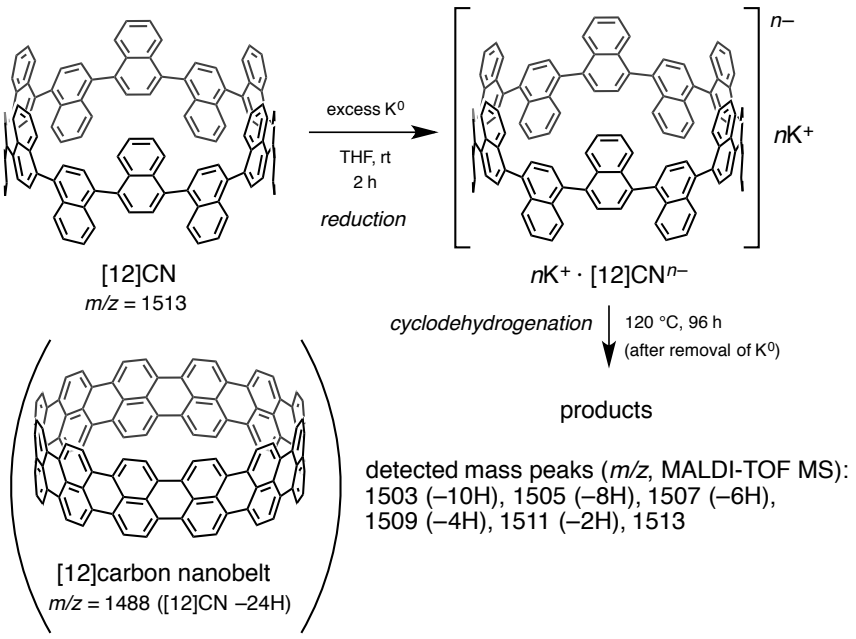

Scheme 5. Anionic cyclodehydrogenation of potassium [12]cyclo-1,4-naphthalenide.

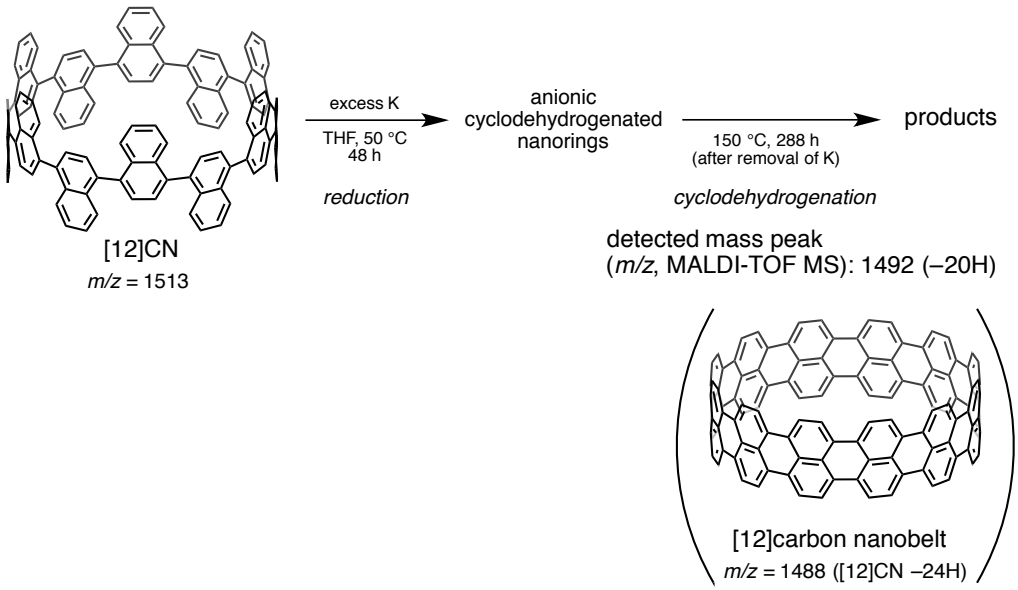

Scheme 6. Sequential cyclodehydrogenation of anionic nanorings after removing potassium metal ([12]CN).

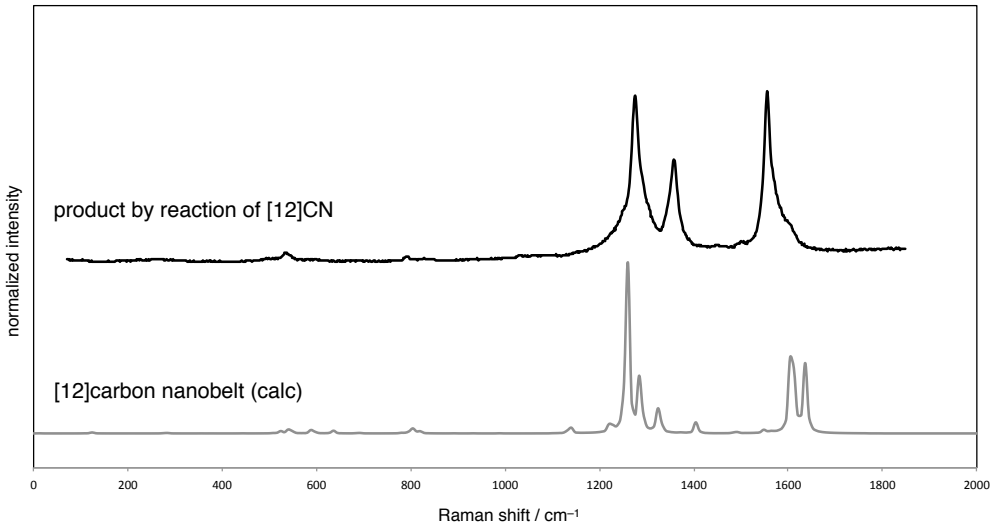

Figure 8. Raman spectra of the product with *m/z* = 1492 (–20H) excited at 532 nm laser (above) and [12]carbon nanobelt (calculation, below).

2-3. Anionic cyclodehydrogenation of [16]CN

By the synthetic study on carbon nanobelt with [12]CN, one potential method for efficient cyclodehydrogenation of CNs was found. Thus, the method was applied to [16]CN (Scheme 7). The condition where potassium metal was removed during the reaction afforded the cyclodehydrogenated product with *m/z* = 1988 (–28H), 1990 (–26H), and 1992 (–24H). The

product was greenish blue solid insoluble to common organic solvents, indicating the extension of π-conjugation in the nanoring. In its Raman spectrum, broaden peaks were observed (Figure 9). This would be caused by the wide range of detected mass peaks compared to those by the reaction of [12]CN.

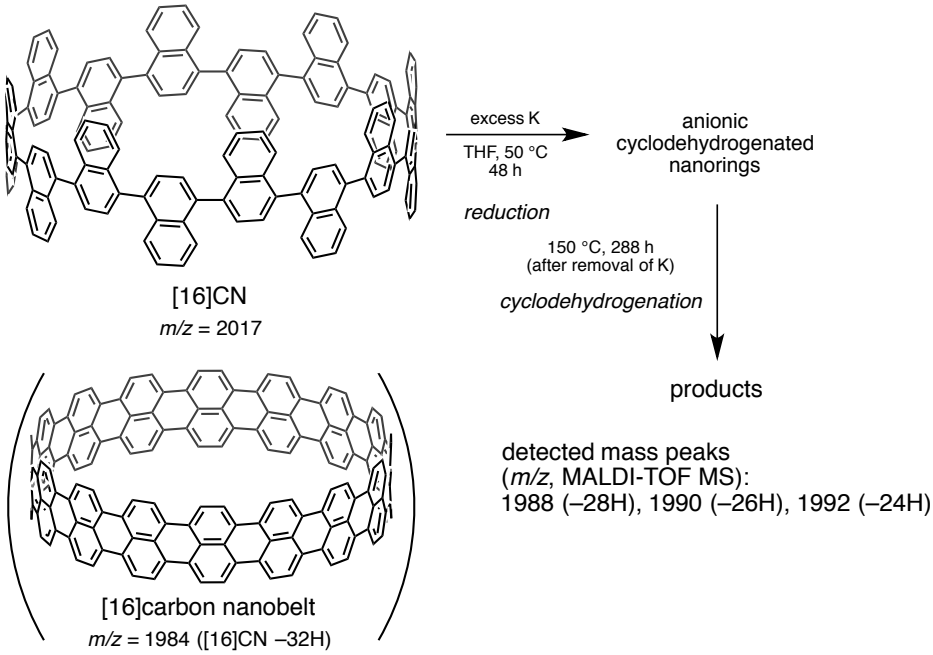

Scheme 7. Sequential cyclodehydrogenation of anionic nanorings after removing potassium metal ([16]CN).

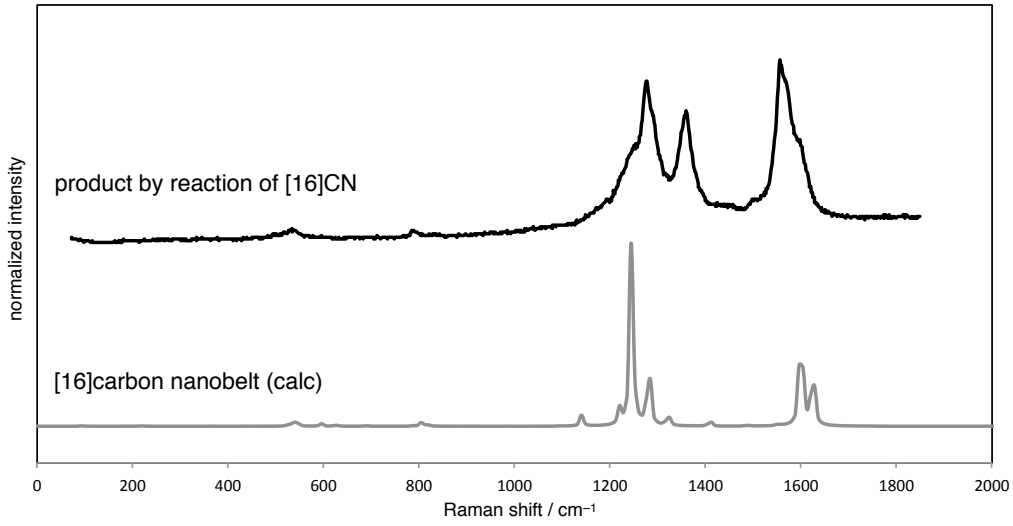

Figure 9. Raman spectra of the product with *m/z* = 1988 (–28H) and 1494 (–26H) excited at 532 nm laser (above) and [16]carbon nanobelt (calculation, below).

2-4. Anionic cyclodehydrogenation of [9]CN

Subsequently, the cyclodehydrogenation of [9]CN was tried in the arranged condition (Scheme 8). However, many mass peaks were detected from the products. The decomposition of nanorings was also indicated by the fact that the mass peaks for rylenes were detected. The strain energy of the CNs increases as the ring size decreases (see Chapter 3). Thus, it is reasonable to assume that the cyclodehydrogenation of [9]CN is more unfavorable than those in [12]CN and [16]CN.

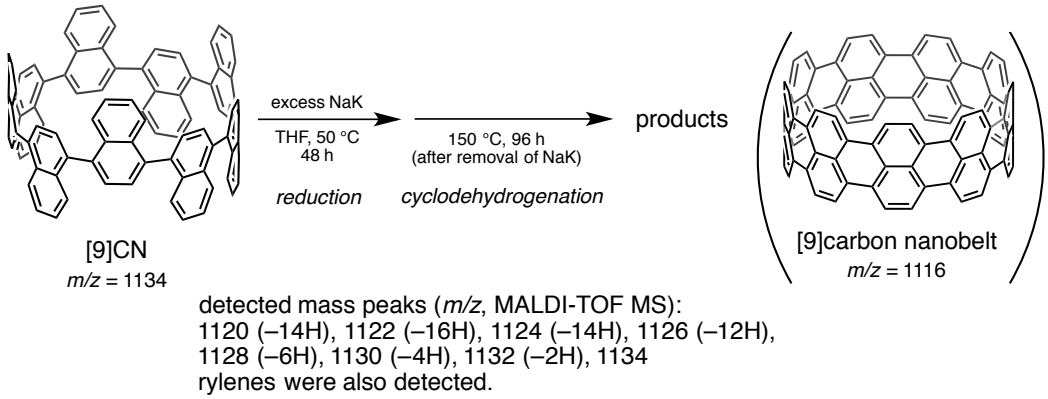

Scheme 8. Sequential cyclodehydrogenation of anionic nanorings after removing potassium metal ([9]CN).

3. Conclusion

In this chapter, the cyclodehydrogenation of CNs were examined toward the synthesis of carbon nanobelts. By anionic cyclodehydrogenation reaction induced by alkali metals such as potassium and NaK alloy, the progress of sequential cyclodehydrogenation of CNs was confirmed. By investigating the reaction conditions, the products expected as cyclodehydrogenated nanorings were obtained from the reaction of [12]CN and [16]CN. On the other hand, the cyclodehydrogenation of [9]CN induced decomposition in the optimized condition for [12]CN and [16]CN. From the results obtained here, large CNs were found to be favorable for the anionic cyclodehydrogenation. It was also found that the sequential anionic cyclodehydrogenation of CNs requires a careful control of the reaction conditions for efficient progression of the reaction. Further investigation is needed to produce carbon nanobelts successfully. For instance, the reaction condition by using potassium naphthalenide might be effective to control the electron-reduction. However, this work also revealed the biggest problem on this approach: the poor solubility of the products, which causes their low reactivity as well as the difficulty in the structural analysis. Because of the problem, enough identification of the products has been prevented. To improve this, the author suggests the introduction of substituents such as alkyl groups into CNs (Figure 10). For example, iridium-catalyzed borylation of CNs should proceed at the 6- and/or 7-positions on their naphthalene rings. The boryl groups can be converted to alkyl groups. The use of alkyl group-substituted naphthalene units in the synthesis of CNs is also promising. These substituents would allow easy treatment of the products, leading to successful synthesis of carbon nanobelts.

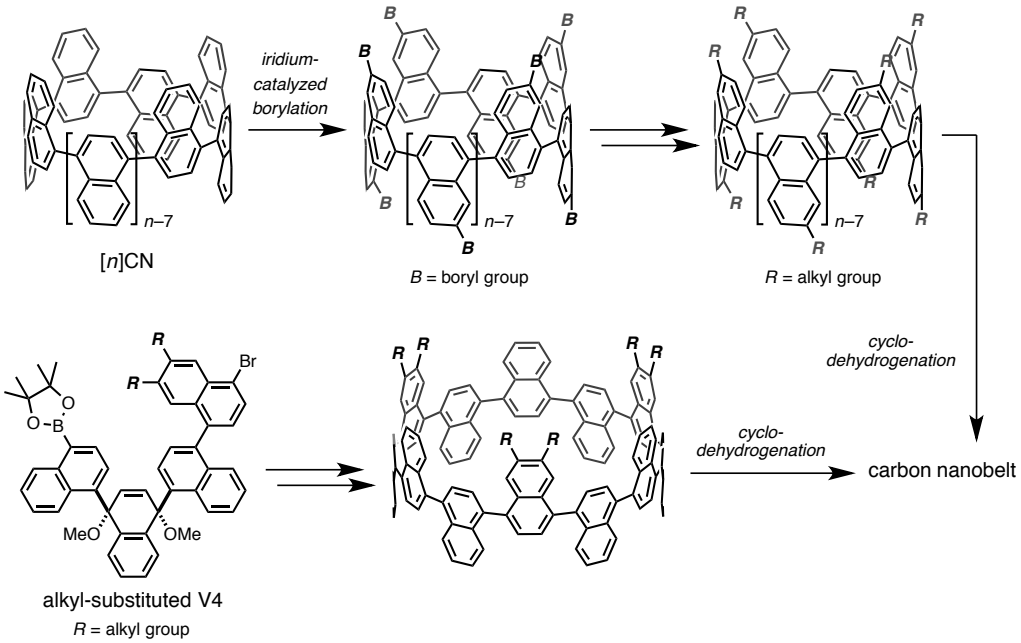

Figure 10. Perspective for the synthesis of carbon nanobelt via alkyl-substituted CNs.

4. Experimental Section

4-1. General

Unless otherwise noted, all materials were obtained from commercial suppliers and used without further purification. Tetrahydrofuran (THF) was purified by passing through a solvent purification system (Glass Contour) and NaK alloy. All reactions were performed under an atmosphere of argon in glass vessels equipped with J. Young® O-ring tap, heated in silicon oil bathes. Work-up and purification procedures were carried out with reagent-grade solvents under air unless otherwise noted. Analytical thin-layer chromatography (TLC) was performed using E. Merck silica gel 60 F254 precoated plates (0.25 mm). High-resolution mass spectra (HRMS) were obtained from a JEOL JMS-S3000 SpiralTOF (MALDI-TOF MS) with *trans*-2-[3-(4-tert-Butylphenyl)-2-methyl-2-propenylidene]malononitrile as matrix. UV–vis absorption spectra of the compounds were recorded on a Shimadzu UV-3510 spectrometer with a resolution of 0.5 nm. Raman spectra of compounds were measured using RENISHAW inVia Raman microscopy equipped with Ar^+ ion lasers operated at 532 nm. A notch filter was used to filter out Rayleigh radiation, and Raman signal was detected by charge-coupled device (CCD). A 50 x, 0.75 NA objective lens was used to focus the laser light onto samples. All measurements were carried out at room temperature and atmospheric conditions.

Typical procedure for anionic cyclodehydrogenation of CNs

In a glove box, CN (1.0 mg, 0.88 μmol for [9]CN, 0.66 μmol for [12]CN, 0.50 μmol for [16]CN), alkali metal (ca. 20.0 mg), purified THF (1.0 mL) was added to a dried Schlenk tube with J. Young® O-ring tap. Then, the vessel was closed with the cap and heated in the silicon oil bath outside the glove box. During the reaction, the progress of cyclodehydrogenation was confirmed by MALDI-TOF MS of the partial sample which was oxidized by DDQ in the glove box for this purpose. As for the experiments in **2-2-3**, the alkali metal was removed inside the glove box. When the reaction was stopped, degassed methanol was added to the solution at room temperature under air. The solvent was removed under reduced pressure. The crude product was then washed with methanol to remove inorganic salts. Subsequently, DDQ (3.0 mg) and benzene (0.5 mL) were added to the obtained products in a test tube. The mixture was heated at 90 °C for 12 h in a 20-well reaction block (heater + magnetic stirrer). After cooling to

room temperature, the solvent was removed under reduced pressure. The reaction mixture was then washed with methanol to remove excess DDQ and reacted DDQ. The products originated from the cyclodehydrogenation of CNs were analyzed by MALDI TOF-MS, absorption spectroscopy, and Raman spectroscopy.

References

1. (a) Sato, T.; Tanaka, M. Yamabe, T. *Synth. Met.* **1999**, *103*, 2525. (b) Li, J.; Zhang, Y. Zhang, M. *Chem. Phys. Lett.* **2002**, *364*, 338. (c) Matsuo, Y.; Tahara, K.; Nakamura, E. *Org. Lett.* **2003**, *5*, 3181. (d) Yumura, T.; Bandow, S.; Yoshizawa, K. Iijima, S. *J. Phys. Chem. B* **2004**, *108*, 11426. (e) Galano, A. *Chem. Phys.* **2006**, *327*, 159. (f) Yumura, T.; Nozaki, D.; Hirahara, K.; Bandow, S.; Iijima, S. Yoshizawa, K. *Annu. Rep. Prog. Chem., Sect. C: Phys. Chem.* **2006**, *102*, 71. (g) Baldoni, M.; Sgamellotti, A.; Mercuri, F. *Org. Lett.* **2007**, *9*, 4267. (h) Liu, L. V.; Tian, W. Q.; Chen, Y. K.; Zhanga, Y. A.; Wang, Y. A. *Nanoscale* **2010**, *2*, 254. (i) Fort, E. H.; Scott, L. T. *J. Mater. Chem.* **2011**, *21*, 1373. (j) Martín-Martínez, F. J.; Melchor, S.; Dobado, J. A. *Phys. Chem. Chem. Phys.* **2011**, *13*, 12844.
2. (a) Bonen, A.; Koch, K.-H.; Lüttke, W.; Müllen, K. *Angew. Chem., Int. Ed. Engl.* **1990**, *29*, 525. (b) Koch, K.-H.; Müllen, K. *Chem. Ber.* **1991**, *124*, 2091.
3. (a) Rao, A. M.; Richter, E.; Bandow, S.; Chase, B.; Eklund, P. C.; Williams, K. A.; Fang, S. Subbaswamy, K. R.; Menon, M.; Thess, A.; Smalley, R. E.; Dresselhaus, G.; Dresselhaus M. S. *Science* **1997**, *275*, 187. (b) Jorio, A.; Saito, R.; Hertel, T.; Weisman, R. B.; Dresselhaus, G.; Dresselhaus, M. S. *MRS Bulletin* **2004**, *29*, 276.
4. Segawa, Y.; Yagi, A.; Ito, H.; Itami, K. *submitted.*
5. (a) Grzybowski, M.; Skonieczny, K.; Butenschçn, H.; Gryko, D. T. *Angew. Chem., Int. Ed.* **2013**, *52*, 9900. (b) Narita, A.; Verzhbitskiy, I. A.; Frederickx, W.; Mali, K. S.; Jensen, S. A.; Hansen, M. R.; Bonn, M.; Feyter, S. D.; Casiraghi, C.; Feng, X.; Müllen, K. *ACS Nano* **2014**, *8*, 11622. (c) Narita, A.; Feng, X.; Hernandez1, Y.; Jensen, S. A.; Bonn, M.; Yang, H.; Verzhbitskiy, I. A.; Casiraghi, C.; Hansen, M. R.; Koch, A. H. R.; Fytas, G.; Ivasenko, O.; Li, B.; Mali, K. S.; Balandina, T.; Mahesh, S.; Feyter, S. D.; Müllen, K. *Nature Chem.* **2014**, *6*, 126.
6. (a) Scholl, R.; Seer, C.; Weitzenböck, R. *Ber. Dtsch. Chem. Ges.* **1910**, *43*, 2202. (b) Seer, C.; Weitzenböck, R. *Ber. Dtsch. Chem. Ges.* **1913**, *46*, 1994.
7. Zhai, L.; Shukla, R.; Wadumethrige, S. H.; Rathore, R. *J. Org. Chem.* **2010**, *75*, 9900.
8. (a) Cai, J.; Ruffieux, P.; Jaafar, R.; Bieri, M.; Braun, T.; Blankenburg, S.; Muoth, M.; Seitsonen, A. P.; Saleh, M.; Feng, X.; Müllen, K.; Fasel, R. *Nature* **2010**, *466*, 470. (b) Diev, V. V.; Schlenker, C. W.; Hanson, K.; Zhong, Q.; Zimmerman, J. D.; Forrest, S. R.; Thompson, M. E. *J. Org. Chem.* **2012**, *77*, 143. (c) Talirz, K.; Söde, H.; Cai, J.; Ruffieux,

P.; Blankenburg, S.; Jafaar, R.; Berger, R.; Feng, X.; Müllen, K.; Passerone, D.; Fasel, R.; Pignedoli, C. A. *J. Am. Che. Soc.* **2013**, *135*, 2060. (d) Basagni, A.; Sedona, F.; Pignedoli, C. A.; Cattelan, M.; Nicolas, L.; Casarin, M.; Sambi, M. *J. Am. Che. Soc.* **2015**, *137*, 1802.

9. Solodovnikov, S. P.; Zaks, Y. B.; Ioffe, S. T.; Kabachnik, M. I. *Radiospektrosk. Kvantovokhim. Metody Strukt. Issled.* **1967**, 106.
10. Michel, P.; Moradpour, A. *Synthesis* **1988**, 894.
11. Rickhaus, M.; Belanger, A. P.; Wegner, H. A.; Scott, L. T. *J. Org. Chem*. **2010**, *75*, 7358.
12. Aprahamian, I.; Bodwell, G. J.; Fleming, J. J.; Manning, G. P.; Mannion, M. R.; Merner, B. L.; Sheradsky, T.; Vermeij, R. J.; Rabinovitz M. *J. Am. Chem*. *Soc.* **2004**, *126*, 6765.

Conclusion of this thesis

Throughout the PhD study, the author has sought the first synthesis of carbon nanobelts. In Chapter 1, cyclo[12]paraphenylene-[2]2,7-pyrenylene ([12,2]CPPyr), a precursor with "foothold" for the construction of belt-structure, was synthesized. Extensive characterization revealed its unique photophysical properties caused by inserted pyrene rings. In the synthesis of carbon nanobelt with [12,2]CPPyr, however, its poor solubility prevented further π-extension on the nanoring. Chapter 2 described the synthesis of another type of precursor, [9]cyclo-1,4-naphthylene ([9]CN). By careful structural analysis, several properties were uncovered, which are characteristic to a carbon nanoring consisting solely of naphthalene rings. Based on the successful synthesis of [9]CN, [8]-, [10]-, [12]-, and [16]CN were also synthesized as shown in Chapter 3. Not only the size-dependent properties of CNs were found, but also the diversity was created in the sizes of potential precursors. With several sizes of CNs in hand, the synthesis of carbon nanobelt was challenged in Chapter 4. To make sequential cyclodehydrogenation of CNs successful, the investigation of reaction conditions for anionic cyclodehydrogenation was conducted. A possible method for efficient cyclodehydrogenaion was found for [12]- and [16]CN, while desired carbon nanobelts have not been obtained yet. This work also disclosed difficulties on the cyclodehydrogenation of CNs and on the analysis of its products.

Carbon nanobelt is one of belt-shaped aromatic hydrocarbons, whose synthesis has long been awaited in the fields of nanocarbon science, materials science, and organic synthesis. In the PhD study, the author has designed and synthesized novel potential precursors. Their structural and electronic properties were extensively studied as a significant part of the synthetic studies on carbon nanobelts. The synthesis of carbon nanobelts from the precursor carbon nanorings was firstly tried, and one possible way that might lead to carbon nanobelts was found. Though further studies are necessary, this research would be in the forefront of synthetic studies on belt-shaped aromatic hydrocarbons. The author believes that this study lead the successful synthesis of carbon nanobelt in future.

List of Publications

（副論文）

1. “Synthesis and Properties of [9]Cyclo-1,4-naphthylene: A π-Extended Carbon Nanoring”
   Akiko Yagi, Yasutomo Segawa, Kenichiro Itami
   J. Am. Chem. Soc. **2012***, 134*, 2962–2965.

2. “Synthesis and Properties of Cycloparaphenylene-2,7-pyrenylene: A Pyrene-containing Carbon Nanoring”
   Akiko Yagi, Venkataramana Gandikota, Yasutomo Segawa, Kenichiro Itami
   Chem. Commun. **2014***, 50*, 957–959.

（参考論文）

“Design and Synthesis of Carbon Nanotube Segments: Toward Controlling the Growth of Carbon Nanotubes”
Yasutomo Segawa, Akiko Yagi, Katsuma Matsui, and Kenichiro Itami
Angew. Chem., Int. Ed. early view. DOI: 10.1002/anie.201508384R1.